Decoding Movement Direction for Brain-Computer Interfaces using Depth and Surface EEG Recordings

Project Report

Federico Bolner and Victor Rohu

Aalborg University,
Department of Health Science and Technology
Biomedical Engineering and Informatics
Fredrik Bajers Vej 7B
DK-9220 Aalborg

AALBORG UNIVERSITY

Department of Health Science and Technology
Fredrik Bajers Vej 7
DK-9220 Aalborg Ø
http://hst.aau.dk

Title:
Decoding Movement Direction for Brain-Computer Interfaces using Depth and Surface EEG Recordings

Theme:
Applied Biomedical Engineering & Informatics

Project Period:
Easter Semester 2012

Project Group:
1086

Participants:
Federico Bolner
Victor Rohu

Supervisors:
Dario Farina
Imran Khan Niazi

External Supervisor:
Karim Jerbi

Copies: 1

Page Number: 102

Date of Completion:
June 1, 2012

Abstract:

A Brain-Computer Interface (BCI) is a communication system that does not depend on the brain's normal output pathways of peripheral nerves and muscles. Thus, it constitutes a new output channel for the brain. In completely disabled patients, it may be used to recognize the patients' "will" directly from the brain in order to command a device, e.g., prosthesis. The purpose of this project is to develop a decoder for a BCI system capable of providing a control output based on decoding of different direction of movement execution, which in turn will enhance the quality of the command to external systems to propitiate the restoration of more complex motor functions than the two-choice commands commonly available in literature. The system will be based on classification of invasive and non-invasive brain signal recordings. The project will be divided into sub-tasks: 1) experimental recording of a data bank of electroencephalographic (EEG) signals for testing the BCI; 2) development of a multi-class, multi-channel translation algorithm that decodes different movement directions based on EEG and intracranial recordings. The late step is subdivided in two main parts: 1) time analysis for movement intention detection based on MRCPs; b) time frequency analysis for movement direction classification. Results of movement intention detection and classification of the direction have shown to be significantly above the level of chance for both iEEG and scalp EEG data. The present study also enabled us to set a comparison of different methods used for spatial filtering, normalization and classification. The method seems promising for the development of asynchronous brain–computer interfaces (BCIs) systems, merging detection and direction classification analyses.

The content of this report is freely available, but publication (with reference) may only be pursued due to agreement with the author.

Preface

This report documents the work of project group 1086, during the 10th semester of the Master of Science in Biomedical Engineering and Informatics with speciality in Medical Systems at the Institute for Health Science and Technology at Aalborg University, Denmark.
The project bases its foundations on the work of laboratory INSERM U1028 (Lyon, France) and the *Institut for Medicin og Sundhedsteknologi, Center for Sanse-Motorisk Interaktion* (Aalborg, Denmark) which both investigate brain activity, respectively through a time frequency approach (*Controle attentionnel, fonctions exectutives et oscillations cerebrales*) and a time analysis based on MRCPs.
The report follows the standard IMRaD structure found in most scientific papers: (I) Introduction and problem statement, (II) Methods, (III) Results and (IV) Discussion and conclusion.

The reference style used in the report is follows the Harvard method: [Last name, Year]. The references are indicated before a full stop. Figures and tables are numbered with reference to the chapter e.g. figure 1 in chapter 2 is "Figure 2.1". The captions are set below the figures or tables.

We would like to deeply thank our supervisors: Dario Farina, Karim Jerbi and Imran Khan Niazi for assistance and availability during the course of this Master thesis work. Our gratitude also goes to Mads Jochumsen and Thomas Lorrain for their useful advises.

Aalborg University, June 1, 2012

Federico Bolner
<fbolne11@students.aau.dk>

Victor Rohu
<vrohu11@students.aau.dk>

Contents

Chapter 1

Introduction

1.1 BCI systems

A brain-computer interface (BCI), also referred as brain-machine interface (BMI), is a device that translates neuronal signals reflecting a persons' intention into commands driving a machine (e.g. prosthesis, cursor, computer, robot, etc.) [Waldert et al., 2008; Birbaumer, 2006]. Typically, BCI control is achieved via classification of mental states or motor intentions using brain signals (such as EEG, iEEG, etc.). It is usually a closed-loop system, which acquires the signals, treats the data (preprocessing, feature extraction and classification are used to make a decision) and provides a feedback to the user through the device (e.g. movement of the prosthesis, etc.) [Pfurtscheller et al., 2008].

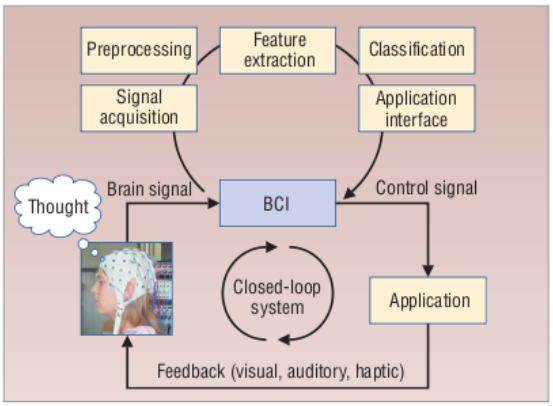

Figure 1.1: Elements of a BCI system. With the user's EEG recording as input, the system digitizes the brain signals, extracts and classifies signal features, and feeds the results to the application interface. The user controls the application and receives visual, auditory, or haptic feedback on the accuracy of the focused thought. In this way, the system becomes a closed-loop [Pfurtscheller et al., 2008].

1.1.1 BCI for communication

The key part of a BCI system is to make brain and computer communicate with each other. To achieve this goal, several physiological phenomena and technical approaches are used. To date the brain signals employed for invasive BCIs include: (1) action potentials from nerve cells or nerve fibers, (2) synaptic and extracellular field potentials and (3) electrocorticograms. The non invasive BCIs used, include instead: (1) the slow cortical potentials (SCP) component of the EEG, (2) other EEG and MEG oscillations, mainly sensorimotor rhythm (SMR), also called μ-rhythm, (3) P300 and other event-related brain potentials, (4) blood-oxygen-level-dependent (BOLD) response in functional magnetic resonance imaging (fMRI) and (5) near-infrared spectroscopy (NIRS), which measures cortical blood flow [Birbaumer, 2006].
A blind approach might also provide interesting results. Instead of using precise and well-known phenomena in given brain areas, classifiers can be trained on several 'random' features. Although this approach may be less efficient at first sight, it might provide new inputs about brain functional areas and brain physiology.

BCI systems are used for many different fields and applications. The principal ones are rehabilitation and multi-media (e.g gaming, etc.).

1.1.2 BCI for rehabilitation

BCI systems have different medical applications. For instance, restorative BCI systems aim at normalization of neurophysiologic activity that might facilitate motor recovery. Rehabilitation methods based on neuroscience seek to stimulate spontaneous functional motor recovery by exploiting the brain potential for plastic reorganization. The example of stroke rehabilitation is meaningful. Motor impairment after stroke is the leading cause of permanent physical disability. A patient who has important difficulty to move his limbs, or can not even move them at all, can use a BCI system with visual feedback in order to improve his condition of disability. By triggering limb movements, even if the movement is not real (e.g. *motor imagery*), and adapting his will to the feedback, the patient activates sensorimotor networks that the lesions affected [Pfurtscheller et al., 2008; Soekadar et al., 2011].

Figure 1.2: Feedback training using virtual hands. The participant's task is to imagine left- and right-hand opening and closing tasks. The BCI generates movement of the right or left (virtual) hand according to classified brain patterns [Pfurtscheller et al., 2008].

On the contrary, the assistive technology (AT), using a BCI system, aims to provide assistance to disabled people in a daily environment (e.g. web browsing, prosthesis control, etc...). Because a BCI device alone is not able to provide 100 % reliable decoding of the real intention of the subject, BCI in AT is mainly used as an additional channel in a so-called hybrid BCI (hBCI) system [Millan et al., 2010].
However, examples of BCI-only AT systems are present in the literature. For instance, Leeb et al. succeeded to make a reliable brain-controlled wheelchair. When the tetraplegic user imagine movements of his paralysed feet, beta oscillations appear in the EEG recordings and are used to control the wheelchair in a virtual environment. The patient is then able to drive himself in a virtual street and go from avatar to avatar.

The navigation in a virtual environment may also have applications in the multi-media/gaming field.

1.1.3 BCI for gaming

Although BCI research will likely continue to focus on medical applications, BCIs may also be used by healthy users for different purposes [Allison et al., 2007].
For instance, the Berlin Brain Computer Interface (BBCI) provides intuitive control strategies in plausible gaming applications through the use bio-feedbacks. In addition, the BBCI paradigm shows encouraging result for patients without previous experiences with BCI systems. Indeed, even an untrained subject can navigate through the Pacman labyrinth (see figure 1.3) in about 40 seconds [Krepki et al., 2003].

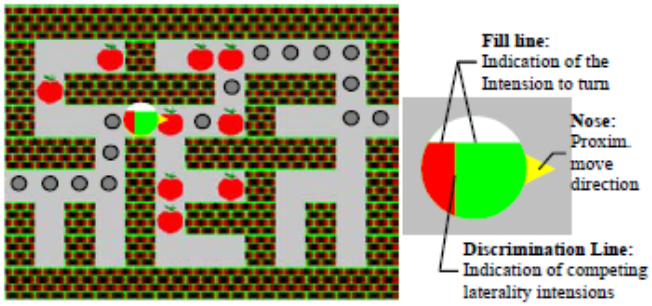

Figure 1.3: Feedback "Brain Pacman" and the head filling strategy for indication of user's upcoming intentions. The Pacman moves every 2 seconds [Krepki et al., 2007].

On top of this, many other applications can be imagined: Middendorf et al. presented a BCI that allowed people to bank a full motion aircraft simulator; some other games or virtual environment allow users to turn or lean left or right. However, this particular kind of BCI usually only allows one degree of freedom with a binary choice [Allison et al., 2007].
A few companies have sold BCIs intended to enable healthy subjects to play simple games (e.g. ibva.com, cyberlink.com and smartbraingames.com). Although the state of art of BCI gaming usually allows only one degree of freedom with a binary choice, further developments are expected in this field [Allison et al., 2007].

1.1.4 Types of BCI systems

BCIs can be categorized according to two main characteristics: synchronization and invasiveness [Besserve, 2007].

1.1.4.1 Synchronous - asynchronous BCIs

The main difference between synchronous and asynchronous BCIs is that synchronous BCI uses the response from the brain to a given stimulus, while asynchronous BCI analyses the signal in continue. The synchronous paradigm is usually used more often [Besserve, 2007]. For example, Leeb et al. uses an asynchronous paradigm, which screens the brain in continue, in order to control a wheelchair in real-time by imagination of feet movements.
On the other hand, in this report we will analyse the brain response to a given signal off-line: the preparation of the movement is triggered by a visual cue, then actual movement initiated by a *"Go signal"*. It involves, therefore, a synchronous BCI.

1.1.4.2 Invasive - non invasive BCIs

Invasive BCI uses intracranial techniques to acquire the signal, such as electrocorticography (ECoG, in which electrodes are on the surface of the cortex) or stereoelectroencephalography (SEEG, where electrodes are placed inside the grey matter). Non-invasive BCI instead uses extracranial recordings of the brain activity, such as electroencephalography (EEG, electrodes on the scalp), magnetoencephalography (MEG, electrodes near the scalp) or functional magnetic resonance imaging (fMRI) [Besserve, 2007]. Unlike invasive systems, which entail the risks associated with any brain surgery, non invasive systems are basically harmless [Pfurtscheller et al., 2008].
For practical reasons, non invasive BCI are more common: from 2007 to 2011, 14.992 publications have cited EEG or MEG, while only 337 mention intracranial EEG [Dalal et al., 2011].

1.2 State of the art

The following report has been written with the goal of detecting the movement intention and classifying four different directions of hand movement, both during the actual movement and the preparation phase, by means of invasive and non-invasive synchronous BCIs.

1.2.1 Overview

Directional tuning of hand/arm movement is present in iEEG, in the low-pass filtered signals (Mehring et al. 2004, Ball et al. 2009; see also figure 1.5) and in the amplitude modulations of different frequency bands (Leuthardt et al. 2004, Ball et al. 2009). Tuning strength is sufficient for relatively accurate directional decoding from low-pass

filtered signals as well as from amplitude modulations of different frequency bands.
As for non invasive EEG, it has been shown that directional tuning for hand/arm movement can also be observed both in low-pass filtered signals and in amplitude modulations of different frequency bands (Waldert et al. 2008, figure 1.6). However, it seems that EEG are less capable of revealing high frequencies (Dalal et al. 2008, Waldert et al. 2008) and only few publications clearly show movement dependent high γ modulations above 90 Hz that are unlikely due to artefacts (Gonzalez et al. 2006, Ball et al. 2008). The common time-frequency pattern during center-out movements (see figure 1.4) is the following: change of amplitude in a low frequency band ($<$ 2 Hz for iEEG, $<$ 7 Hz for EEG) during the movement, decrease of amplitude in an intermediate frequency band (6-30 Hz for iEEG, 10-30 Hz for EEG) shortly before and lasting until the end of the movement, and movement related amplitude increase in high frequency band (34-128 Hz for iEEG, 62-87 Hz for EEG).

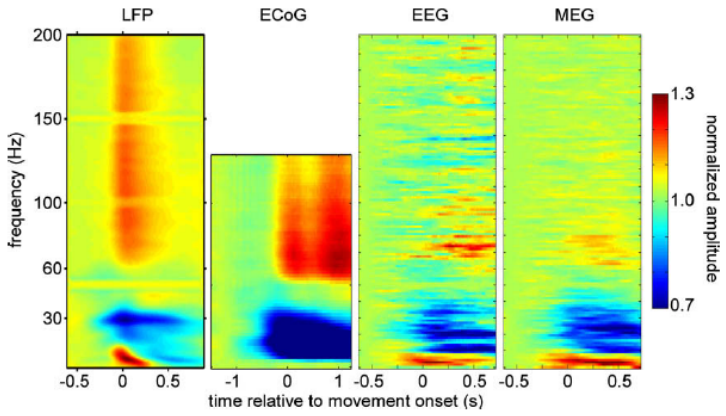

Figure 1.4: Grand-average time-resolved amplitude spectrograms during centre-out movements for the different recording techniques (LFP, ECoG, EEG, MEG) [Waldert et al., 2009].

1.2.2 Particular cases

Rickert et al. showed that the local field potential (LFP) recorded by an intracranial procedure can be used to discriminate 8 directions in a centre-out arm movement. On the one hand, analysis of the LFPs in the time domain showed that the amplitude of a slow complex waveform beginning shortly before the onset or arm movement is modulated with the direction of the movement (see figure 1.7. Direction-dependant modulations are found also in other frequency ranges ($<$4 Hz, 6-13 Hz and 63-200 Hz), where the components of the signal typically increase their amplitudes before and during movement execution (see figure 1.8). As shown in figure 1.9, the low frequency band yields the best decoding power (DP = 0.24 on $<$ 4 Hz and 1 electrode). The combination of the high frequency band and the low frequency band (63-200 Hz and $<$ 4 Hz) can increase the decoding power.

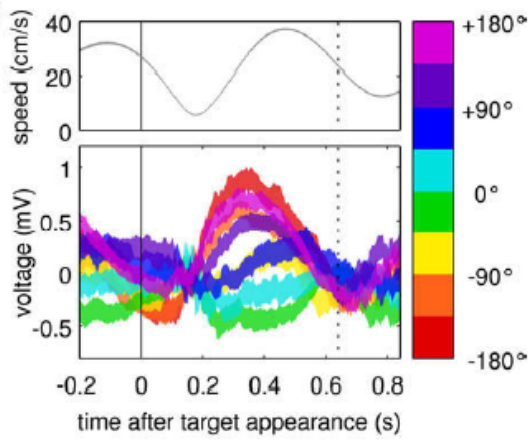

Figure 1.5: Average human ECoG from one electrode on hand/arm motor cortex, measured during continuous target-to-target movement and sorted for eight different instantaneous movement directions (lower plot). The vertical solid line shows the time of a new target appearance (t = 0) while the dotted line indicates the median time of target reaching. Coloured bands display the mean over all single traces of one direction +/- standard-error of the mean. The upper inset shows the average magnitude of hand velocity [Waldert et al., 2009].

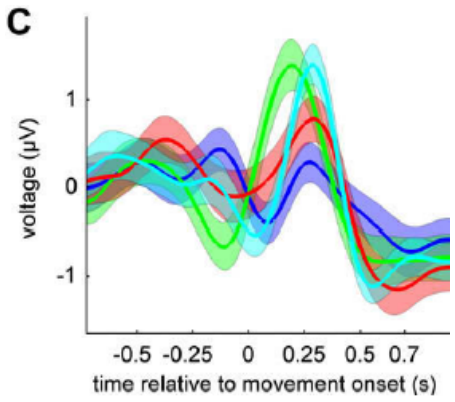

Figure 1.6: Averaged movement related potential recorded with one EEG electrode above the contralateral motor area of one subject (average +/- standard-error of the mean across all trials for each direction, blue – right, green – up, red – left, cyan – down) [Waldert et al., 2009].

Leuthardt et al. used ECoG recordings decoding to control a one-dimensional computer cursor. This binary task can be a achieved with up to 74 % accuracy while opening and closing the right hand (combination of frequency bands within 10.5 and 50.5 Hz) and 83 % of accuracy while imagining opening and closing right hand (in which a decrease in 30.5-32.5 Hz band has been seen). This result may seem curious, as the best result is achieved with the imagination task. This can be explained by the effort Leuthardt et al. made in order to optimize the imaginary task, which is indeed more relevant for BCI. Direction-dependant modulations are also found for a bidimensional joystick movement direction task (4 directions), particularly in 40-180 Hz (see figure 1.10).

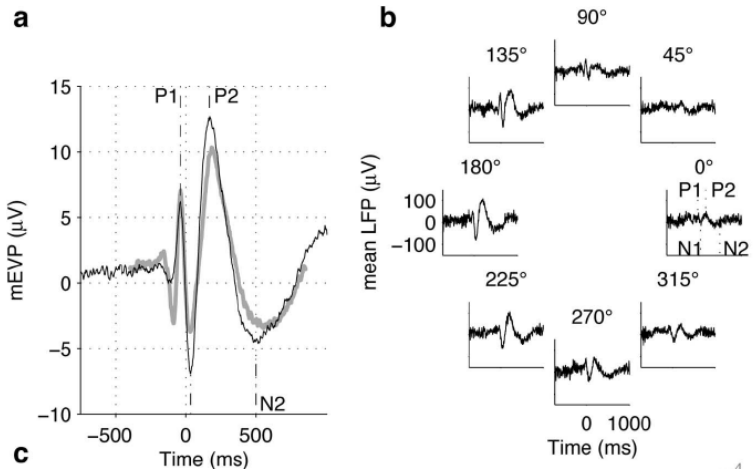

Figure 1.7: Tuning of the movement-evoked potential. Time 0 ms indicates movement onset. (a) Grand average movement evoked potentials (averaged across all recorded LFPs). Trials were aligned either to movement onset (black curve) or to cue onset (grey curve). P1, P2, N1, and N2 indicate the points in time of the positive and negative peaks of the average LFP. (b) Directional tuning of a movement evoked potential obtained from a single electrode: trial-averaged activity shown separately for each movement direction [Rickert et al., 2005].

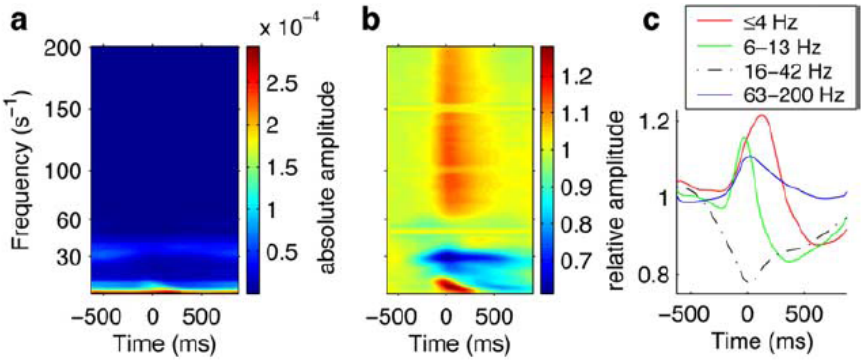

Figure 1.8: (a) Time-resolved amplitude spectrum, (b) Each frequency bin normalized by its baseline amplitude, (c) Changes in the amplitude exhibited by four different frequency bands (<4, 6–13, 16–42, and 63–200 Hz) during the task [Rickert et al., 2005].

Ball et al. proposed a general study about how arm movement direction in neuronal activity of the cerebral cortex (ECoG technique) can be used for movement control mediated by a BCI. The results shown in figures 1.11 and 1.12 are found using regularized linear discriminant analysis (RLDA) in a center-out arm movement task in 4 directions.

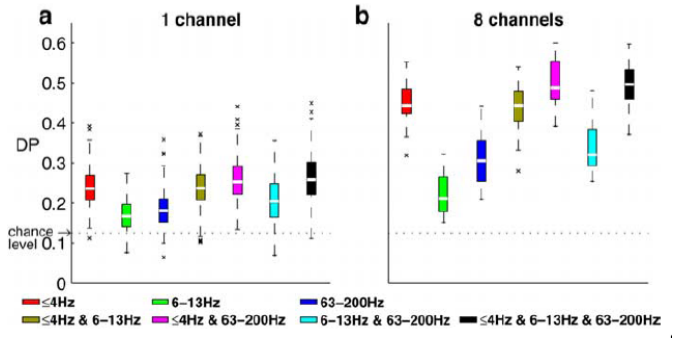

Figure 1.9: Decoding power of different frequency bands [Rickert et al., 2005].

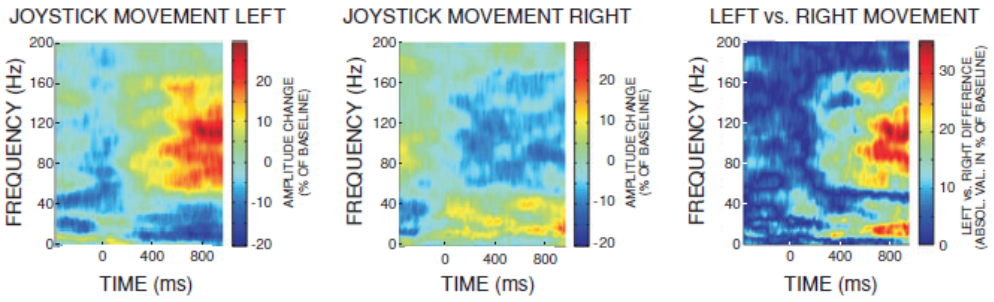

Figure 1.10: ECoG correlations with joystick movement direction before and during movement [Leuthardt et al., 2004].

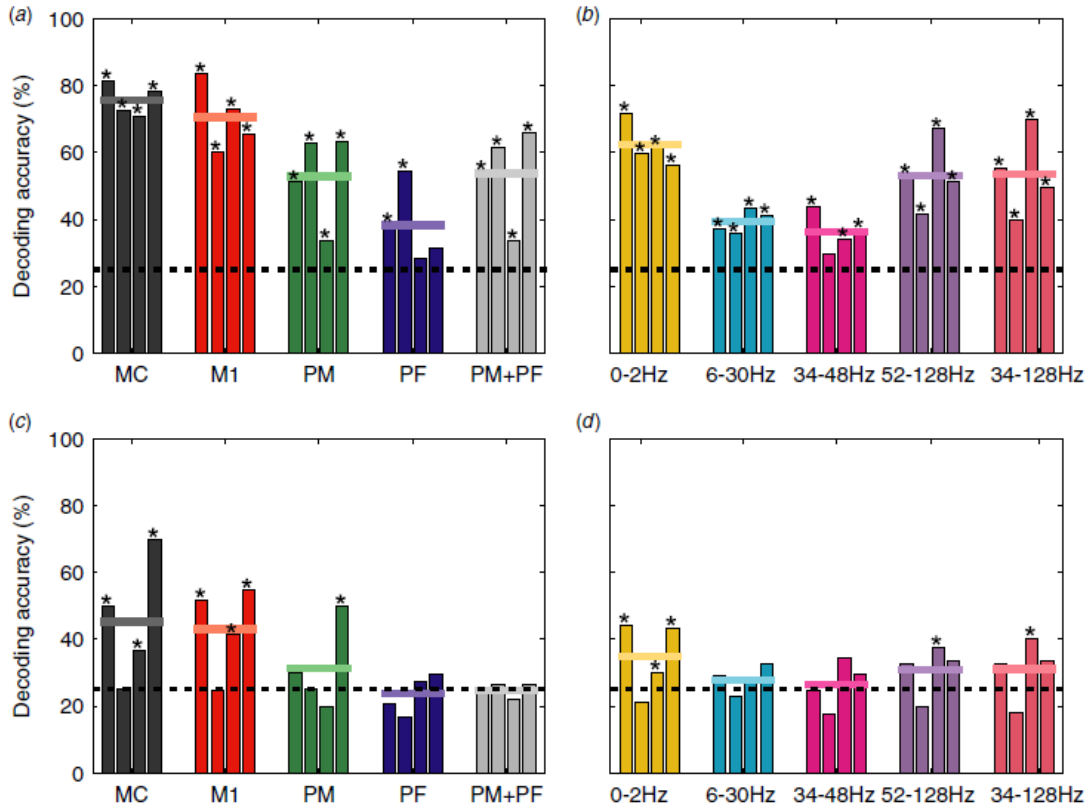

Figure 1.11: Decoding accuracy from different frontal anatomical subregions and signal frequency bands (four movement directions). The dashed line depicts the chance level. Stars indicate bars with significant decoding accuracy. (a) Decoding results for the movement-related potentials from the whole mean duration of the reaching movement, including activity up to 250 ms prior to movement onset. The five groups of bars correspond to the anatomical subdivisions MC (entire motor cortex = M1 + PM), M1 (primary motor cortex), PM (premotor cortex), PF (prefrontal cortex) and PM + PF (premotor and prefrontal cortex). Each of the five bars in the individual groups of bars represents one recording session (two sessions from subject 1, and one session from each of the subjects 2, 3 and 4). Horizontal coloured lines mark the mean DA for each anatomical subdivision (b) Frequency domain decoding results for MC, for the same time window as in (a), for the low, intermediate and different gamma bands (low, high and broad). The corresponding results as in (a) and (b) are given for activity during the pre-movement time window only, ranging from 250 ms to 0 ms before arm movement onset [Ball et al., 2009].

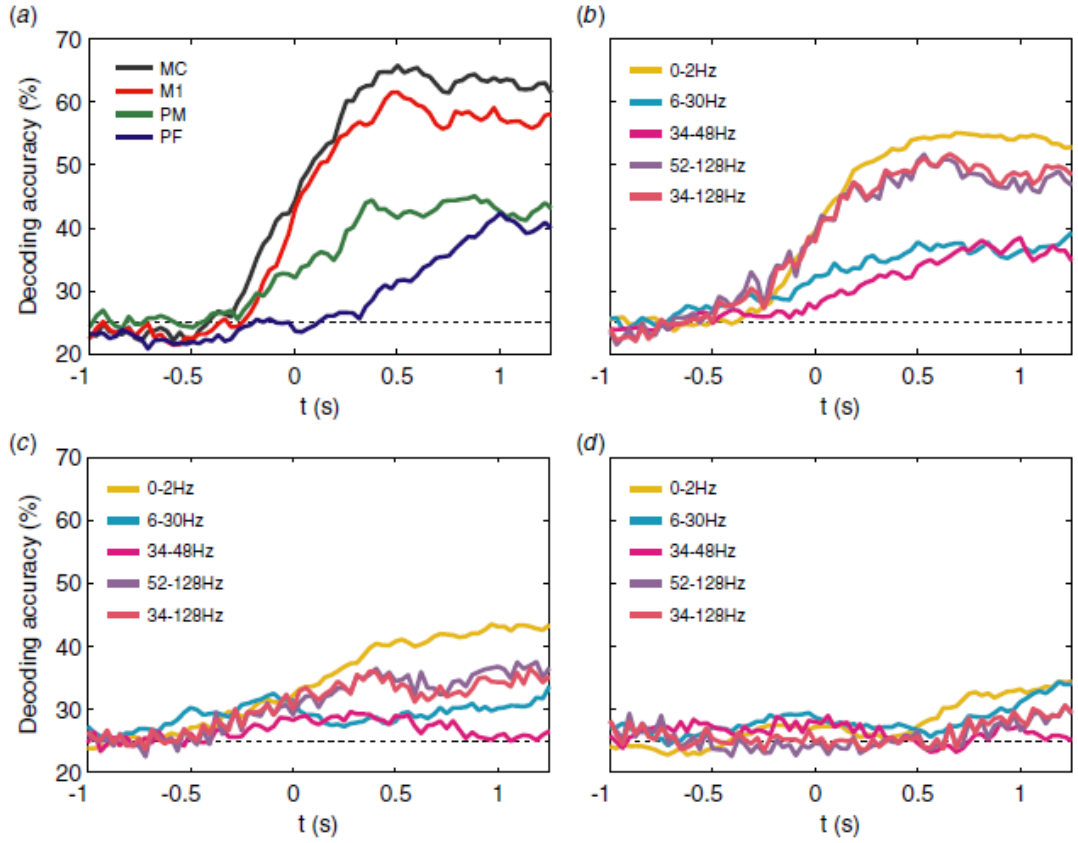

Figure 1.12: Temporal evolution of decoding accuracy. Graphs show the DA of the time window lasting from 500 ms before until the time indicated on the x-axis. Time is given relative to movement onset. (a) Time course for decoding of the movement-related potentials for M1, PM, MC and PF. (b) Time course of DA for decoding from the amplitude spectra using the low, intermediate and different gamma bands for M1. The black line indicates the chance level. (c) Time course for PM and (d) for PF [Ball et al., 2009].

1.3 Problem statement

Movement intention detection can be achieved studying EEG waveforms which occur before the movement onset. One of the major challenges in detecting EEG waveforms from single trials is the poor signal to noise ratio (SNR) of the EEG. Since EEG signals represent the summation of potentials generated by a large population of cortical neurons, the amplitude of the spontaneous EEG activity is relatively large (in the range of 100 μV) with respect to the activity related to motor planning and execution, such as the initial negative phase of MRCP (range 8–10 μV, see appendix C for a MRPC insight). In order to improve the SNR of EEG signals, spatial filtering can be used, however, commonly used spacial filters such as Laplacian filters, may not be optimal for detection of MRCPs from single trials [Niazi et al., 2011].
Once the movement intention is confirmed, the decoding of the direction is the next challenge. By considering the signal in the frequency domain, new information about the movement direction might be found. The ability to decode the direction of upper-limb motor tasks from its underlying neural signature is even more intriguing for brain computer interface used for rehabilitation. Although a lot of progress has been achieved in the recent years, numerous methodological and physiological questions remain open or need deeper exploration. Specifically, what type of information about movement direction can be extracted from surface and invasive recordings of brain activity? Which brain signals provide the best decoding of limb movements direction? What signal classification algorithms are best suited for this endeavour and how can we optimize them to achieve efficient BCIs in the future?

Aim

The goal of this research project is to implement and apply multiple detection and decoding techniques to scalp and depth EEG recorded in subjects performing motor tasks in different directions. The accuracy of the various decoding strategies will be compared at various levels: (a) the classification methods, (b) the discriminant neuronal signatures, known as the features, (c) the type of EEG recordings, and (d) robustness to artifacts and noise.

Methods

This interdisciplinary project consists of two main parts: (1) electrophysiological recordings of brain activity such as MRCPs, LFPs and different brainwaves, both from iEEG and scalp EEG; and (2) implementation and comparison of signal detection, classification and decoding approaches to infer movement intention and direction from invasive and non-invasive brain signal recordings.

Part 1

Experimental data acquisition in subjects performing a delayed motor task was conducted. In addition to already existing intracranial EEG recordings acquired from an

epileptic patient (Grenoble hospital (France)), new surface EEG recordings were acquired (Aalborg University laboratory (Denmark)). The latter experiment used scalp EEG in a delayed center-out motor task. The scalp EEG data will be cleaned from blinks or muscle artifacts and will be pre-processed prior to implementation of detection and classification tests.

Part 2

- Two types of signals will be explored: (a) surface EEG (acquired during the project in Aalborg University laboratory), and (b) depth intracranial EEG (provided by Lyon laboratory).
- Two types of analyses will be considered, (a) movement intention detection and (b) movement direction detection, either intended (during the delay period) or executed (during real movement).
- Two types of features will be assessed: (a) time-domain features such as motor cortical potentials for movement intention detection, and (b) frequency-domain features for movement detection/direction decoding.
- Different spatial filter are used in the time-domain analysis. For the frequency-domain, features will be examined with a number of appropriate signal processing tools that include: (i) wavelets transform to compute the frequency features from the EEG signals, (ii) Linear Discriminant Analysis (LDA), Support Vector Machine (SVM), k-Nearest Neighbor (KNN) and Neural Network (NN) for classification of (intended/executed) movement directions.

Expected impact

The results of this ambitious project will have implications at least at three levels: (a) from a methodological point of view, the comparison of the classification approaches on experimental data will provide important insights into the strengths and limitations of existing methods and might suggest ways to improve them; (b) from a physiological perspective, identification of the best discriminant features will advance our knowledge of motor encoding/decoding in the context of motor-related BCIs; (c) in the long-term, the expertise and results obtained in this project may have useful implications on the future use of BCI to control a robotic prosthesis (neural prosthesis) on one hand, and on the use of BCI in the context of neuro-rehabilitation in patients with motor deficiencies on the other.

Chapter 2

Methods

2.1 Introduction

In this chapter, we will first describe the experimental protocol. Then we will explain the methods used for time analysis (whose the goal is movement detection). Finally, we will go through the methods used for time frequency analysis (whose the goal is movement direction classification).

2.2 Experimental protocol

2.2.1 Subjects

2.2.1.1 Intracortical EEG

The subject is a patient affected by a drug-resistant epilepsy who decided to be operated. As the EEG/MEG investigations are not sufficient to find the epileptic focus, in-depth electrodes are used until the site was located. During the investigation period, the patient gave us her agreement to carry the present experiment.

2.2.1.2 Scalp EEG

Five subjects were used for this purpose. The subjects were all right-handed males with an age that ranged from 23 to 30. None of the subject suffered from hand or arm pathologies or neurological disorders. The participants gave their informed written consent before inclusion in the study. The entire test was conducted accordingly to "The Rights of a Volunteer in a Biomedical Research Project", issued by the Danish National Committee on Biomedical Research Ethics.

2.2.2 Experimental setup

2.2.2.1 Intracortical EEG

Intra-cerebral recordings were conducted using a video-SEEG monitoring system (Micromed, Treviso, Italy), which allowed the simultaneous data recording from 128 depth-EEG electrode sites. The data from the recorded patient were bandpass filtered online from 0.1 to 200 Hz and sampled at 1024 Hz. During the acquisition, the data are recorded using a reference electrode located in white matter.
The in-depth electrodes are placed in agreement with the surgeon needs so as to identify the epileptic focus. As a result, they are spread in the brain without any relations to the investigated task. More than 128 recording sites (channels) are present but only the most interesting sites according to the surgeon are scanned for our experiment.
As shown on figures 2.2 and 2.3, each electrode is labelled by a letter, and each dot represents an electrode site where a signal can be recorded. On each electrode, the different sites are labelled by a number: from 1 (closer from the scalp), to usually 16: e.g. *v14* is the 14th site on the electrode *v*. The figure 2.1 shortly displays the link between an electrode and the corresponding brain area.

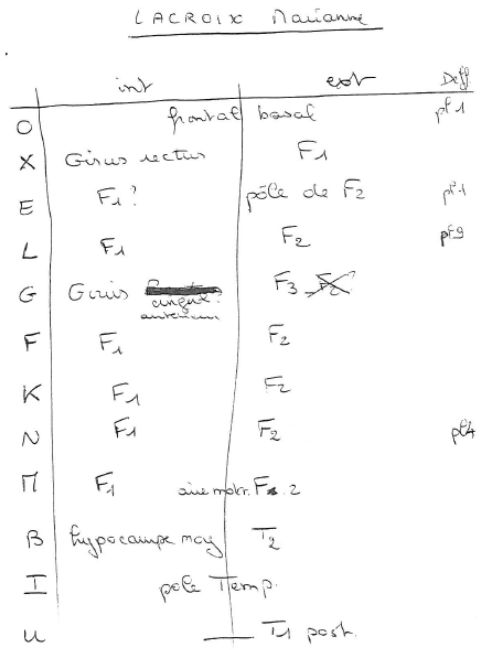

Figure 2.1: Correspondence between electrodes and functional areas of the brain. Column Ext. represents the channels which are closer to the scalp. Column Int. represents the channels which are more deeply in the brain. On a given electrode, the site number 1 is the more internal, while the site number 16 is the more external.

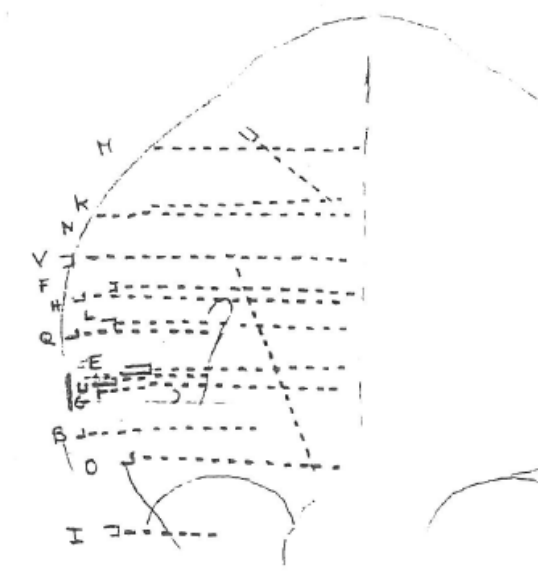

Figure 2.2: Electrodes implantation diagram, each dot represents a recording site.

Figure 2.3: Electrodes implantation diagram, each dot represents a recording site.

2.2.2.2 Scalp EEG

The experiment took place in an electrically shielded room. Subjects were seated on a chair, in front of a LCD screen placed on a table, with the arm on the table and the hand holding a mouse. EEG signals were recorded from Ag/AgCl scalp electrodes. Twenty electrodes were placed accordingly to the International 10-20 system, located in F3, F1, Fz, F2, F4, FC3, FC1, FCz, FC2, FC4, C3, C1, Cz, C2, C4, CP3, CP1, CPz, CP2, CP4, P3, P1, Pz, P2, P4. The right ear lobe (A2) was used as a reference. The subjects were grounded at the forehead. EOG was measured from FP1. The EEG recording was performed with a forty channels digital DC EEG amplifier (Nuamps Express, Neuroscan, USA) and data recorded with the Acquire Software Scan 4.5 (Neuro Scan Labs) following

the mentioned protocol (using Presentation software). Electrode impedances should be kept below 5 $k\Omega$. The EEG and EOG signals were sampled with a rate of 500 Hz and amplified with a gain of 19. The signals were converted by a 32-bit A/D converter. Early preprocessing has been performed with EEGLAB and Neuroscan.

2.2.3 Task

The experimental task consisted in asking the subjects to perform a simple movement of the arm in the given direction, while holding the mouse (no constraints on the speed of the movement), reaching a point on the screen and finally coming back to the central starting point. Presentation software was used to display synchronized cues on the screen both for the iEEG and surface EEG recordings. The task consisted, in detail, of:

- A "rest period", from 0 to 1 sec, during which the screen is blank.
- At 1 sec a visual cue (illuminated target) in a random direction, is given to the subject.
- A "preparation period", from 1 to 2.5 sec, during which the subject is instructed not to perform the movement.
- At 2.5 sec a "go signal" is displayed. This means that the subject can start to perform the movement in the suggested direction.
- A "movement period", starting from 2.5 to 3.9 sec. The subject moves the pointer of the mouse towards the target, reaches it, and comes back to the starting point on the screen.

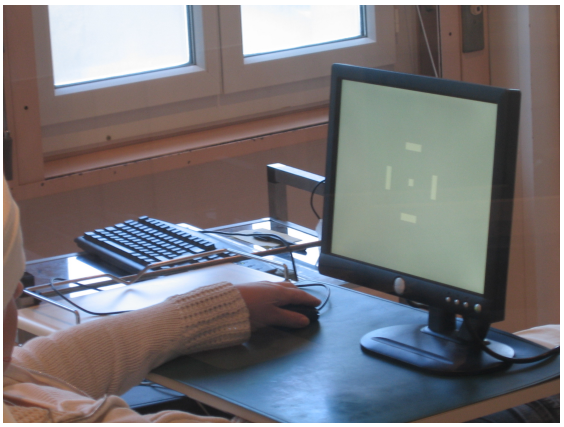

Figure 2.4: Picture of the experiment setup. The central point and the 4 different targets (up, down, right, left) can be seen on the screen.

This protocol was used both for the iEEG and surface EEG, with some differences between the number of direction and number of trials recorded. As for the iEEG recordings, the subject performed 50 trials (movement tasks) for each of the four directions

(up, down, left and right), both for the left and the right hand. As for the surface EEG recordings, 100 trials for each of the four directions (up, down, left and right) were collected for the right hand, whereas only two directions (up and down, 100 trials) were collected from the left hand. The increase in the number of trails recorded from the scalp EEG can be explained by the loss of quality of the scalp recordings compared with the intracortical ones.

2.3 Early preprocessing

2.3.1 Detrend

The iEEG signal is 0.1 to 200 Hz bandpassed online then detrendend so as to remove the continuous part (offset). The EEG signal is 0.05 - 150 Hz bandpassed offline then detrended. However, the bandpassing and detrending do not remove the muscular artifacts.

2.3.2 Bipolarization

As the muscular artifacts were widespread into the brain, we could partially remove their influence by using bipolarization on iEEG data. E.g. instead of using the voltage of the site 6 of electrode n (calculated from a reference electrode in the white matter) we used n7-n6. If there was an artefact, it is most likely present on the two sites due to the short inter-site distance (around 3 mm) and thus the artifact could be removed by bipolarization [Jerbi et al., 2009].

2.3.3 Eye artifacts

As proposed by Imran and Mads (and also referenced in Waldert et al.) who already worked with the Aalborg University EEG system, we used a 50 microvolts threshold detection of eyes artifacts in the EEG signal. For each epoch, if the signal acquired on one electrode is above the threshold, we decided to discard the entire epoch (and not only the couple epoch-electrode). Indeed, an artifact which leads the signal to be above the threshold on one electrode is certainly also present on other electrodes, maybe without being strong enough to cross the threshold.
Bipolarized iEEG signal is far less vulnerable to muscular artifacts than EEG signal Leuthardt et al. [2004]. We used the averaged across epochs time-frequency maps of each electrodes in order to find and discard artifacted channels (see example in *Results*).

2.4 Signal processing

2.4.1 Movement intention detection

Here follows a brief introduction to the protocol and the techniques used to analyse the data set, which later will be treated more extensively. The experimental data were

analysed with two different spatial filters and a cross-correlation approach was used to determine the movement intention detection accuracy. Since the aim is detecting an *intention* of the movement, the initial negative phase of the MRCP was used (see appendix C for a MRPC insight). The signal analysis methods will be discussed in the following subsections. It was divided in two steps, first MRCP template extraction from the training data, then the movement intention detection part.
The aim of spatial filtering is to improve the signal-to-noise ratio by creating a virtual channel which is a (linear, in the following cases) combination of the input channels of the filter. The first filter was a large Laplacian spatial filter (LSF), which has been proved to be a valuable choice among other fixed coefficient spatial filters [Niazi et al., 2011]. The second filter was an optimized spatial filter (OSF), where the optimization process is achieved with the aim of maximizing the SNR of the filtered data. After the spatial filtering, the MRCP template was extracted from the resulting channel (named surrogate channel from now on).
In the second part of the analysis, the negative phase of the MRCP template was used on the data to calculate the movement intention detection accuracy. This was achieved by measuring the cross-correlation between template and signal and obtaining the number of correct and incorrect detections. The results are expressed using statistical parameters as true positive rate (TPR) and false positives rate (FPR). Finally, the performance of the different spatial filters was compared.
The protocol described above was applied on: (a) each data set containing the single task performed by each subject (for example 'down' movement with the right hand for subject no. 3), and (b) combining for each subject each hand movement tasks (for example: all the epochs from left hand of subject no. 3), allowing to have more epochs, but losing the direction information.

2.4.1.1 Electrode selection

iEEG After the bipolarization process, we were left with 91 channels located in 16 electrodes (see figure 2.7). Out of these 91, 7 channels were selected to be used in the analysis; their location is showed in figure 2.7. This number of channels might seem restricted compared to the starting point mentioned above, but the procedure it was necessary for at least two reasons: (a) the optimization process for the OSF filter on 91 channels would have been too long, and (b) from an MRCP extraction point of view, these seven channels were the ones showing a shape that reminded the one of the MRCP. Among these seven channels, two channels were chosen from two electrodes near sensorimotor areas, three channels from other two electrodes located in the frontal lobe and the two last channels came from two electrodes which passed through the temporal lobe. The locations of the chosen electrodes are near the motor cortex, the prefrontal areas and basal ganglia, places in which the MRCP is likely to be generated (see appendix C).

Scalp EEG For the same reason mentioned above, for the spatial filtering 9 channels out of 20 were chosen. As figure 2.8 shows, they were:

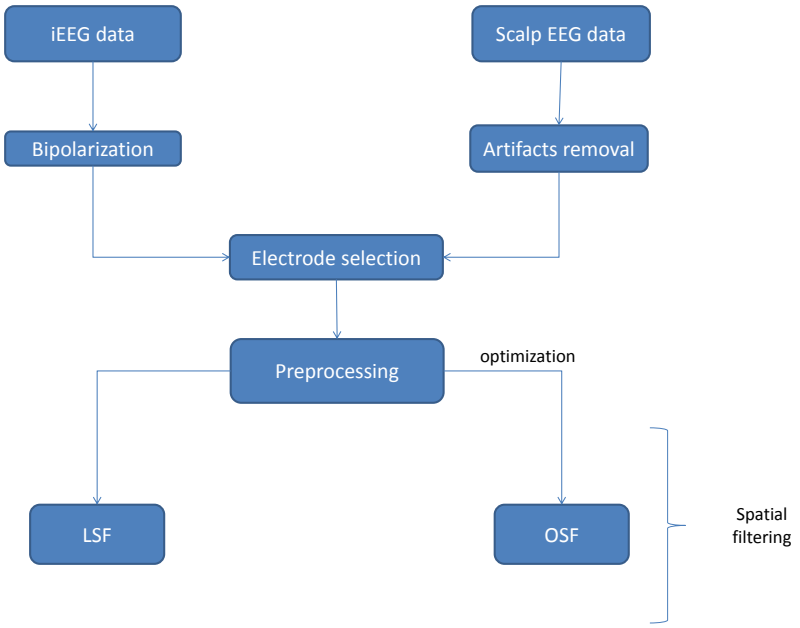

Figure 2.5: The flux diagram describes the first part of the protocol (signal processing)

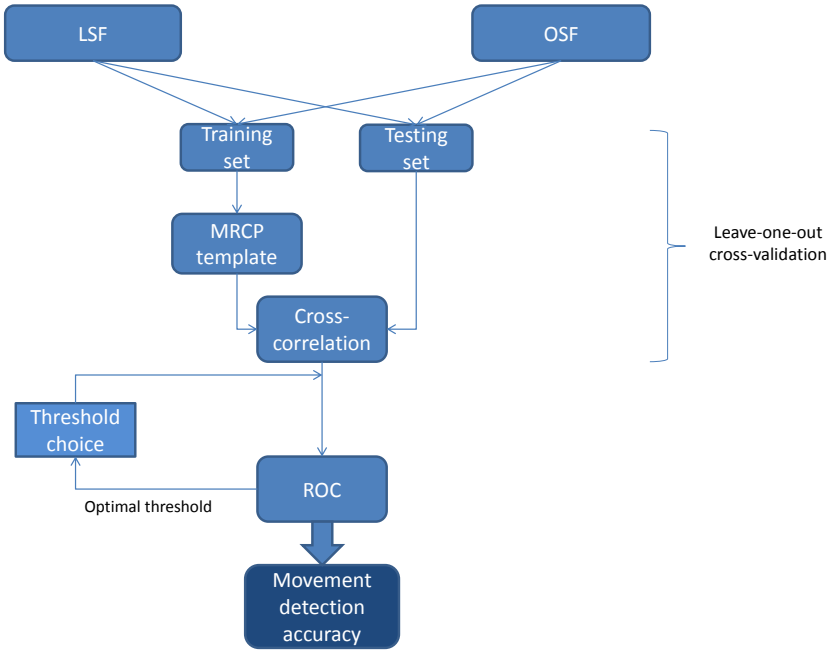

Figure 2.6: The flux diagram describes the second part of the protocol (template extraction and movement detection)

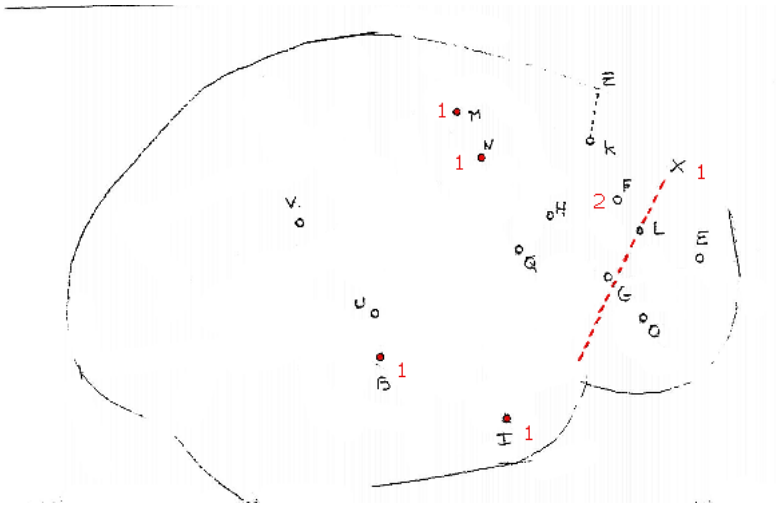

Figure 2.7: Electrodes location and number of the channels chosen for the iEEG data analysis.

- C3, C1, Cz, CP3, CP1, CPz, P3, P1, Pz for right hand movements and
- Cz, C2, C4, CPz, CP2, CP4, Pz, P2, P4 for left hand movements.

This choice is justified by the fact that these electrodes as they are located above the premotor, motor and somatosensory cortices and are not expected to be easily contaminated by task related auditory or visual artifacts. Nine channels were considered enough for this type of analysis, and so F3, F1, Fz, F2 and F4 electrodes were not used, both to make the optimization process faster and because they are the nearest to the subject face. The position of the electrodes was not centered on the z axis, but shifted contralaterally with respect to the hand used for the motor task.

2.4.1.2 Signal analysis

2.4.1.3 Preprocessing

Both the iEEG and the EEG data were detrended, band-pass filtered with a third order Butterworth zero-phase filter from 0.05 Hz to 5 Hz.

2.4.1.4 Spatial filtering

Spatial filtering has been used for source localization in EEG. In particular, the surface Laplacian is a technique that has been used to improve the spatial resolution of the electroencephalographic signals. Through a liner combination of the input channels, the filtering process ends with a single virtual channel (later referred as *surrogate channel*) which contains greater spatial information than does the raw potential measured by EEG montages [Bradshaw and Wikswo, 2001].
The spatial filtering has been applied both on iEEG and scalp EEG data for each movement the subject performed.

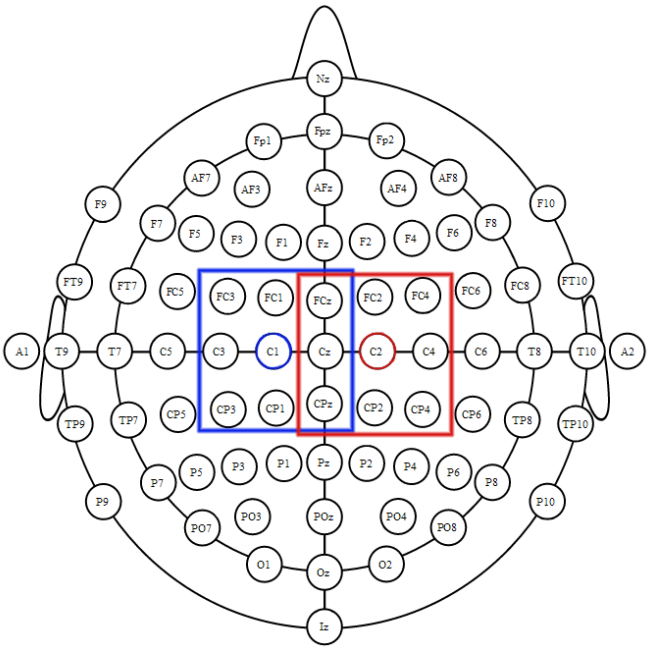

Figure 2.8: Electrodes selection for the scalp EEG. The squares indicate which electrodes were selected for the analysis, depending on the hand used during the movement (right hand:blue square, left hand:red square). The circle indicated which electrode had 1 as weight coefficient in the Laplacian filtering process.

The two spatial filters (LSF and OSF) were applied on the pre-processed data sets (iEEG channels and EEG channels) and resulted in a surrogate channel for each one of them. A spatial filter is defined and changes its characteristics depending on its set of coefficients. In this study, we investigated two different spatial filters: a Laplacian spatial filter (LSF) and an optimal spatial filter (OSF) [Niazi et al., 2011].

Laplacian filter The Laplacian filter is a commonly used source localization and it has fixed coefficients. The channel coefficients in this case were:

$$x_i = \begin{cases} 1, & i = 1 \\ -\frac{1}{(N_{ch}-1))}, & \forall i \neq 1, \end{cases}$$

where N_{ch} is the number of channels, so 7 for the iEEG and 9 for the scalp EEG. The sum of the N_{ch} coefficients is zero so that the spatial dc (mean value of the waveform) components are rejected [Niazi et al., 2011]. Channel 1, which has weight equal to 1 in the Laplacian filter, ($x_i = 1$) changed according to the type of data.
For iEEG data, the channel 1 was chosen empirically among the ones that were located in the frontal areas and above the motor cortex. Because of their location, a preference was initially reserved to M and N electrodes (see figure 2.7 for detailed position). As it could be expected, the signal recorded from them presented good information about the movement phase (after the 'go' signal in the protocol), but not as much for the MRCP

negativity phase. A more recurrent negative phase came instead from a channel located on electrode F, in the frontal lobe of the brain. In order to find the best channel, a preliminary analysis was anyway conducted and confirmed that channel F performed from 0 % up to 10-15 % better in terms of TPR compared to M or N, and so it was chosen as channel 1 for the Laplacian filter during the final analysis.
As for the scalp EEG, instead, x_1 corresponded to C1 for right hand movements and C3 for left hand movements: C1 and C3, respectively, are the centers of the matrix of electrodes (see figure 2.8) positioned contralaterally with respect of the used hand, and due to their position overlaying the hand area in the brain, are most likely the ones that can provide a good source of information [Ramoser et al., 2000].
Here follows an example for scalp EEG data (right hand movement):

$$surrogate\,channel = \begin{bmatrix} x_1 & x_2 & ... & x_{N_{ch}} \end{bmatrix} \begin{bmatrix} channel\,C1 \\ channel\,C3 \\ ... \\ channel\,Pz \end{bmatrix}$$

Optimized Laplacian Filter The Optimal Spatial Filter (OSF) provides an optimized coefficient set in order to maximize the signal-to-noise ratio in the surrogate channel.
The filter coefficients were optimized on the data set with the following procedure. First, 'signal' epochs of about 1 s were selected (more or less the entire MRCP length). These epochs contained the initial negative phase of an MRCP; more precisely, they started from the beginning of the negativity phase of the MRCP and finished shortly before its peak positivity in the movement period. Then, 'noise' epochs of 1 second (by protocol it corresponds to the whole *rest period*) were selected.
The aim of the optimization process was to find a set of channels that maximizes the 'signal' energy while minimizing the 'noise' energy, with the constraint that the sum of the coefficients was zero. Thus, signal-to-noise ratio was the function ($SNR(\mathbf{x})$, dependent on $\mathbf{x}$) to be maximised in the optimization process [Niazi et al., 2011]. The SNR is calculated as follows:

$$SNR = \frac{P_{signal}}{P_{noise}},$$

where P_{signal} and P_{noise} are respectively the powers of the signal and noise.
A quasi-Newton method was used for the optimization: from an initial guess, a series of steps were repeated iteratively until $\mathbf{x}$ converges to the solution. The initial vector of coefficients $\mathbf{x_0}$ was based on the EEG large Laplacian montage [Niazi et al., 2011].

2.4.1.5 Template extraction and detection of movement intention

The template was built on the descending phase of MRCP extracted from the training data of (a) the surrogate channel and (b) the virtual channel obtained with the Laplacian

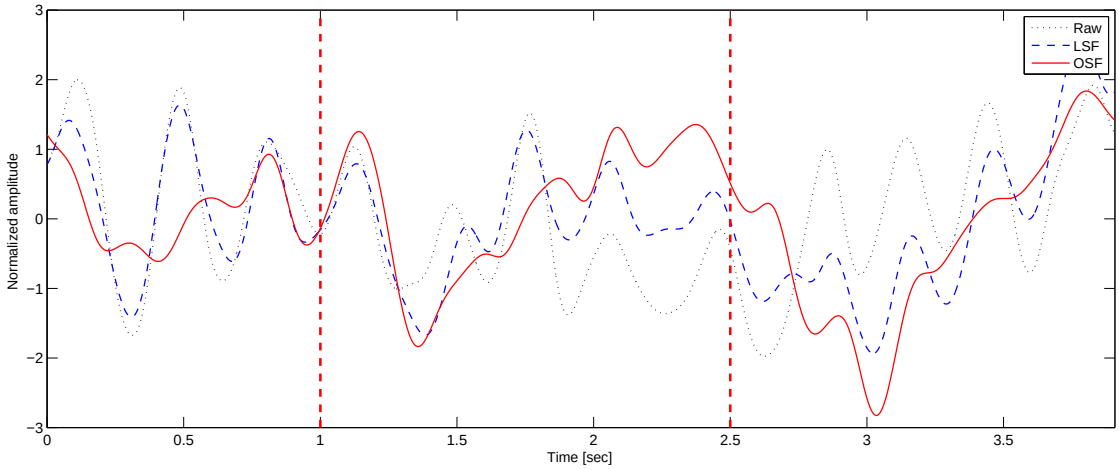

Figure 2.9: Normalized epoch traces (mean over all the epochs) for the 'up' movement with the left hand for the iEEG data for the raw signal and the two spacial filters outputs. More precisely: (a) normalized 'raw' signal (after bandpass filtering) acquired from the channel which was given weight 1 in the Laplacian filtering (coefficient $x_1 = 1$)('Raw',dotted line), (b) normalized output of the Laplacian filter ('LSF', dashed line), and (c) output of the Optimized Spacial Filter ('OSF',continuous line). The vertical dashed lines correspond to the 'visual cue' and the 'go signal' (see protocol in the Methods chapter 2).
The descending phase of the MRCP was used as template for the movement detection.

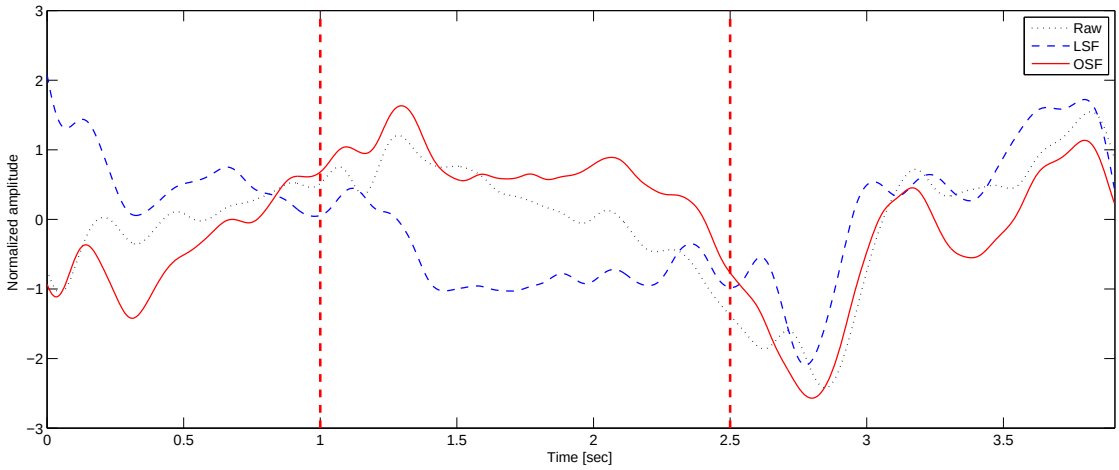

Figure 2.10: Normalized epoch traces (mean over all the epochs) for the 'up' movement with the left hand for the EEG data (subject no. 2) for the raw signal and the two spacial filters outputs. More precisely: (a) normalized 'raw' signal (after bandpass filtering) acquired from the channel which was given weight 1 in the Laplacian filtering (coefficient $x_1 = 1$)('Raw',dotted line), (b) normalized output of the Laplacian filter ('LSF', dashed line), and (c) output of the Optimized Spacial Filter ('OSF',continuous line). The vertical dashed lines correspond to the 'visual cue' and the 'go signal' (see protocol in the Methods chapter 2).
The descending phase of the MRCP was used as template for the movement detection.

filter, allowing later comparison between the two spacial filters. Then, through cross-validation (using leave-one-out technique) between template and testing signal epochs, a ROC curve was built, allowing to measure the true positive rate and false positive rate of the movement detection. The threshold of the cross-correlation was selected on the midpoint of the turning phase of the ROC in order to obtain a balance between number of correct detections and number of false positives.

Template extraction The template was obtained from the OSF and LSF outputs, performing an average over the epochs of the training set, and then extracting the MRCP portion of interest: from the initial of the depression phase till the negativity peak (see figure 2.11). The length of this template was in most cases of about or less than 1 second of signal, depending on subject, hand or movement in question.

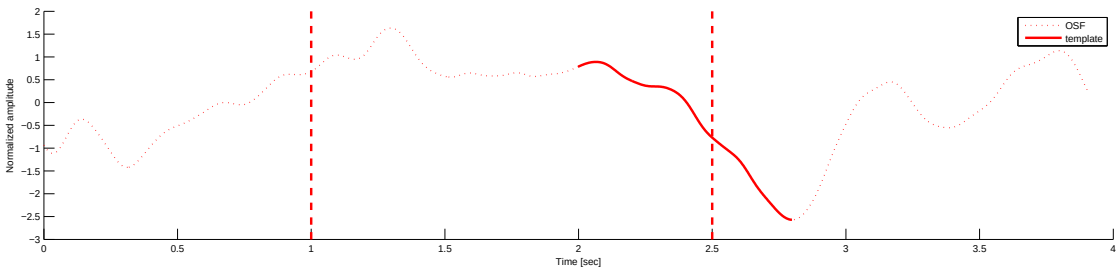

Figure 2.11: Example of template extracted from the training set (subject 2, left hand movement in the 'up' direction from scalp EEG data). The template corresponds to the descending phase of the MRCP (thick line).

2.4.1.6 Movement detection

For the movement detection, a leave-one-out cross-validation approach was used (more information about can be found in subsection 2.4.2.3 in the Methods chapter). The cross-correlation between the template (built on training data) and testing data was measured. After setting a certain threshold, the true and false positive rates can be calculated, and so on with different threshold values. This process ended with a receiver operating characteristic (ROC), which finally led to choose the "optimal" threshold as the one that allows to have the highest number of correct movement detections while having the lowest of incorrect detections; this translates in having the highest TPR while minimizing the FPR. In our analysis, we decided to identified our 'optimal' threshold as the one which provides the nearest value (Euclidean distance) in the ROC curve to $(TPR, FPR) = (100\%, 0\%)$. This value was in the well known midpoint of the turning phase of the ROC. By doing this, a balance between TPR and FPR can be obtained.
After selecting the "optimal" threshold, the corresponding TPR and FPR were extracted as results of the movement intention detection accuracy. The TPR and FPR were calculated as:

$$TPR = tp/(tp + fn), \quad FPR = fp/(fp + tn),$$

where tp, tn, fp, fn indicate the number of true positives, true negatives, false positives and false negatives, respectively.

- tp (true positive): a movement is detected in the 'signal' portion of the epoch ('preparation' + 'movement' phase in the protocol);
- tn (true negative): absence of movement is detected in the 'noise' portion of the epoch ('rest period' in the protocol description);
- fp (false positive): a movement is detected in the 'noise' portion of the epoch;
- fn (false negative): absence of movement is detected in the 'signal' portion of the epoch.

The "detection" corresponded to finding a cross-correlation value higher than the "optimal" threshold found in the previous step by means of the ROC plot.

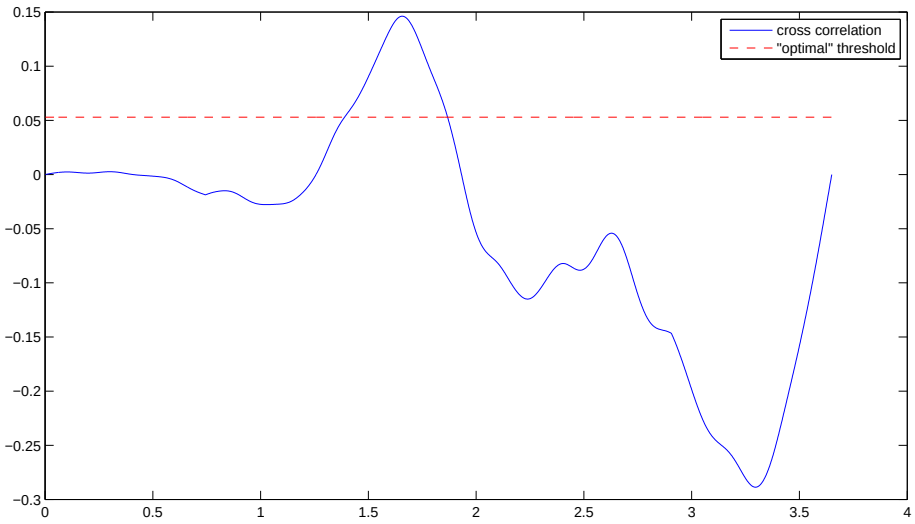

Figure 2.12: Example of cross correlation signal between template and the portion of the 'signl' portion of one epoch. The dotted red line shows the "optimal" threshold found with the above method. So, in this case, a true positive is identified.

Artificially generated noise By protocol, the 'rest' period (here referred also as 'noise' signal) lasted 1 second. This duration is almost three times shorter than the remaining part of the signal (2.9 sec) and it is nearly the same as the MRCP template, probably not enough to lead to a correct detection accuracy. In order to obtain a more realistic result, epochs of artificial noise of the same length of the rest of the epoch (2.9 sec) were generated.
This was done estimating an auto-regressive (AR) model of every 'noise' epoch and

using that instead of the 'real' noise. The order of the model was decided using the Akaike Final Prediction Error estimate (FPE). When the FPE does not improve a lot while increasing the order, it means that our model cannot be enhanced by incrementing its order. Using this criteria, with the provided set of data, the order was stopped at 15. The Burger's method, which has been proved to be a good method to estimate the parameters of an AR model, was used [De Hoon et al., 1996].
Since the model input is white noise, it estimates a slightly different output every time. The TPR and FPR were thus calculated as the mean over the values given by running the algorithm 10 times.

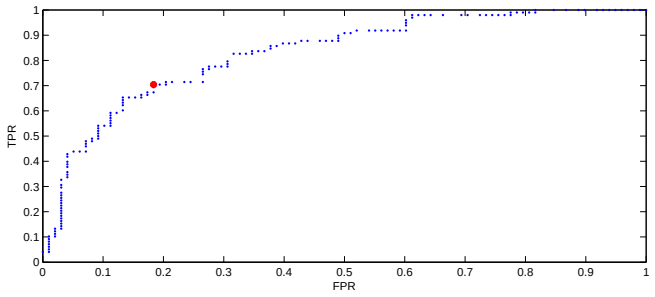

Figure 2.13: The figure show a ROC plot that measure the detection accuracy of right arm direction towards the right of subject no. 2 (scalp EEG data, artificially generated noise).

2.4.2 Movement direction classification

Following, you will find the different methods we used for the time-frequency analysis of iEEG and EEG data. The current chapter follows the order of our analysis (pre-processing, feature building, feature extraction and classification) and the methods are chronologically sorted within each section (see figure 2.14).

2.4.2.1 Feature extraction

After obtaining a clean signal, the first step was to set a process in order to extract features.

Time-frequency map A time-frequency (TF) map is a two dimensionnal graph of time against frequency. There are two main ways of computing a TF map: the windowed Fourier transform and the wavelet transform.
The **windowed Fourier transform** replaces the Fourier transform's sinusoidal wave by the product of a sinusoid and a window which is localized in time. It takes two arguments: time and frequency. The windowed Fourier transform has a constant time frequency resolution. This resolution can be can be changed by rescaling the window g. It is a complete, stable, redundant representation of the signal (see figure 2.15). Hence it is invertible. The redundancy implies the existence of a reproducing kernel. The time

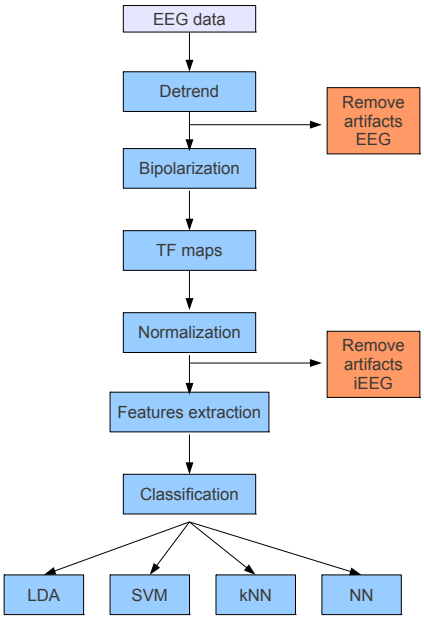

Figure 2.14: Plan of the data analysis process. On top, the raw EEG data from the acquisition system, then the different steps followed in order to perform the classification. (1) preprocessing: detrend and bipolarization, (2) feature building: time-frequency (TF) maps and normalization, (3) feature extraction, (4) classification with different methods: linear discriminant analysis (LDA), support vector machine (SVM), k-nearest neighbour (kNN), neural network (NN). The artifacts removing is done at different steps whether we are working with intracranial EEG (iEEG) or extracranial EEG (EEG).

and frequency spreads of these functions are constant. The family is generated by time and frequency translations of one atom [Chaplais, 1998].

The **wavelet transform** replaces the Fourier transform's sinusoidal waves by a family generated by translations and dilations of a window called a wavelet. It takes two arguments: time and scale. Its time spread is proportional to scale s, while its frequency spread is proportional to the inverse of s [Chaplais, 1998].
The main advantage of wavelet transforms is the variation of windows length. In order to isolate signal discontinuities, one would like to have some very short basis functions. At the same time, in order to obtain detailed frequency analysis, one would like to have some very long basis functions. A way to achieve this is to have short high-frequency basis functions and long low-frequency ones. This "happy medium" is exactly what we get with wavelet transforms (see figure 2.16) [Graps, 1995].
One thing to remember is that wavelet transforms do not have a single set of basis

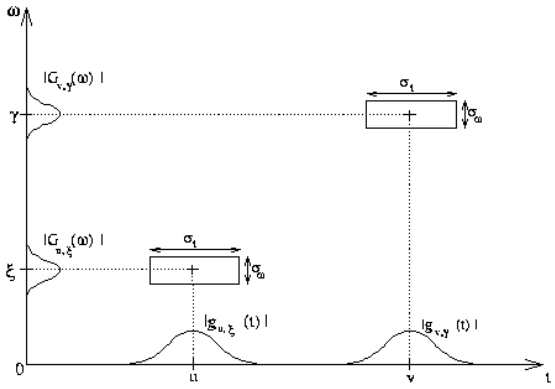

Figure 2.15: *Fourier* - The boxes show the localization of an atom in the time frequency space computed by the windowed Fourier transform. Notice the same resolution in all the space [Chaplais, 1998].

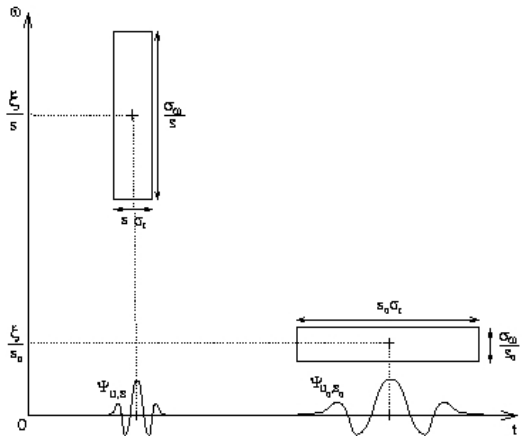

Figure 2.16: *Wavelet* - The boxes show the localization of an atom in the time frequency space computed by the wavelet transform. The time resolution is better when punctual changes occur in the signal (high frequencies) while the frequency resolution is better when the signal is stable in time (low frequencies) [Chaplais, 1998].

functions like the Fourier transform, which utilizes just the sine and cosine functions. Instead, wavelet transforms have an infinite set of possible basis functions. Thus wavelet analysis provides immediate access to information that can be obscured by other time-frequency methods such as Fourier analysis [Graps, 1995].
Because we are running an offline analysis trying to catch specific changes in the brain signals due to punctual stimuli, wavelet transform is the most appropriate method to use although it takes much more time to compute.

Baseline normalization Temporal evolution of the power of different frequencies is determined by a time-frequency analysis using the wavelet transform. To enhance the power modulation within a trial, the power spectra is normalized by different methods

using a baseline. The baseline is a period on which the subject is at rest. The baseline is computed for each sample in a time interval within the rest period (100-500 ms, 400-800 ms, 100-800 ms) [Rickert et al., 2005; Waldert et al., 2008]. Then, each frequency is normalized by the average value of the baseline for the same frequency, enabling to enhance low amplitudes and smooth high amplitudes so as to obtain homogeneous time frequency maps.
Here are the 4 methods mainly used to perform baseline normalization:

- (1)$TF - baseline$
- (2)$\frac{TF}{baseline}$
- (3)$\frac{TF-baseline}{baseline}$
- (4)$\frac{TF-baseline}{std_{baseline}}$

Where TF is the time-frequency and *std* is the standard deviation.

Choice of the features We now have a process to extract time-frequency features from the signal. However, we could choose an infinity of different features considering all the frequencies or all the time intervals. A way to restrict our analysis is to consult the BCI related literature:

iEEG Usual frequency bands are extensively referenced in the iEEG-related literature. Frequencies up to 200 Hz can be used for iEEG without getting too much noise ([Leuthardt et al., 2004]). In addition, we are working with a 1024 Hz sample frequency, which enables us to perform a frequency analysis up to 512 Hz without losing information (Shannon-Nyquist theorem).
Using multiple references ([Leuthardt et al., 2004; Rickert et al., 2005; Ball et al., 2009; Waldert et al., 2009; Jerbi et al., 2011]), and after discussions with Karim, we selected the following common frequency ranges for our first analysis: $2-4, 2-7, 4-7, 8-13, 6-30, 15-30, 30-130, 60-130, 60-160$ (Hz). The very low and very high bands (0-2 Hz, 160-200 Hz) are difficult to use due to the wavelet transform lack of resolution in extreme frequencies.
For each part of the task (0-1000 ms: rest, 1000-2500 ms: movement preparation, 2500-3900 ms: actual movement), all the time intervals could be considered.

EEG Usual frequency bands are extensively referenced in the EEG-related literature. One might be careful when using high frequencies due to a lot of perturbations caused by the extracranial EEG recordings. Usually, the maximal using frequency is around 90 Hz but recent references report the use of frequencies up to 150 Hz. Using multiple references ([Ball et al., 2008; Waldert et al., 2008, 2009; Jerbi et al., 2011]), and after discussions with Karim, we selected the following common frequency ranges for our first analysis: < 3 Hz, < 5 Hz, < 7 Hz, 2-4 Hz, 10-30 Hz, 15-30 Hz, 30-50 Hz, 60-85 Hz, 62-87 Hz, 50-128 Hz, 30-130 Hz. These two lasts are particularly high, but we would

like to take a look at the results they can provide.
For each part of the task (0-1000 ms: rest, 1000-2500 ms: movement preparation, 2500-3900 ms: actual movement), all the time intervals could be considered.

2.4.2.2 Classification

The chosen features were given as inputs to classification algorithms which try to find a link between the value of a feature and a task (e.g. movement preparation, movement of the right hand to the left, etc...).
Classification algorithms are used to identify 'patterns' of brain activity. Considering some features and a classification algorithm, the BCI tries to recognize different mental states in a given data set (e.g. hand movement). As a result, the performance of a pattern recognition system depended on both the features and the algorithm employed [Lotte et al., 2007].
Basically, given some features, a classifier was trained on an experimental data set so as to adjust a boundary between the classes by means of a classification algorithm. In our case we used supervised methods, meaning we had a prior knowledge on which sample belongs to which class and we used it to design the classifier [Duda et al., 2001].
Formally, classification consists in finding the true label $y*$ of a feature vector $\mathbf{x}$ using a mapping function f. This mapping is learnt from a training set T [Lotte et al., 2007].
A classifier can easily reach 100 % of good classification on a given set of data (e.g. by learning by heart which sample belongs to which class) and, at the same time, provide poor performance on a new data set. As a result, it is important to find a way to evaluate the classifier performance.
In this section, we will first briefly explain the different classification methods used in this project, then we will see how to choose the appropriate features and we will finally explain how to compare classifier performance.

k-nearest-neighbor The k-nearest-neighbor (kNN) rule is a supervised method for data classification. This method assumes no prior knowledge of the statistics of the data in question. kNN is also a 'lazy method', meaning there is very little training and the method does not try to generalize from the data.
Simply the k-nearest-neighbor rule classifies a sample by the majority of k nearest training samples around it, as shown on figure 2.17. K is often an odd number to ensure majority. The outcomes are strongly linked with the choice of k. A high k removes noise but decreases the accuracy of the boundaries [Duda et al., 2001].
The distance between samples can be calculated using different measures. The Euclidean distance formula is the most used:

$$D(\mathbf{a}, \mathbf{b}) = \left(\sum_{k=1}^{d} (a_k - b_k)^2 \right)^{\frac{1}{2}}$$

Where d is the dimensionality of $\mathbf{a}$ and $\mathbf{b}$.

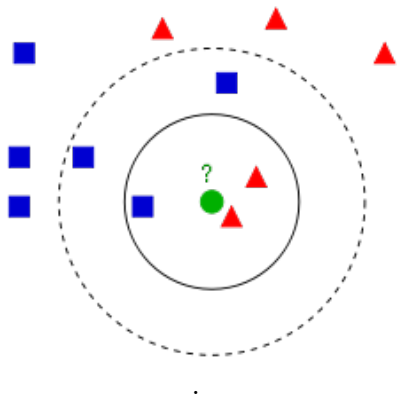

Figure 2.17: This plot shows the principle behind K-Nearest-Neighbor Rule. It is a two dimensional feature space. The blue squares represent class 1 and the red triangles represent class two. The green dot will be classified according to the nearest samples (image from Wikipedia)

Linear discriminant analysis Linear discriminant analysis (LDA) is a method used in statistics, pattern recognition and machine learning to find a linear combination of features which separates two or more classes of objects or events. Linear Discriminant Analysis (LDA) is characterized as a supervised and parametric method. LDA is performed under the hypothesis of multivariate normal distribution, different mean for each class, same conditional covariance matrix and same a priori probability for each class [Duda et al., 2001].
LDA is a very fast method but, depending on the underlying distribution of the samples, performances may decrease. When classes need to be classified, a decision boundary is needed. LDA looks for the linear combination of features which best describes the data, then it creates a decision boundary which is a hyperplane $g(\mathbf{x}) = 0$ (or multiple hyperplanes to solve a N-class problem with N>2) of the feature space.

$$g(\mathbf{x}) = \mathbf{w}^t \cdot \mathbf{x} + w_0,$$

where $\mathbf{x}$ is the input features vector, $\mathbf{w}$ is the weight vector, which determines the direction of the decision boundary, and w_0 is the bias, which determines the location of the decision boundary. In a two classes problem, each sample has to be assigned to either w_1 (class 1) or w_2 (class 2). To perform the classification of a sample $\mathbf{x}$, we are following the rule: if $g(\mathbf{x}) < 0$ then decide w_1, if $g(\mathbf{x}) > 0$ then decide w_2. On figure 2.18 all the training points are plotted and the best linear decision hyperplane separates the points [Duda et al., 2001].

Figure 2.18 shows the result of LDA through a set of data, it can be observed how LDA divides the two classes with a linear boundary.

Support vector machine Support Vector Machine (SVM) is very closely related to the Linear Discriminant Analysis and uses both k-nearest-neighbor rule and linear discriminant analysis classification [Press et al., 2007]. SVM aims to find one (or several)

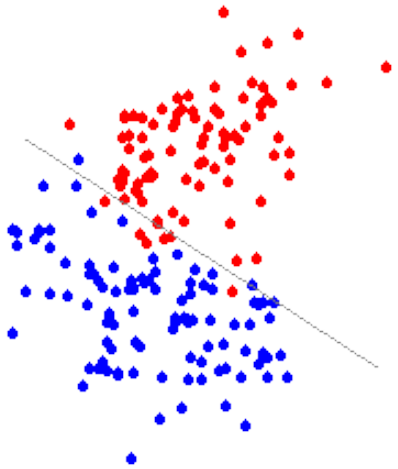

Figure 2.18: LDA performed in a two dimensional feature space. The red points and the blue circles belong to different classes, the straight line is the boundary computed by LDA [Mirkin, 2011]

separating hyperplane(s) between two or more classes. The difference is that Support Vector Machine finds the hyperplane with the largest margin between the classes. A larger margin between the classes should ensure a better generalization of the classifier. Furthermore support vector machine does not assume multivariate normal distribution of the features [Noble et al., 2004].
The best possible case of separation and generalization is illustrated in figure 2.19 by the red hyperplane labelled H_2 . The blue hyperplane labelled H_3 could be a result of a linear discriminant analysis and while it separates the classes well enough it is less generalizable than hyperplane calculated by the support vector machine, because it only separates the classes by a small margin [Duda et al., 2001].
SVM finds at least three support vectors (two from class 1 and one from class 2), which are the most difficult samples to classify. The hyperplane is then situated with equal distance to the support vectors. In fact, it is not realistic to expect the two classes to be completely separable, the terms soft margins are introduced to allow samples of one class to push trough the margin and into the area of the other class [Noble et al., 2004].

Neural network One other interesting method is the neural network (NN) based classification, since the architecture of neural networks is inspired by the brain. A neural network is made of several simple communication processors (called neurons) distributed in at least two layers. Usually, one neuron is connected to every other neuron of the following layer [Hudson and Cohen, 1999].
The inputs of the neural network will be the different features, and each output will be a class: depending on the output values, given an input, the sample will be classified. To perform the classification, the neural network is trained on a training data set [Hudson

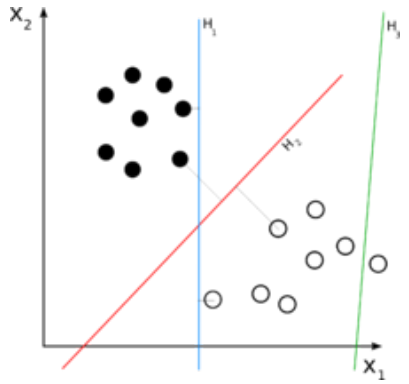

Figure 2.19: The hyperplanes H_1, H_2 and H_3 represent difference separation and generalizability. H_1 separates the classes but only with a small margin. H_2 is calculated by a support vector machine and it separates the classes by the maximum margin. H_3 does not separate the classes (image from Wikipedia).

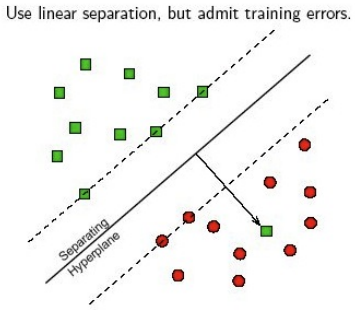

Figure 2.20: Two point clouds separated by a hyperplane. The hyperplane does not separate the classes cleanly. In this situation the margin are soft (image from *dtreg.com*).

and Cohen, 1999].
There are three characteristics which describe a neural network: the neuron model, the architecture and the training algorithm [Hudson and Cohen, 1999].

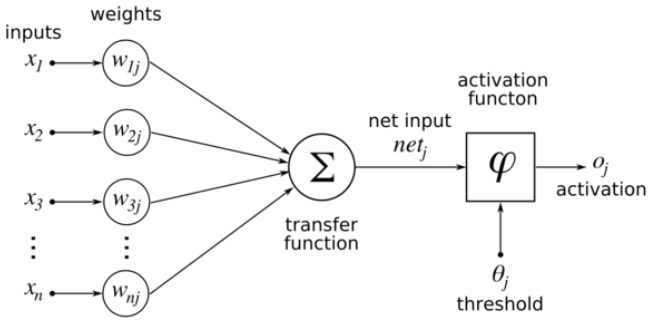

Figure 2.21: Description of a neuron using a NN (image from Wikipedia)

Neuron model As showed in figure 2.21, each input are first weighted. Then all the weighted inputs are summed by the so-called transfer function. Finally, the activation function will provide a final single output. The activation function ϕ can be very different from a neural network to another: we can either use a threshold to provide a binary output (e.g. if $net > \theta$ then the output is 1, otherwise it is 0) or also more complex continuous functions [Hudson and Cohen, 1999].

Architecture For supervised neural network, at least three layers are usually used. A three-layer neural network is enough to solve all the problems if the activation function is not linear (e.g. figure 2.22, notice that the layers between the input and output layers are called hidden layers) [Hudson and Cohen, 1999].

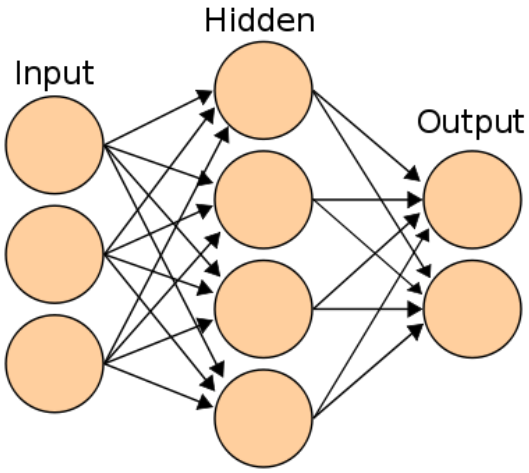

Figure 2.22: Architecture of a neural network (image from Wikipedia)

However, more than three layers can be used: this basically enables a more adaptive neural network with greater processing power but at the cost of more complex training algorithm [Hudson and Cohen, 1999].
We will use a feed forward neural network with three layers. As illustrated on 2.22: there is no feedback from one layer to a previous layer. Each input represents a dimension of the features vector and each output represents a dimension of the class vector [Hudson and Cohen, 1999].

Training algorithm As we have prior knowledge of the actual classes the samples from the training data set belong to, we use a widespread supervised training method called back-propagation [Hudson and Cohen, 1999].
When there is a mistake in the outputs, the difference between the expected outputs and the actual outputs is computed. This difference is called error. The error is then propagated backwards through the hidden layers. The output of each neuron is multiplied by the error, so as to get the gradient of the weight. For each neuron the weight is

increased according to a given learning rate, if the gradient is negative, and vice versa [Hudson and Cohen, 1999].

Choice of classifiers KNN algorithms are not very popular in the BCI community, probably because they are known to be very sensitive depending on the dimensionality, which can make it easily fail. However, when used in BCI systems with low dimensional feature vectors, kNN may prove to be efficient [Lotte et al., 2007].
Due to its quick computation and good performance, LDA is particularly well suited for online classification (e.g. P300 speller) or multiclass analysis [Lotte et al., 2007]. In addition, many references across the literature perform LDA for the classification of hand movement using EEG signals [Rickert et al., 2005; Mehring et al., 2004].
The review wrote by Lotte et al. helped us to make our choice of investigated classifier. We can see from table 2.23 that LDA, RFLDA, SVM, KNN and Perceptrons provide good results in different studies. However, the RFLDA is only useful if the sample size is small compared with the size of feature vector [Dai and Yuen, 2003], which is not our case. It should also be remarked that perceptron does not actually refer to the historical perceptron, but to the pattern recognition feedforward neural networks.

Protocol	Preprocessing	Features	Classification	Accuracy (%)	References
Finger: on BCI competition 2003 data set IV	CSSD	ERD and Bereitschaftspotential based features	Perceptron	84	[48]
	14–26 Hz band pass + CSP	Activity in two brain regions with sLORETA	Perceptron	83	[18]
	bandpass	PCA+CSP+OLS	SVM	90	[77]
Speech muscles	0.5–15 Hz band pass	Raw EEG	MLP	100	[43]
Finger/toe		Raw EEG	TDNN	<90	[57]
			GDNN	≃90	
Finger: on different data sets	0–5 Hz band pass	Amplitude values of smoothed EEG	kNN	78.4	[38]
			Linear SVM	96.8	
			RFLDA	96.7	
			LDA	96.3	
		Amplitude values of smoothed EEG	Gaussian SVM	93.3	[39]
			Linear SVM	92.6	
			RFLDA	93.7	
			LDA	90.7	
			kNN	78	
		BP	Voting with LVQ NN	≃85	[54]
Finger: in asynchronous mode	1–4 Hz band pass	Bi-scale wavelet features	1-NN	up to 81	[76]
	1–4 Hz band pass + PCA	Normalized bi-scale wavelet features		97	[67]

Figure 2.23: Accuracy of classifiers in movement intention based BCI [Lotte et al., 2007].

2.4.2.3 Evaluation of classifier performance

To perform a classification the first step is to train the classifier using a training data set. The next step is to test the classifier and answer the question: *how well does the classifier perform on other data than the training data?*

Cross-validation The best choice would be to separate the total amount of data into a training data set and a test data set, so the training data would never be used to test the classifier. Unfortunately, two sets are often expensive and time-consuming to generate because it requires extensive amount of data. The limited amount of data makes it necessary to apply a method that reuses the training data [Hawkins, 2004]. The method applied in this study is the leave-one-out cross validation.
The leave-one-out-method trains the classifier on the entire episode set except one episode. The one episode left-out is then used to test how well the classifier can predict which class this episode belongs to. It iterates this operation for every episode then provides a final confusion matrix [Duda et al., 2001].
A good result given by the cross-validation method ensures that there is no over-fitting of the classifier [Hawkins, 2004]. This result has to be compared to the level of chance (for example 33 % for 3 classes).

Decoding information, decoding accuracy, decoding power Specific measurements of classifier performance are found in the BCI related literature. Three of them are used in different publications closely linked to our work.
The decoding accuracy (DA) (also called decoding power (DP), [Rickert et al., 2005]) is defined as the percentage of correctly decoded trials [Waldert et al., 2009; Mehring et al., 2004] (given in our case by cross-validation), while the decoding information (DI) quantifies the amount of information extracted about movement direction [Waldert et al., 2009].

$$DA = DP = \frac{N_c}{N},$$

where N_c is the number of correct classification given by cross-validation and N is the total number of samples.
Under the assumptions of equal probabilities for correct predictions for each direction and equal distributions of false predictions across directions, we can use the following formula which relates the DI to the DA:

$$DI(DA) = \frac{DA}{100} \ln \frac{DA}{DA_{chance}} + \frac{100 - DA}{100} \ln \frac{100 - DA}{100 - DA_{chance}},$$

where DA_{chance} is the level of the chance (e.g. 25 (%) for 4 classes) [Waldert et al., 2008].
The DI enables to directly compare the decoding performance of studies using different number of classes.

2.4.2.4 iEEG analysis

From a practical point of view, we do not have sufficient data storage capacity to save a TF map for each trial, each channel and each event. The first solution, which would have been to reduce the frequency resolution, presents two main issues. First, without saving each frequency bin independently we can not apply normalization any more; or we have to directly save the normalized data, which limits our analysis. Secondly, although the frequency resolution is not important in the high frequencies, it is in the low frequencies. Together with Karim, we decided to keep all the frequency bins but save our data on the given time windows: 100-500 ms, 400-800 ms, 100-800 ms for the rest, 1000-1400 ms, 1000-2300 ms, 2000-2500 ms for the preparation, 2500-3000 ms, 2700-3700 ms, 3200-3700 ms for the movement.
To select the channels on which we ran a more detailed analysis (influence of normalization, 2 features, etc.), we made the following hypothesis: if a good DA is found for a couple channel-task on a large time window, the DA can be improved by choosing other close time windows, other frequency bands or a multiple features approach, for the same couple channel-task. On the contrary, a good DA on a narrow time-window will not necessarily lead to a better DA on a wider one. As a result, our first analysis is performed on the widest time-windows. Further analysis was performed on the 3 channels which provide the best DA for each couple channel-task during the first analysis. Another approach would have been to fix a threshold for each couple channel-task, and select all the channels for which the DA is above this threshold. However, doing this, the best classifiers of the first analysis will keep more electrodes than the others, giving them more chance of achieving a high DA after other analysis. With the purpose of classifier comparison in mind, this method would have created a bias.

2.4.2.5 EEG analysis

In order to perform EEG analysis, we used the conclusions from iEEG analysis, which can be found in *Discussion*. We therefore performed a single channel one feature classification on the widest time windows with a *subtraction then division by the baseline* normalization. Due to computation time issues, we did not investigate SVM and NN.

Chapter 3

Results

Time and time frequency results are successively displayed in this chapter.

3.1 Movement intention detection

In general, the results demonstrated that it is possible to detect voluntary movement intentions using the descending phase of the MRCPs. The TPR (true positive rate) is always above 70 % (OSF data) and often above 75 %, which roughly means that we are able to detect correctly three intended movement out of four. Most of the FPRs (false positive rate) are, instead, around 25 % . Considering the complexity of the task the subject had to perform, and the amount of 'noise signal' available, we can consider these results as rather satisfactory.

The following tables present the TPRs (%) and FPRs (%) for the datasets already described in 'Methods'. They point out the detection performances on (a) the particular movement performed by each subject (e.g. 'down' movement with the right hand for subject no. 3), and (b) the movement data performed by the left hand and the right hand joined together. An average over the different movements for every subject can also be evaluated easily (Tables 3.1, 3.2, 3.5, 3.6 and 3.3, 3.4 3.7, 3.8, respectively).
The data used for the detection comprises iEEG and EEG data (Tables from 3.1 to 3.4 and from 3.5 to 3.9, respectively). For both iEEG and scalp EEG, the detection accuracy has been calculated for two data sets: the first provided by the recordings, and the second by the ones which use estimated 'noise signals' based on the 'real' noise signals (corresponding to the first second of the recorded epochs). In the latter case, an average of the TPRs and FPRs has been measured over the values given running the algorithm 10 times. The standard deviation of the mentioned average is not reported in the tables to avoid confusion and because it was always lower than 5 %. As expected, using only the rest period (see protocol) as 'noise signal' provided greater performances, but we can expect that the results obtained using estimated noise to be more realistic.
A comparison between the performance of the two spatial filters is highlighted in the tables as well, finding no relevant improvement using the OSF. In particular, Table 3.9

shows the detection accuracy for the two filter, averaging TPRs and FPRs over all the movements and all the subjects.
Finally, Table 3.10 shows the mean over the five subjects for the six tasks used during scalp EEG recordings (using estimated noise).

Since the legend is common for every table, it will be listed here:

- OSF Optimized Spatial Filter
- LSF Laplacian Spatial Filter
- LH Left Hand movement
- RH Right Hand movement
- _u movement towards 'up' direction
- _d movement towards 'down' direction
- _l movement towards 'left' direction
- _r movement towards 'right' direction

Mov.	OSF - TPR (%)	LSF - TPR (%)
LH_u	84.0	80.0
LH_r	90.0	82.0
LH_d	96.0	82.0
LH_l	90.0	72.0
RH_u	80.0	70.0
RH_r	94.0	80.0
RH_d	86.0	74.0
RH_l	80.0	88.0
sd	6.0	6.0
Mean	**87.5**	**78.5**

Mov.	OSF - FPR (%)	LSF - FPR (%)
LH_u	18.0	20.0
LH_r	12.0	24.0
LH_d	30.0	26.0
LH_l	12.0	10.0
RH_u	18.0	32.0
RH_r	18.0	24.0
RH_d	32.0	38.0
RH_l	20.0	32.0
sd	7.4	8.6
Mean	**20.0**	**25.8**

Table 3.1: The table shows the detection accuracy for the iEEG data for the particular movement task performed by the subject.

Mov.	**OSF - TPR (%)**	**LSF - TPR (%)**
LH_u	79.9	70.1
LH_r	79.6	74.1
LH_d	71.4	81.5
LH_l	81.5	69.9
RH_u	72.7	78.0
RH_r	73.4	75.3
RH_d	68.3	72.4
RH_l	75.0	77.9
sd	4.7	4.1
Mean	**75.2**	**74.9**

Mov.	**OSF - FPR (%)**	**LSF - FPR (%)**
LH_u	26.7	38.9
LH_r	34.7	42.2
LH_d	34.4	36.7
LH_l	29.3	32.8
RH_u	34.8	45.6
RH_r	35.0	38.2
RH_d	52.5	43.6
RH_l	31.4	41.1
sd	7.8	4.1
Mean	**34.9**	**39.9**

Table 3.2: The table shows the detection accuracy for the iEEG data for the particular movement task performed by the subject, using estimated noise signal for the analysis.

Mov.	OSF - TPR (%)	LSF - TPR (%)
LH	81.5	84.5
RH	83.0	83.0
sd	1.1	1.1
Mean	**82.3**	**83.8**

Mov.	OSF - FPR (%)	LSF - FPR (%)
LH	14.5	23.5
RH	20.5	27.0
sd	4.2	2.5
Mean	**17.5**	**25.3**

Table 3.3: The table shows the detection accuracy for the iEEG data, for the joined movement tasks performed by the subject, for both hands.

Mov.	OSF - TPR (%)	LSF - TPR (%)
LH	75.2	77.9
RH	78.7	80.3
sd	2.5	1.7
Mean	**77.0**	**79.1**

Mov.	OSF - FPR (%)	LSF - FPR (%)
LH	31.9	32.0
RH	35.2	34.3
sd	2.3	1.6
Mean	**33.6**	**33.2**

Table 3.4: The table shows the detection accuracy for the iEEG data, for the joined movement tasks performed by the subject, for both hands, using estimated noise in analysis.

	OSF - TPR (%)					LSF - TPR (%)				
Mov.	**sub1**	**sub2**	**sub3**	**sub4**	**sub5**	**sub1**	**sub2**	**sub3**	**sub4**	**sub5**
LH_u	66.3	60.0	76.6	57.1	71.7	70.4	64.7	64.9	66.3	71.7
LH_d	83.4	79.3	61.3	77.9	77.3	63.6	70.1	54.8	72.6	75.3
RH_u	70.4	87.8	69.0	75.2	81.0	68.4	79.6	75.0	65.0	66.0
RH_r	69.0	72.4	72.2	84.0	91.2	75.0	78.6	58.8	69.0	84.3
RH_d	63.3	78.8	75.3	65.0	86.5	79.6	88.9	69.1	65.0	64.4
RH_l	69.4	81.2	85.7	82.0	78.8	80.6	68.7	65.3	64.0	73.1
sd	6.9	9.5	8.2	10.4	6.9	6.7	8.9	7.2	3.3	7.2
Mean	**70.3**	**76.6**	**73.4**	**73.5**	**81.1**	**72.9**	**75.1**	**64.7**	**67.0**	**72.5**
	OSF - FPR (%)					**LSF - FPR (%)**				
Mov.	**sub1**	**sub2**	**sub3**	**sub4**	**sub5**	**sub1**	**sub2**	**sub3**	**sub4**	**sub5**
LH_u	45.9	31.8	45.7	27.6	44.6	45.9	36.5	40.4	36.7	29.3
LH_d	21.2	44.8	35.4	42.1	26.8	33.3	51.7	37.6	35.8	39.1
RH_u	17.3	25.5	24.0	30.9	21.0	27.6	34.7	50.0	25.8	38.0
RH_r	27.0	27.6	26.8	27.0	3.9	31.0	35.7	21.6	34.0	17.6
RH_d	33.7	20.2	29.9	36.0	19.2	19.4	39.4	27.8	27.0	50.0
RH_l	48.0	36.4	32.7	26.0	22.1	21.4	25.2	18.3	23.0	52.9
sd	11.3	9.3	8.6	6.3	14.7	9.6	7.0	11.1	5.1	12.1
Mean	**32.2**	**31.1**	**32.4**	**31.6**	**22.9**	**29.8**	**37.2**	**32.6**	**30.4**	**37.8**

Table 3.5: The table shows the detection accuracy for the scalp EEG data for the particular movement task performed by the subject.

	OSF - TPR (%)					LSF - TPR (%)				
Mov.	**sub1**	**sub2**	**sub3**	**sub4**	**sub5**	**sub1**	**sub2**	**sub3**	**sub4**	**sub5**
LH_u	70.0	62.0	73.7	65.3	65.7	73.8	62.6	65.1	58.1	69.3
LH_d	80.9	84.8	72.8	70.6	69.6	56.4	84.0	57.7	66.1	63.7
RH_u	76.7	78.0	69.7	69.8	75.9	68.8	79.0	76.7	63.6	58.3
RH_r	81.4	77.1	80.7	69.2	86.1	80.0	78.3	66.5	69.3	77.2
RH_d	57.7	77.0	70.0	78.5	78.8	68.6	85.1	64.1	64.4	64.6
RH_l	61.2	64.7	60.7	69.0	72.0	73.2	74.6	60.5	64.6	66.0
sd	10.1	8.7	6.5	4.4	7.2	7.9	8.2	6.5	3.7	6.3
Mean	**71.3**	**73.9**	**71.3**	**70.4**	**74.7**	**70.1**	**77.3**	**65.1**	**64.4**	**66.5**

	OSF - FPR (%)					LSF - FPR (%)				
Mov.	**sub1**	**sub2**	**sub3**	**sub4**	**sub5**	**sub1**	**sub2**	**sub3**	**sub4**	**sub5**
LH_u	40.1	20.2	32.2	28.7	19.7	19.8	18.8	17.1	16.9	23.6
LH_d	30.0	19.3	27.8	33.4	22.2	23.3	29.4	32.7	30.8	28.2
RH_u	19.4	22.2	16.9	21.6	21.5	18.0	25.3	25.1	22.5	21.8
RH_r	26.5	22.1	25.6	25.9	17.5	15.3	23.1	24.0	22.5	21.5
RH_d	20.4	18.3	23.3	23.3	17.2	19.8	25.1	24.7	19.5	29.9
RH_l	31.9	29.6	22.4	25.1	25.0	24.2	25.0	25.6	24.8	32.4
sd	7.7	4.1	5.2	4.2	3.0	3.3	3.5	5.0	4.8	4.6
Mean	**28.1**	**22.0**	**24.7**	**26.3**	**20.5**	**20.1**	**24.5**	**24.9**	**22.8**	**26.2**

Table 3.6: The table shows the detection accuracy for the scalp EEG data for the particular movement task performed by the subject, using estimated noise signal for the analysis.

	OSF - TPR (%)					LSF - TPR (%)				
Mov.	**sub 1**	**sub 2**	**sub3**	**sub4**	**sub5**	**sub 1**	**sub 2**	**sub3**	**sub4**	**sub5**
LH	74.5	87.8	70.0	84.0	81.0	69.4	79.6	78.0	69.0	66.0
RH	75.0	72.4	72.1	75.3	91.2	80.0	78.6	58.8	64.9	84.3
sd	0.4	10.9	1.5	6.2	7.2	7.5	0.7	13.6	2.9	12.9
Mean	**74.8**	**80.1**	**71.1**	**79.7**	**86.1**	**74.7**	**79.1**	**68.4**	**67.0**	**75.2**
	OSF - FPR (%)					**LSF - FPR (%)**				
Mov.	**sub 1**	**sub 2**	**sub3**	**sub4**	**sub5**	**sub 1**	**sub 2**	**sub3**	**sub4**	**sub5**
LH	24.5	25.5	23.0	27.0	21.0	23.5	34.7	51.0	34.0	38.0
RH	35.0	27.6	27.8	30.1	3.9	35.0	35.7	21.6	25.8	17.6
sd	7.4	1.5	3.4	2.2	12.1	8.1	0.7	20.8	5.8	14.4
Mean	**29.8**	**26.6**	**25.4**	**28.6**	**12.5**	**29.3**	**35.2**	**36.3**	**29.9**	**27.8**

Table 3.7: The table shows the detection accuracy for the iEEG data, for the joined movement tasks performed by the subject, for both hands.

	OSF - TPR (%)					LSF - TPR (%)				
Mov.	**sub 1**	**sub 2**	**sub3**	**sub4**	**sub5**	**sub 1**	**sub 2**	**sub3**	**sub4**	**sub5**
LH	80.8	76.7	67.3	69.8	76.4	69.4	81.0	76.0	63.9	58.5
RH	74.4	76.2	80.1	72.4	85.1	82.7	78.0	66.3	69.1	76.4
sd	4.5	0.4	9.1	1.8	6.2	9.4	2.1	6.9	3.7	12.7
Mean	**77.6**	**76.5**	**73.7**	**71.1**	**80.8**	**76.1**	**79.5**	**71.2**	**66.5**	**67.5**
	OSF - FPR (%)					**LSF - FPR (%)**				
Mov.	**sub 1**	**sub 2**	**sub3**	**sub4**	**sub5**	**sub 1**	**sub 2**	**sub3**	**sub4**	**sub5**
LH	29.8	23.2	16.8	24.3	24.3	24.2	28.1	25.5	22.3	20.4
RH	25.8	19.8	26.3	29.1	19.5	19.7	21.5	26.6	22.4	20.1
sd	2.8	2.4	6.7	3.4	3.4	3.2	4.7	0.8	0.1	0.2
Mean	**27.8**	**21.5**	**21.6**	**26.7**	**21.9**	**22.0**	**24.8**	**26.1**	**22.4**	**20.3**

Table 3.8: The table shows the detection accuracy for the iEEG data, for the joined movement tasks performed by the subject, for both hands, using estimated noise in analysis.

TPR (%)		FPR (%)	
OSF	**LSF**	**OSF**	**LSF**
72.3	69.7	24.3	23.2

Table 3.9: Mean over all the movement tasks and all the subjects, for the same spatial filter (estimated noise data)

	TPR (%)		FPR (%)	
Mov.	**OSF**	**LSF**	**OSF**	**LSF**
LH_u	67.3	65.8	28.2	19.2
LH_d	75.7	65.6	26.5	28.9
RH_u	74.0	69.3	20.3	22.5
RH_r	78.9	74.3	23.5	21.3
RH_d	72.4	69.4	20.5	23.8
RH_l	65.5	67.8	26.8	26.4

Table 3.10: The table shows the mean over the five subjects of the everyone of the six tasks performed during scalp EEG recordings (estimated noise data).

3.2 Movement direction classification

In this part, we will follow the order of *Methods* to display the results the time frequency analysis. A more deep analysis has been performed on iEEG signals because we got the iEEG data quite quickly. The conclusions (see *Discussion*) of this first iEEG analysis have been used to set up the EEG analysis.

3.2.1 iEEG data

3.2.1.1 Preprocessing and feature extraction

Bipolarization By bipolarization, we are keeping 91 channels out of 128. The isolated recording sites (e.g. n9 if there is neither n8, nor n10) are removed.

Time-frequency maps Time-frequency (TF) maps have been plotted using wavelet transform. Figure 3.1 shows a classic TF map. In order to find the artifacts, we plotted TF map for each channel across all the events and all the trials (e.g. figure 3.2). We listed the channels on which we found artifacts and we removed them for further analysis.

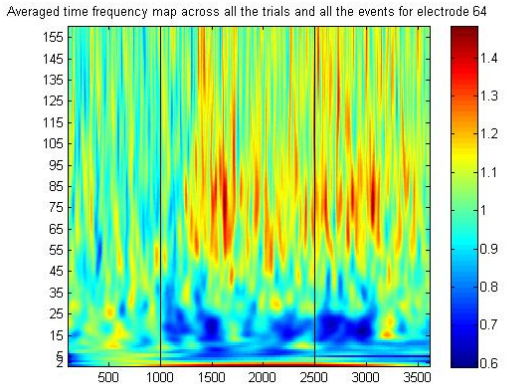

Figure 3.1: TF map for channel f10-f9, across all the event and all the samples. The vertical black lines show respectively (1) the visual cue, (2) the go signal. The effect of wavelet transform in high frequencies (stretching) and low frequencies (crushing) are noticeable. We also notice an increase of power in the high frequencies during the preparation and the movement, while the power of the intermediate frequency band decrease. The power of the very low frequencies is particularly high during the movement preparation.

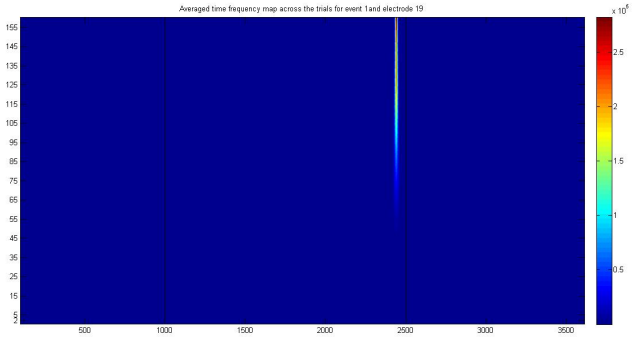

Figure 3.2: Example of a synchrone high amplitude artifact around 2450 ms in the time frequency (TF) map. This artifact is found on channels number 18 and 19 (i5-i4 and i6-i5), which have been employed to send information about the experiment so as to synchronize the data.

3.2.1.2 Classification analysis

Pattern recognition methods are optimized by trial and error. We have 91 bipolarized channels so far, and we could run an analysis on all the possible time windows and frequency ranges, which would take both too much time and too much memory. Our main goal with this first analysis is to aim the channels which provide the best results for each classification method. Beside that, a secondary goal is to provide a first comparison of the different classifiers and their parameters (e.g. k in kNN).
As explained in section 2.4.2.1, the analysis is ran on the frequency ranges: $2-4, 2-7, 4-7, 8-13, 6-30, 15-30, 30-130, 60-130, 60-160$ (Hz).
For each part of the task (0-1000 ms: rest, 1000-2500 ms: movement preparation, 2500-

3900 ms: actual movement) we chose a wide time-window (see section 3.2.1.6) and we avoided the edges to not consider the wavelet-transform artifacts: 100-800 ms: rest, 1000-2300 ms: preparation (2300 ms instead of 2500 ms to avoid the effect of anticipation of the *go signal*), 2700-3200 ms: execution (2700 ms instead of 2500 ms to catch the actual movement execution, which begins on average 200 ms after the *go signal*).
Figure 3.5 displays the DAs found with Neural Network method. Due to long computation time, an extensive analysis closed to what we have done with LDA, SVM and kNN was impossible (more than 10 days of computation). As a result, we decided to test the NN on the best features of both LDA and kNN. E.g. the best feature for rest vs. movement with LDA is 60-130 Hz on channel v14-v13, as a result, we tested the neural network on 60-130 Hz on v14-v13 for the classification rest vs. movement.
A summary of the analysis is displayed in figures 3.6 and 3.7. TF maps of some representative channels which yield to good DAs are displayed in figures 3.8, 3.9 and 3.10.
Because the kNN results are very similar depending on k, we will keep $k = 3$ (which seems to provide the best results globally) and $k = 5$ (which is interesting because more robust to the noise) for further analysis.

	LDA			SVM		
	DA	*chan.*	*freq.*	*DA*	*chan.*	*freq.*
RM	82.25	60-130	v14-v13	86	2-7	i2-i1
RP	81.5	6-30	b2-b1	86.25	2-7	v14-v13
LRM	67	60-160	u2-u1	67	60-160	u2-u1
LRP	64	60-130	v3-v2	63	60-130	v3-v2
UDM	66	60-160	g13-g12	65	60-160	g13-g12
UDP	64	8-13	u2-u1	63	2-4	x14-x13
4M	36	15-30	o10-o9			
4P	35	30-130	x14-x13			

Figure 3.3: For LDA and SVM, for each comparison, the best decoding accuracy (DA) found across the cchannels and across the frequency bands is displayed. In lines, RM: rest vs. movement, RP: rest vs. preparation, LRM: left vs. right during the movement, LRP: left vs. right during the preparation, UDM: up vs. down during the movement, UDP: up vs. down during the preparation, 4M: classification of the 4 directions during the movement, 4P: classification of the 4 directions during the preparation. Good DA yielded by channels with artifacts are not displayed (see figure 3.2)

	kNN, k=3			kNN, k=5		
	DA	*chan.*	*freq.*	*DA*	*chan.*	*freq.*
RM	99.5	60-130	x13-x12	99	15-30	g14-g13
RP	99.75	2-7	k11-k10	98.75	30-130	m11-m10
LRM	78	8-13	f3-f2	78	8-13	f3-f2
LRP	71	2-7	e8-e7	69	60-160	o9-o8
UDM	73	15-30	q7-q6	66	60-130	v2-v1
UDP	68	2-4	e6-e5	71	4-7	o2-o1
4M	37	60-130	f9-f8	40.5	15-30	o9-o8
4P	40	2-7	q8-q7	36.5	2-7	e8-e7

Figure 3.4: For kNN (k=3 ands k=5), for each comparison, the best decoding accuracy (DA) found across the channels and across the frequency bands is displayed. In lines, RM: rest vs. movement, RP: rest vs. preparation, LRM: left vs. right during the movement, LRP: left vs. right during the preparation, UDM: up vs. down during the movement, UDP: up vs. down during the preparation, 4M: classification of the 4 directions during the movement, 4P: classification of the 4 directions during the preparation. Good DA yielded by channels with artifacts are not displayed (see figure 3.2)

	NN-LDA	NN-kNN
RM	95.7	95.7
RP	95.2	94
LRM	55	50
LRP	59	44
UDM	50	50
UDP	50	41

Figure 3.5: In NN-LDA column, the DA found by using the best couples channel-frequency found with LDA method for each task is displayed. In NN-kNN column, the DA found by using the best couples channel-frequency found with kNN (k=3) method for each task is displayed. In lines, RM: rest vs. movement, RP: rest vs. preparation, LRM: left vs. right during the movement, LRP: left vs. right during the preparation, UDM: up vs. down during the movement, UDP: up vs. down during the preparation. Good DA yielded by channels with artifacts are not displayed (see figure 3.2)

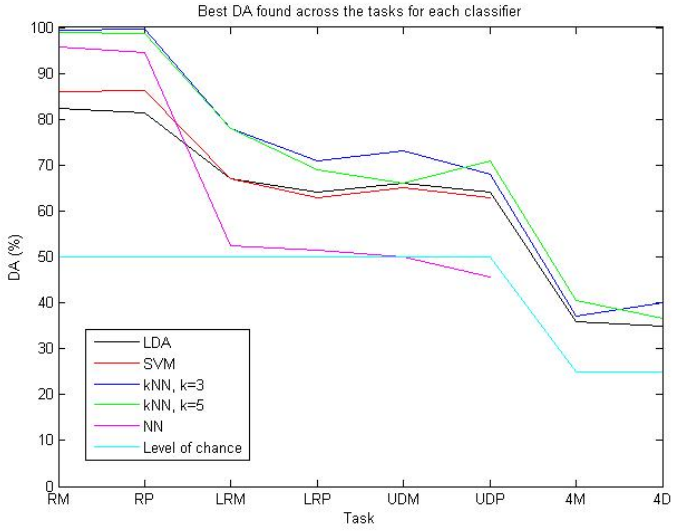

Figure 3.6: Display the best DA found for each task and each classifier. LRM: left vs. right during the movement, LRP: left vs. right during the preparation, UDM: up vs. down during the movement, UDP: up vs. down during the preparation, 4M: classification of the 4 directions during the movement, 4P: classification of the 4 directions during the preparation. In order to plot the NN, we averaged the results found for NN-LDA and NN-kNN (see figure 3.5)

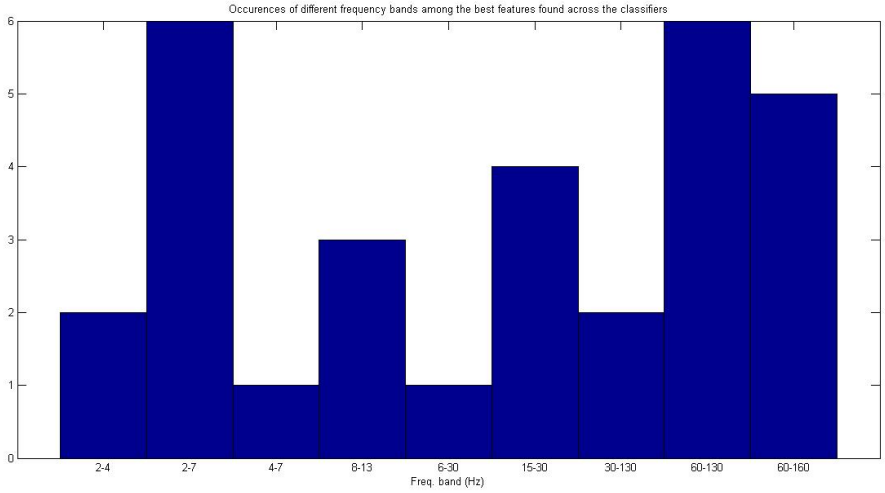

Figure 3.7: Display the number of occurrences of each frequency band among the best features found across the classifiers.

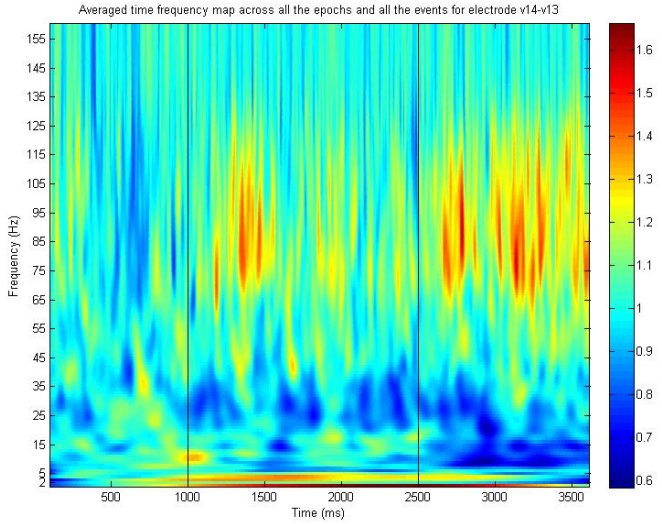

Figure 3.8: Averaged time frequency map across all the events and all the epochs for channel v14-v13. We notice an increase of power in high and low frequencies during the preparation and the actual movement. This channel yields to 82.25 % of correct classification of rest vs. movement on 60-130 with LDA and 86.25 % of correct classification of rest vs. preparation on 2-7 with SVM.

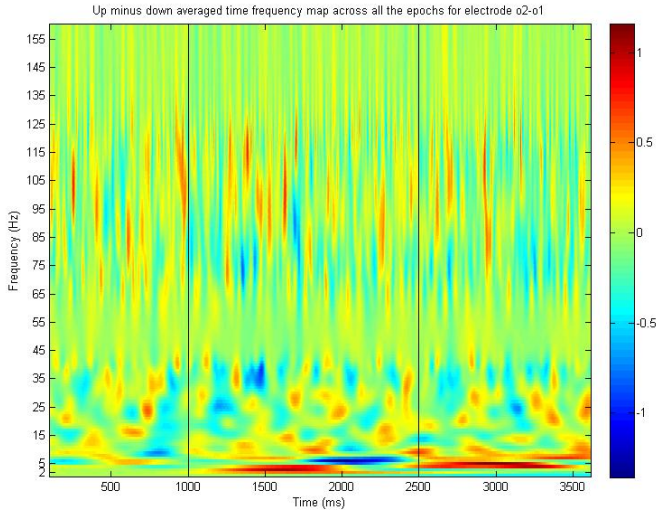

Figure 3.9: Up minus down averaged time frequency map across all the epochs for channel o2-o1. We notice an increase of power in 2-5 with a decrease of power in 5-8 during the preparation and an increase of power in 3-7 during the movement. This channel yields to 71 % of correct classification of up vs. down during the preparation on 4-7 with kNN, k=5.

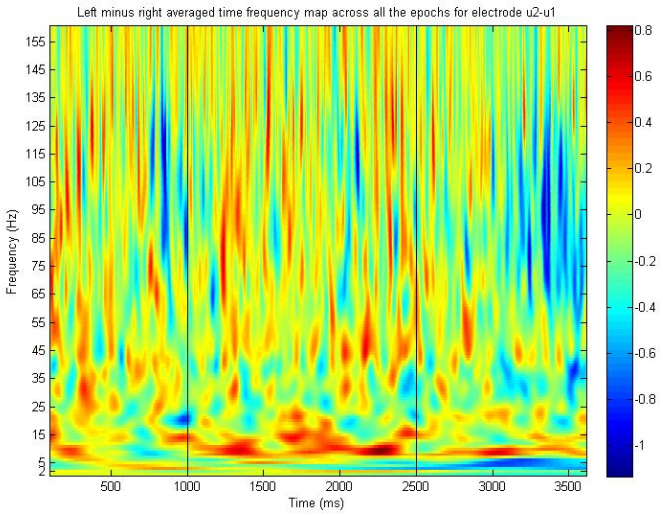

Figure 3.10: Left minus right averaged time frequency map across all the epochs for channel u2-u1. We notice a global decrease of high frequencies power during the movement. This channel yields to 67 % of correct classification of right vs. left during the movement on 60-160 with both LDA and SVM.

3.2.1.3 Influence of normalization

We studied the influence of normalization on the DA of the three best channels for each couple classifier-task. Absence of normalization, and the methods (1) (2) (3) of normalization (see section 2.4.2.1) has been considered. The method (4) is not used as we can not access the standard deviation with our way of saving the TF maps. The results for kNN (k=3) and LDA are respectively displayed in figures 3.11 and 3.12. The results for kNN (k=5) are very similar to the ones obtained for kNN (k=3), the results for SVM are also very similar to the ones obtained for LDA. Methods (1) *substract the averaged baseline then divide by the averaged baseline* and (2) *divide by the averaged baseline* provide the same results in term of DA but lead to different time-frequency map display.

kNN, k=3			
	no norm.	sub. & div.	sub.
RM	57/x13-x12	99.5/x13-x12	99/n14-n13
RP	58.75/h13-h12	99.25/v3-v2	99.25/g14-g13
LRM	68/e8-e7	78/e8-e7	64/q3-q2
LRP	64/f3-f4	71/f3-f4	62/i5-i4
UDM	61/e12-e11	73/q7-q6	62/q7-q6
UDP	63/b3-b2	68/e6-e5	66/f11-f10
4M	32/v3-v2	37/q8-q7	34.5/q8-q7
4P	33/f9-f8	40/f9-f8	32.5/e7-e5

Figure 3.11: Comparison: absence of normalization (No norm.) and two normalization methods: subtraction and division by the baseline, subtraction of the baseline. The third method (division by the baseline) provide the same results as the first method. The comparison is performed on the three best channels of kNN (k=3) for the 8 tasks (RM: rest vs. movement, RP: rest vs. preparation, LR: left vs. right during the movement (LRM) and the preparation (LRP), UD: up vs. down, 4: classification of the 4 directions). The best DA and the corresponding channel are displayed.

LDA			
	no norm.	sub. & div.	sub.
RM	66.5/l14-l13	82.25/k7-k6	83.75/v14-v13
RP	58.75/b2-b1	81.5/b2-b1	80.25/b2-b1
LRM	64/u7-u6	67/v3-v2	66/v3-v2
LRP	62/e3-e2	64/u2-u1	62/e3-e2
UDM	62/i4-i3	66/g13-g12	63/v2-v1
UDP	60/x14-x13	64/u2-u1	60/u2-u1
4M	33/x14-x13	29.5/x14-x13	33/x14-x13
4P	32.5/o10-o9	35/o10-o9	31.5/o10-o9

Figure 3.12: Comparison: absence of normalization (No norm.) and two normalization methods: subtraction and division by the baseline, subtraction of the baseline. The third method (division by the baseline) provide the same results as the first method. The comparison is performed on the three best channels of LDA for the 8 tasks (RM: rest vs. movement, RP: rest vs. preparation, LR: left vs. right during the movement (LRM) and the preparation (LRP), UD: up vs. down, 4: classification of the 4 directions). The best DA and the corresponding channel are displayed.

3.2.1.4 Time windows influence

See figures 3.14 and **??** for the analysis results. The protocol is explained in captions. The combination 222 will be kept for further analysis.

kNN, k=3									
	111	*122*	*133*	*211*	*222*	*233*	*311*	*322*	*333*
RM	98.5	98.75	99	98.75	99.5	98.75	99	99.25	99.25
RP	98.75	99	99	99	99.75	99	98.75	99.25	99
LRM	62	65	63	62	78	60	62	57	63
LRP	61	64	69	73	71	65	60	69	64
UDM	65	64	63	63	73	63	59	61	65
UDP	64	58	67	62	69	62	64	65	58
4M	31.5	33	31	34.5	37	32.5	30	32	31
4P	33	30.5	31	31	40	32	31	33	30

Figure 3.13: Display the best DA found for each task and each time windows combination for kNN, k=3. The considered time windows are: 100-500 ms, 400-800 ms, 100-800 ms for the rest, 1000-1400 ms, 1000-2300 ms, 2000-2500 ms for the preparation, 2500-3000 ms, 2700-3700 ms, 3200-3700 ms for the movement. The time windows are referenced by a code. E.g. 122 means we use the first range for the rest, the second for the preparation and the second for the movement (thus 100-500 ms, 1000-2300 ms and 2700-3700 ms). We use the same task notations as previously.

LDA									
	111	*122*	*133*	*211*	*222*	*233*	*311*	*322*	*333*
RM	78.75	81.75	81.75	77.5	82.25	80.25	81.25	79.75	83.25
RP	81	81.25	78.75	77.75	81.5	80.75	79	79.25	82
LRM	60	62	63	61	67	66	62	64	65
LRP	64	61	62	61	64	61	63	59	61
UDM	59	67	62	61	64	61	60	64	65
UDP	61	60	61	61	64	61	58	64	62
4M	31	32.5	32.5	30.5	36	32.5	30	31.5	34
4P	31.5	30.5	30	32	33	33.5	32.5	36	33

Figure 3.14: Display the best DA found for each task and each time windows combination for the LDA. The considered time windows are: 100-500 ms, 400-800 ms, 100-800 ms for the rest, 1000-1400 ms, 1000-2300 ms, 2000-2500 ms for the preparation, 2500-3000 ms, 2700-3700 ms, 3200-3700 ms for the movement. The time windows are referenced by a code. E.g. 122 means we used the first range for the rest, the second for the preparation and the second for the movement (thus 100-500 ms, 1000-2300 ms and 2700-3700 ms). We used the same task notations as previously.

3.2.1.5 Two features analysis

The two features analysis (see figures 3.15 and 3.17) has to be compared with the one feature analysis (see figure 3.3, 3.4 and 3.5). All the combinations of the chosen frequency ranges (see 2.4.2.1) has been investigated on the three best channels.

LDA, 2 features			
	DA	*Channel*	*Freq. ranges*
RM	84.25	v14-v14	2-4 – 60-160
RP	82.75	b3-b2	2-7 – 30-130
LRM	66	u2-u1	2-4 – 30-130
LRP	65	g13-g12	4-7 – 60 160
UDM	65	v3-v2	2-4 – 60-160
UDP	68	x14-x13	2-4 – 6-30
4M	33	o10-o9	2-7 – 30-130
4P	36	x14-x13	2-4 – 4-7

Figure 3.15: Display the best results found using LDA with two features (two frequency ranges) applied on the 3 best channels.

SVM, 2 features			
	DA	*Channel*	*Freq. ranges*
RM	88.5	i2-i1	2-7 – 6-30
RP	90	v14-v13	2-7 – 30-130
LRM	66	u2-u1	4-7 – 60-160
LRP	63	v3-v2	2-4 – 60 130
UDM	64	g13-g12	60-130 – 60-160
UDP	66	x14-x13	2-4 – 6-30

Figure 3.16: Display the best results found using SVM with two features (two frequency ranges) applied on the 3 best channels.

kNN, k=3, 2 features			
	DA	*Channel*	*Freq. ranges*
RM	97.75	x13-x12	2-4 – 15-30
RP	97.75	v3-v2	15-30 – 30-130
LRM	74	f3-f2	8-13 – 60-160
LRP	66	e8-e7	6-30 – 15-30
UDM	64	n9-n8	2-4 – 30-130
UDP	62	b3-b2	2-4 – 2-7
4M	35	f10-f9	2-7 – 60-160
4P	36	q8-q7	2-7 – 30-130

Figure 3.17: Display the best results found using kNN, k=3, with two features (two frequency ranges) applied on the 3 best channels.

kNN, k=5, 2 features			
	DA	*Channel*	*Freq. ranges*
RM	97.75	g14-g13	6-30 – 15-30
RP	98	m11-m10	2-7 – 15-30
LRM	74	f3-f2	8-13 – 60-160
LRP	68	o9-o8	15-30 – 60-130
UDM	64	n9-n8	2-4 – 30-130
UDP	62	n9-n8	6-30 – 30-130
4M	40	g12-g11	4-7 – 60-130
4P	37	e8-e7	2-7 – 30-130

Figure 3.18: Display the best results found using kNN, k=5, with two features (two frequency ranges) applied on the 3 best channels.

LDA, 2 features			
	DA	*Channel*	*Freq. ranges*
RM	84.25	v14-v13	2-4 – 60-160
RP	83.75	v14-v13	2-7 – 60-130
LRM	68	n2-n1	2-7 – 4-7
LRP	66	k12-k11	8-13 – 6-30
UDM	66	o10-o9	2-7 – 30-130
UDP	69	e7-e6	30-130 – 60-160
4M	39.5	z5-z4	8-13 – 6-30
4P	36.5	n10-n9	4-7 – 60-130

Figure 3.19: Display the best results found using LDA with two features (two frequency ranges) applied on **all** the channels.

3.2.1.6 Channels combination

Another analysis has been launched to see if summing some channels could lead to more discriminant features. We investigated all the possible combinations (by summation) of the three best channels for each couple classifier-task (see). The frequency window combination 222 is used, all the frequency ranges are tested. Compared to the previous results (see 3.2.1.2), we notice a global decrease of the DA.

LDA			
	DA	*Channel(s)*	*Frequency range*
RM	82.25	v14-v13	60-130
RP	81.5	v2-v1,b2-b1	6-30
LRM	67	u2-u1	60-160
LRP	64	v3-v2	60-130
UDM	65	g13-g12, v2-v1, i3-i2	60-130
UDP	62	m10-m9, u2-u1	2-7
4M	30	o10-o9, q3-q2,f13-f12	60-160
4P	35	x14-x13	2-4

Figure 3.20: The 3 best channels (see previous) has been combined as follow: chan1+chan2, chan2+chan3, chan3+chan1, chan1+chan2+chan3. The best DAs across the combinations are displayed. If one channel is used multiple times (e.g. chan1=chan2 and chan1+chan2 provides the best DA) we only display one time the name of this channel.

SVM			
	DA	*Channel(s)*	*Frequency range*
RM	86	e8-e7, i2-i1	2-7
RP	86.25	v14-v13,b3-b2	2-7
LRM	67	u2-u1	60-160
LRP	63	v3-v2	60-130
UDM	63	g13-g12, i3-i2	60-160
UDP	59	m10-m9, x14-x13	2-4

Figure 3.21: The 3 best channels (see previous) has been combined as follow: chan1+chan2, chan2+chan3, chan3+chan1, chan1+chan2+chan3. The best DAs across the combinations are displayed. If one channel is used multiple times (e.g. chan1=chan2 and chan1+chan2 provides the best DA) we only display one time the name of this channel.

kNN, k=3			
	DA	*Channel(s)*	*Frequency range*
RM	99.5	x13-x12, n14-n13	60-160
RP	99.25	v3-v2,g14-g13	6-30
LRM	65	i4-i3, f3-f2	8-13
LRP	64	q3-q2, e8-e7	6-30
UDM	61	e12-e11, q7-q6	60-130
UDP	67	e6-e5, b3-b2	30-130
4M	35	e6-e5, f10-f9	60-160
4P	33	v3-v2, f12-f11	30-130

Figure 3.22: The 3 best channels (see previous) has been combined as follow: chan1+chan2, chan2+chan3, chan3+chan1, chan1+chan2+chan3. The best DAs across the combinations are displayed. If one channel is used multiple times (e.g. chan1=chan2 and chan1+chan2 provides the best DA) we only display one time the name of this channel.

kNN, k=5			
	DA	*Channel(s)*	*Frequency range*
RM	99	m11-m10, g14-g13	15-30
RP	98.75	b7-b6, m11-m10	30-130
LRM	57	f3-f2, l12-l11	4-7
LRP	66	b7-b6, l4-l3	2-7
UDM	67	q7-q6	60-160
UDP	59	n9-n8, h13-h12	30-130
4M	34.5	o9-o8, z2-z1	60-160
4P	31	z2-z1, e8-e7	30-130

Figure 3.23: The 3 best channels (see previous) has been combined as follow: chan1+chan2, chan2+chan3, chan3+chan1, chan1+chan2+chan3. The best DAs across the combinations are displayed. If one channel is used multiple times (e.g. chan1=chan2 and chan1+chan2 provides the best DA) we only display one time the name of this channel.

3.2.2 EEG data

3.2.2.1 Eye artifacts monitoring

The threshold methods used to discard the eye artifacts worked correctly. Up to 10 epochs has been removed for each couple subject-event.

3.2.2.2 Classification results

Due to large amount of data (5 subjects with 100 epochs per event for EEG, instead of one subject with 50 epochs per event for iEEG) and lack of time, we decided to

set the analysis protocol with regards to the iEEG results (see 2.4.2.5). We then kept long time windows: 300-800 ms, 1000-2300 ms, 2500-3700 ms, used 'subtraction then division' normalization, and ran a single feature analysis with LDA, kNN (k=3) and kNN (k=5). We also tried other more specific time windows (e.g. 2500-2800 on subject 1) from scratch without getting a better DA. SVM has been ran on subject 1, and we checked that, as for the iEEG analysis, the results were very similar to those we have got from LDA. As a result, because this classifier is very time consuming, we decided to discard it. For the same time reason, we did not investigate NN classifier. The results of the 4 directions comparisons were close to the level of the chance (25 %) and are consequently not displayed.
A summary of the analysis is displayed in figures 3.29 and 3.30. TF maps of some channels which yield to good DAs are displayed in figures 3.31, 3.32 and 3.33.

	Subject 1, right hand								
	LDA			KNN3			KNN5		
	DA	chan.	freq.	DA	chan.	freq.	DA	chan.	freq.
RM	81.6	30-130	C3	99.6	60-85	C3	99.5	30-130	C2
RP	81.6	62-87	F3	99.6	15-30	CZ	99.3	2-3	CP1
LRM	65.3	50-128	CZ	63.2	15-30	C1	64.3	15-30	C1
LRP	60.7	62-87	F3	66.3	50-128	CP4	64.3	50-128	C4
UDM	63.8	30-50	FZ	62.2	2-4	F3	63.8	60-85	F1
UDP	58	15-30	CPZ	62.2	50-128	F4	64.8	50-128	F4

Figure 3.24: For each classifier, for each comparison, display the best decoding accuracy (DA) found across the channels and across the frequency bands for the first subject. In lines, RM: rest vs. movement, RP: rest vs. preparation, LRM: left vs. right during the movement, LRP: left vs. right during the preparation, UDM: up vs. down during the movement, UDP: up vs. down during the preparation.

	Subject 2, right hand								
	LDA			KNN3			KNN5		
	DA	chan.	freq.	DA	chan.	freq.	DA	chan.	freq.
RM	83.5	30-130	CP1	99.6	15-30	FCZ	99.6	60-85	CP2
RP	79.6	2-7	FC1	99.6	2-4	C3	99.5	4-7	F1
LRM	61.3	30-130	CZ	66.5	4-7	C1	64.4	15-30	C1
LRP	61.3	2-5	FC1	65.5	4-7	C1	64.9	50-128	C1
UDM	60.8	15-30	FZ	63.9	60-85	CP4	64.9	50-128	FC3
UDP	59.8	15-30	F1	62.9	60-85	C1	69	60-85	C1

Figure 3.25: For each classifier, for each comparison, display the best decoding accuracy (DA) found across the channels and across the frequency bands for the second subject. In lines, RM: rest vs. movement, RP: rest vs. preparation, LRM: left vs. right during the movement, LRP: left vs. right during the preparation, UDM: up vs. down during the movement, UDP: up vs. down during the preparation.

	Subject 3, right hand								
	LDA			KNN3			KNN5		
	DA	chan.	freq.	DA	chan.	freq.	DA	chan.	freq.
RM	88.7	15-30	F4	99.7	10-30	C4	99.4	30-130	FC4
RP	79.1	2-7	FC2	99.7	30-130	FCZ	99.3	2-3	FC1
LRM	62.4	30-130	FC1	61.3	4-7	F3	63.9	30-130	F1
LRP	61.3	30-50	CZ	61.9	4-7	F2	63.9	60-85	CP1
UDM	58.2	60-85	F3	63.9	60-85	CPZ	63.4	2-4	FC4
UDP	60.8	62-87	CP3	69	2-3	F3	65.4	2-5	C1

Figure 3.26: For each classifier, for each comparison, display the best decoding accuracy (DA) found across the channels and across the frequency bands for the third subject. In lines, RM: rest vs. movement, RP: rest vs. preparation, LRM: left vs. right during the movement, LRP: left vs. right during the preparation, UDM: up vs. down during the movement, UDP: up vs. down during the preparation.

	Subject 4, right hand								
	LDA			KNN3			KNN5		
	DA	chan.	freq.	DA	chan.	freq.	DA	chan.	freq.
RM	78.3	30-130	CZ	99.6	30-50	CP1	99.5	30-50	CP1
RP	79.7	10-30	FZ	99.6	30-50	FC2	99	30-130	FC2
LRM	62.8	30-50	FC2	62.3	30-130	CZ	63.9	30-50	FC2
LRP	60.8	10-30	CZ	64.9	2-7	CP3	66.5	50-128	C3
UDM	62.9	2-5	F1	63.4	30-50	CZ	62.9	2-5	F1
UDP	58.8	10-30	C3	66.5	2-5	FZ	68.6	2-5	FZ

Figure 3.27: For each classifier, for each comparison, display the best decoding accuracy (DA) found across the channels and across the frequency bands for the fourth subject. In lines, RM: rest vs. movement, RP: rest vs. preparation, LRM: left vs. right during the movement, LRP: left vs. right during the preparation, UDM: up vs. down during the movement, UDP: up vs. down during the preparation.

	Subject 5, right hand								
	LDA			KNN3			KNN5		
	DA	chan.	freq.	DA	chan.	freq.	DA	chan.	freq.
RM	82	30-130	F3	99.7	10-30	CP1	99.2	2-5	C3
RP	79.8	60-85	CPZ	99.9	2-4	CP3	99.4	60-85	F4
LRM	70.6	60-85	F3	65.5	2-7	CP2	64.4	2-7	FC2
LRP	64.9	30-130	F3	66	2-4	CP1	65.5	10-30	CP4
UDM	72.7	50-128	F3	71.6	50-128	F3	69.6	50-128	F3
UDP	64.4	50-128	F1	63.4	15-30	FC4	64.9	60-85	CZ

Figure 3.28: For each classifier, for each comparison, display the best decoding accuracy (DA) found across the channels and across the frequency bands for the fifth subject. In lines, RM: rest vs. movement, RP: rest vs. preparation, LRM: left vs. right during the movement, LRP: left vs. right during the preparation, UDM: up vs. down during the movement, UDP: up vs. down during the preparation.

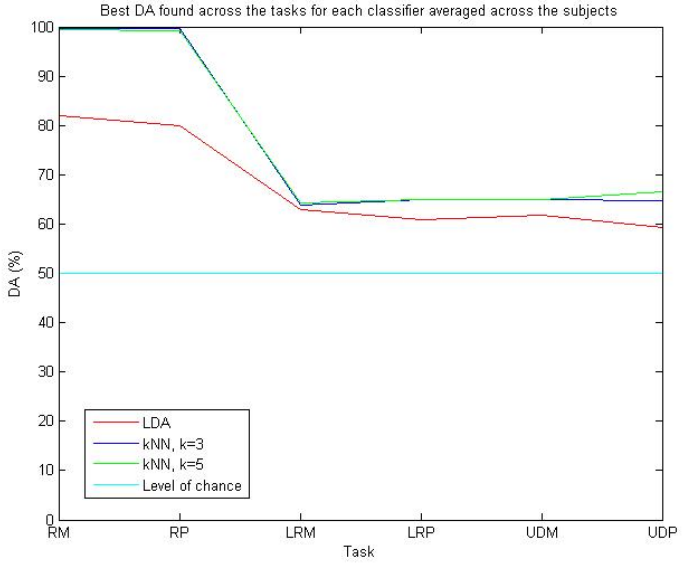

Figure 3.29: Display the best DA found for each task and each classifier. For each couple classifier-task, we averaged the best DA found across the 5 subjects. LRM: left vs. right during the movement, LRP: left vs. right during the preparation, UDM: up vs. down during the movement, UDP: up vs. down during the preparation.

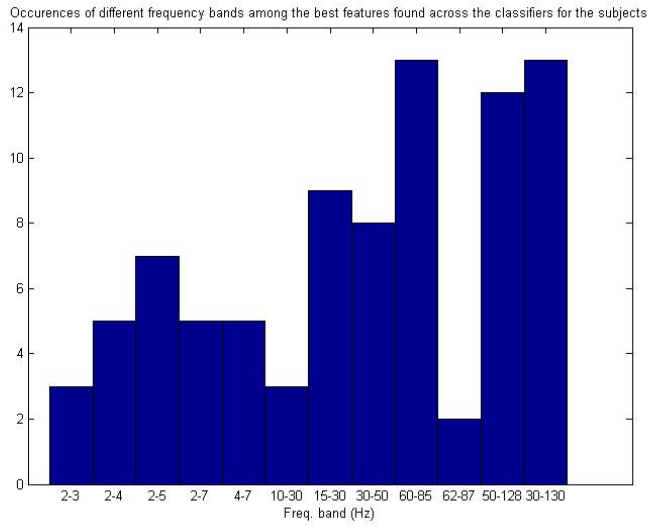

Figure 3.30: Display the number of occurrences of each frequency band among the best features found across the classifiers. The analysis is performed across the 5 subjects.

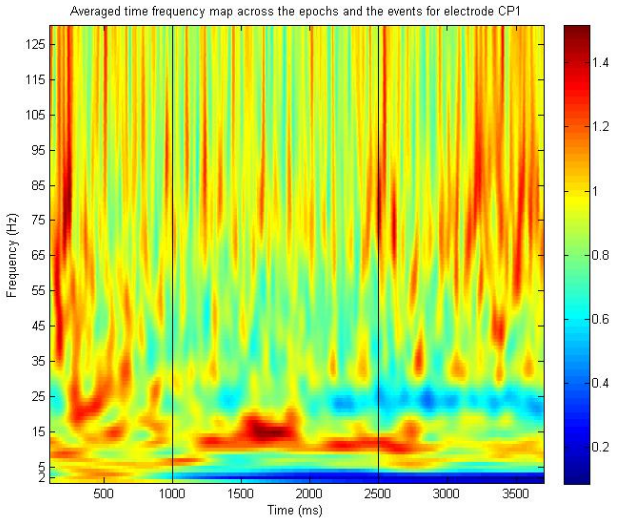

Figure 3.31: Averaged time frequency map across all the events and all the epochs for channel CP1 (subject1). We notice a decrease of the power in low frequencies during both the preparation and the movement, while the intermediate frequencies power increases only during the preparation, and the high frequencies power increases only during the movement. This channel yields to 99.3 % of correct classification of rest vs. movement on 2-3 with kNN, k=5.

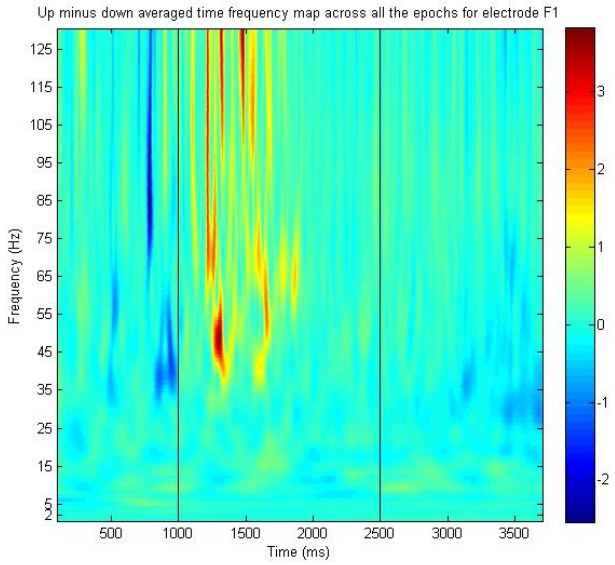

Figure 3.32: Up minus down averaged time frequency map across all the epochs for channel F1 (subject 1). We notice a decrease of power in high frequencies during the preparation. It is difficult to say whether or not artifacts are involved though. This channel yields to 63.8 % of correct classification of up vs. down during the movement on 60-85 with kNN, k=5.

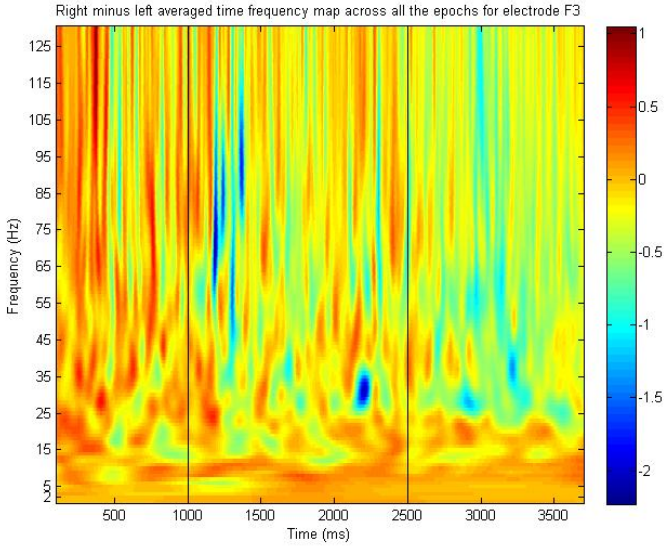

Figure 3.33: Right minus left averaged time frequency map across all the epochs for channel F3 (subject 5). We notice a first decrease of intermediate and high frequencies during the preparation, then a more clear decrease of intermediate and high frequencies during the movement. This channel yields to 70.6 % of correct classification of right vs. left during the movement on 60-85 with LDA. F3 also yields to 64.9 % of correct classification of right vs. left during the preparation on 30-130 with LDA.

Chapter 4

Discussion

In this part, we try to have a critical view on various aspects of our work, first by summarizing the results and then by confronting our outcomes to the BCI-related literature. We will finally draw a conclusion and try to propose a way for going further.

4.1 Results summary

In general, the results demonstrated the feasibility to detect voluntary movement intention using the negative phase of MRCPs or the time frequency maps from executed movements trials in four directions. Despite the relative complexity of the protocol followed by the subject (see Chapter 2), the true positive rates obtained from both iEEG data and scalp EEG with time analysis show that the proposed methods can be used for movement intention detection purposes. The TPR (true positive rate) is always above 70 % (OSF data) and often above 75 %, while the majority of the FPRs (false positive rate) are around 25 %. It is also possible to use time frequency analysis in this purpose: the DA (decoding accuracy) obtained from both iEEG and EEG data with time frequency analysis is above 80 % (LDA and SVM) and goes up to 99 % (kNNs) for the movement intention detection.
Once the movement intention is validated, the movement direction analysis can be taken into account. Time frequency analysis enables movement direction classification on intracortical EEG during the intended movement (around 70 % with kNN, 64 % with LDA or SVM for two directions classification; around 38 % with kNN and 35 % with LDA for four directions classification) and actual movement (around 75 % with kNN and 67 % with LDA or SVM for two directions classification; around 39 % with kNN and 36 % with LDA for four directions classification). Direction classification is possible for two directions on scalp EEG data (on average 66 % with kNN across the subjects and 62 % with LDA; however, up to 72 % can be reached for subject number 5), while the four directions classification is around the level of chance.

The most striking outcome from EEG results is the big differences which can be seen across the different subjects in many fields: frequency ranges, results of the LDA, results

of the kNN. As for the employed methods, one can notice an important increase of the DA on the comparisons rest vs. movement/preparation by using normalization. The best results are found with the 'sub. & div.' normalization at one exception (4 directions movement for LDA). We can therefore conclude that normalization enhance the decoding accuracy for time frequency analysis. Concerning the time windows, according to figures 3.14 and 3.13 the choice of the three longer time intervals (222, see figure caption for explanation) yields to the best results. Our effort to combine the two or three best channels did not work (see 3.2.1.6)). Finally, by using two features instead of one, we noticed an increase of the DA for the comparisons RM and RP with LDA and SVM, while the DAs for the other comparisons were similar. However, the use of two features for kNN (k=3 and k=5) led to a globally decreased DA.

4.2 Similar BCI paradigms

The novelty of the **movement intention detection** analysis of our report stands in the application of the movement *intention* detection based on the negative phase of the MRCP, for four different directions of movement, with no prior training of the subjects. Since there are no similar studies, no direct comparison is possible.
We can though report several studies which concentrated their attention on low frequencies (1-4 Hz) switch designs mainly intended for communication purposes [Bashashati et al., 2006; Yom-Tov and Inbar, 2003]. Their results show lower TPR (50 -70 %) than ours, but one of the goals relies in minimal FPR (which was around 1-2 %).
The most similar work compared to ours comes from a recent study conducted by Niazi et al., whose work has been of great inspiration for the movement intention method during the development of the project. The accuracy of movement detection intention from single trial MRCPs for both movement imagination and execution was measured using a portion of the negative phase of the MRCP (until movement onset) as a template in order to be tested against the testing data (scalp EEG, 9 channels). The same Optimized Laplacian Filter (OSF) was used to improve the SNR of the MRCP over the noise. The mean of TPR was 82.5 % (FPR not reported in the article), which is slightly better than our findings. However, unlike us, the subject performed always the same task (ankle dorsiflexion) and they had to undergo a training session. In this study it was demonstrated that the OSF outperforms the LSF.
Relying on our results, we can state the Optimized Spatial Filter brings a slight improvement (or sometimes no improvement) over the Large Laplacian filter. One of the reasons may stand in the fact that, by protocol, we dispose only of 1 second of noise signal (the 'rest period') to be used in the SNR optimization. These results anyway confirm the robustness of the Optimized Spatial filter in this type of analysis, where four different movement directions were performed by 5 (scalp EEG) + 1 (iEEG) subjects at their preferred speed, following a rather "complex" set of instructions. The validity of the OSF is also indicated in a study conducted on MRCP classification [Boye et al., 2008]. The analysis was conducted on imagination of plantar-flexions with the right foot. Features were extracted with principal component analysis and classification be-

tween MRCPs and noise was performed with kNN and SVM. In this case, the TPR were high (80-90 %), but given the differences in the protocol, e.g. a larger data set, only one task rather than four, and usage of the entire MRCP waveform was used in the analysis, a comparison seems inappropriate.
Some of the above mentioned papers tend to give priority to a low FPR rather than high TPRs. Depending on the purpose of the BCI system which this study is be applied to, a different threshold can be set, which results in a different weight of TPRs over FPRs. In our study, the threshold was set trying to get the highest TPR while having the lowest FPR possible, but other approaches can be used. For instance, higher TPR could be achieved increasing the number of false positives, or even using the entire MRCP as template instead of the negative phase. In the second case, thought, the detection could only be made once the movement is already started, loosing the predictive design of the study.
Further considerations can be made about the movement detection accuracy. The first note can be the distinction between results obtained using 'real' noise ('rest period' in the protocol, 1 sec. of duration) and longer artificial noise, estimated from the real one. As it can be expected, the performances decrease using estimated noise. Nevertheless, we base most of our considerations on these results, as the same length of 'noise' and 'signal' (see Chapter 2) is used for the movement detection and so the results can be expect to be more "realistic".
A second reflection is that there is an improvement brought by using a bigger data set. Using all the data from one hand (with no distinction of two/four movements) leads to higher TPRs and lower FPRs, particularly for the iEEG data. This result could be explained by the fact that a larger training set leads to built a better MRCP template. This difference is indeed more beneficial to the iEEG, as we dispose only of half (50) epochs for each movement in respect of the scalp EEG data (100 epochs per movement). Furthermore, the iEEG results, in general, show +10 % of FPRs, despite the fact that intracortical recording have greater spatial resolution than standard scalp EEG. This could be because the electrodes in the epileptic patient were placed in order to treat his illness, rather than in optimal locations (e.g the motor cortex). Furthermore, the locations of the electrodes were not spatially disposed on a surface like for the scalp EEG data, nor one next to the other, but spread around the brain. This probably affected the performance since we use a spatial filter for our analysis also on the iEEG data.
Finally, a consideration about the detection accuracies of movement in the four directions can be made. The tables show (in particular, but not only, Table 3.10) no general trend of a better detection of movement intention for a particular direction rather than another.

Moving to **direction classification**, as first notice, it should be specified that our time frequency analysis compares different classification methods (LDA, SVM, kNN, NN) on both scalp and intracranial EEG recordings, which has not be done previously according to our knowledge. In addition, the different normalization methods comparison is not referenced in the literature as well. As a result, the used paper for this section only partially cover the analysis performed in our study. For instance, we did not focus

our main attention on the optimization of the classifiers, while most of the published studies did it.

Channel combination In a similar EEG experiment, Jerbi et al. reported a peak of the DA when 34 out of 55 channels were used (and a drop for more than 34 channels). According to Waldert et al. the decoding performance of iEEG could be increased by using additional recording sites. Indeed, the weaker inter-channel correlation and thus less redundancy between channels, could lead to better results. Waldert et al., in another study, reports that the use of few sensors exclusively above contralateral motor-related areas after movement onset can improve the DA of a similar EEG experiment. Finally, Mehring et al. in figure 4.1 shows how the use of multiple channels can increase the DA.

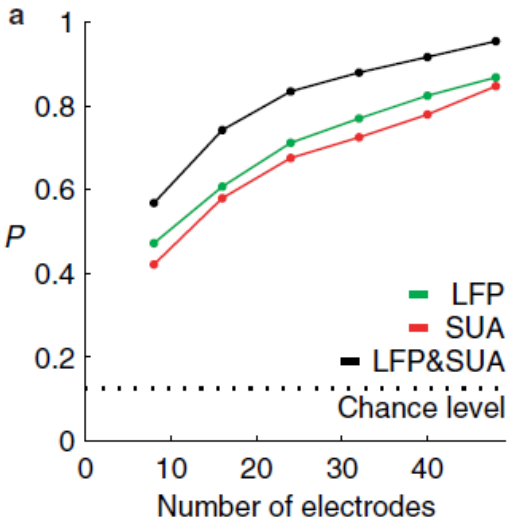

Figure 4.1: Decoding of movement target and trajectories from multiple local field potentials (LFP). Average probability of correctly discriminating between eight targets as a function of the number of recording electrodes. LFPs (green) and single-unit activity (SUA, red), both recorded simultaneously from identical sets of micro-electrodes yielded a similar decoding power. Using LFPs in conjunction with simultaneously recorded SUAs (black) further increased the average decoding power [Mehring et al., 2004].

Feature combination According to Jerbi et al., simultaneous multichannel recordings from large neuronal ensembles used in the context of brain machine interfaces further support the notion of a distributed representation of limb kinematics in multiple cortical areas. This assertion supports the use a multi-feature approach. In addition, Rickert et al. shows that combining two frequency ranges can increase the DA (e.g. <4 Hz and 63-200 Hz, see figure 4.2).

iEEG analysis According to Jerbi et al. highest directional tuning is found in <4 Hz and 60-140 Hz. From our analysis, we can observe that most of the frequencies

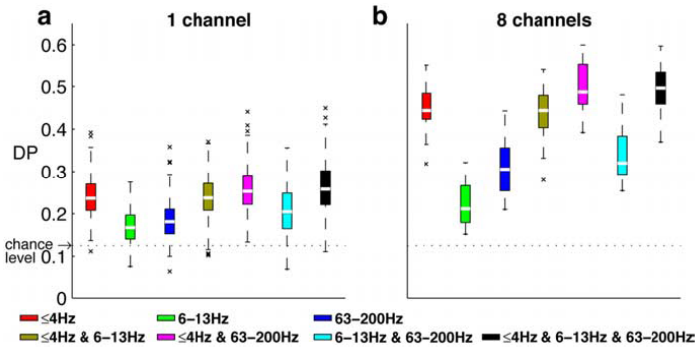

Figure 4.2: Decoding power of different frequency bands. a, The box plots show the distribution of decoding power of single LFPs for various frequency bands and their combinations indicated at the bottom. White bars depict the median, the box ranges from the lower to the upper quartiles, the dashed whiskers extend to the most extreme decoding power within the 1.5-fold interquartile range from the borders of the bars, and the symbols mark outliers. b, Decoding power of simultaneous LFP recordings from eight electrodes (symbols as in a) [Rickert et al., 2005].

ranges which provided the best DAs are either in the low frequency or in the high frequency bands. Yet, some intermediate bands also yield to good results, especially for kNN and LDA. Rickert et al. shows that the amplitude of <13 Hz is modulated with the direction of movement and that the amplitude of 16–42 Hz band decreases during movement execution, which supports our use of intermediate frequency bands. Furthermore, Mehring et al. uses the changes in relative spectral power for 8-30 Hz in order to classify limb movements.
The reached DA can be seen as satisfactory and can be compared to what is found in the literature. E.g. Leuthardt et al. used ECoG recordings decoding to control a one-dimensional computer cursor. This binary task can be a achieved with up to 74 % accuracy while performing opening and closing movements of the right hand and with 83 % of accuracy while the subject is performing the same imagined task. Other binary tasks referenced by Leuthardt et al. are performed with a 60 to 70 % DA before training. However, many papers are focused on the 4 directions or 8 directions classification (see figure 4.2). Our results can be considered valid, considering the fact that we use only one channel where most of the results referenced in the literature use a multiple channels approach.

EEG analysis First of all, it has to be said that the movement direction decoding from extracranial EEG data is still a challenge and has only been performed recently for the first time by Waldert et al. in 2008. Therefore, it has been largely assumed that non invasive recordings cannot decode limb movement directions because of the low SNR and bandwidth limitation [Jerbi et al., 2011]. Jerbi et al. reports 80 % in a binary single trial EEG classification left vs. right across 4 subjects in his review. If we consider the left vs. right classification across our 5 subjects, we achieved 64.5 % on average.

4.3 Limitations

We first deal with the limitations leaded by the experimental protocol, then we dig into more specific limitations: first for the time-based analysis, then for the time frequency analysis. As mentioned above, due to specific methods used for each technique, we judged the display our comments in two different parts to be clearer for the reader.

4.3.1 Experimental protocol

4.3.1.1 iEEG

For obvious ethical reasons, iEEG recordings in human are only performed on non healthy epileptic subject during the pre surgical investigation. iEEG is then only recorded in patients with intractable epilepsy who are sometimes cognitively impaired due to various pain/sedating medication or frequent seizures. In addition, between recovery of the patient from channel implantation and channel removal there is often very limited time, and sometimes a low patient interest to perform BCI experiments ([Waldert et al., 2009]). Furthermore, epileptic EEG shows characteristics peaks from time to time during the 'normal' state. During a crisis, those peaks gain in amplitude and the different EEG channels begin to synchronize on each other. If there is a crisis during an experiment, the data have to be discarded. However, the 'normal state' peaks remain and might induce a bias in our data. Furthermore, we can also wonder if there are other hidden epileptic-related phenomena which could impact classifiers accuracy.
Because electrode placement is solely determined by the requirements of epilepsy surgery, we miss some areas which could be relevant for our purpose. Indeed, according to Leuthardt et al., the decoding performance is dependant on the location of the implanted electrodes, the number of electrodes, and the inter-electrodes distance. It might also depend on electrode size and impedance. These parameters are determined by the requirements of pre-neurosurgical evaluations. As a result, in case of low DA, a general conclusion about whether or not iEEG is able to decode limb movements can not be drawn. On the contrary, an iEEG analysis can randomly reveal the importance of a very specific zone for some tasks.

4.3.1.2 EEG

Concerning scalp EEG data, we face the opposite problem: the recorded area is wide for each electrode. Although EEG enables to cover all the surface of the brain, it is not able to aim a very specific zone.
As reviewed by Jerbi et al., the presence of eye artifact shows a notable drop in accuracy. Even is we are discarding blinks by the mean of a threshold comparison [Waldert et al., 2008], some eye saccades might remain and impact the results. In addition, at least another person was present in the same room while the experiment was running, leading to an increased risk of eye saccades.
Finally, although the room in which the EEGs have been recorded is shielded from the outside (roads, other buildings, etc.), numerous electromagnetic sources were present

inside: computers, cellphones, etc. These sources are impossible to monitor and may induce random artifacts in the signal.

4.3.1.3 iEEG and EEG

There are limitations which are common for EEG and iEEG.
In the protocol, visual cues trigger the execution of a task (one visual cue to indicate the direction and another visual cue to display the 'go signal'). The impact of visual trigger on the EEG signals is not known. We could imagine that a punctual drop in the power of a given frequency band right after the visual cue is not due to the movement planification, but to the apparition of the visual cue itself. In order to have a better understanding about its influence, it would be interesting to propose visual cues to a subject without letting him know the goal of the experiment and without allowing him to move his arm.
On top of this, after the visual cues, each subject reacted differently: some of them performed the movement quickly, some others moved their arm slowly, etc. As a result, the protocol is not exactly the same and some results might be biased, especially when the detection accuracy across the 5 EEG subjects is averaged. We could have used the mouse position information in order to locate precisely the interesting movement, which would have eliminated the movement onset uncertainty. However, using such a technique would have raised algorithmic issues due to a different samples lengths for every trial.
Finally, although we tried to carefully reproduce the intracranial experiment ran in Grenoble (France), the two setups are not exactly the same: positions (sat in a bed in France, sat on a chair in Denmark), distance from the screen, etc. These differences might lead to unknown bias.

4.3.2 Time frequency analysis

Normalization As the value taken for the rest and the value taken for the baseline are the same, the normalization leads to compare the value 1 (rest) to the average power in a given time frequency area (movement or preparation). This obvious comparison provides good classification results despite of the chosen channel. Furthermore, the best DA is not directly yielded by physiological parameters. As a result, the DA without normalization for the best channels found with normalization is quite low (see figure 3.11).
Besides, the best results are found with the sub. & div. normalization at one exception (4 directions movement for LDA). We can therefore conclude that normalization enhances the decoding accuracy for time frequency analysis.
A limit to our normalization approach is that we use a specific baseline for each epoch taken in the rest period (prior to the first visual cue). In a real-time online analysis, such a method can not been used (we would have to use a unique baseline to normalize each epoch). In a previous study conducted by Rohu V. at INSERM (Lyon, France), it has been shown that the use of an averaged baseline across the epochs (in order to normalize each epoch) leads to a decrease of the DA on the rest vs movement/preparation

classifications.

Time windows As we previously selected our 3 channels using the time intervals which provide the best results, a specific conclusion cannot be withdrawn. The hypothesis (see 3.2.1.6) according to which we could find better DA by narrowing the time windows is not validated. However, due to data storage limitations we have not been able to perform a more refined time windows analysis. Therefore, we can neither invalidate our hypothesis.

Channels combination Channels combination could improve the DA. Indeed, we used the best channels without regards to the physiological meanings. Two channels in two different parts of the brain can yield to good DA if taken separately, but give a low DA if taken together. We could have performed an analysis from scratch, trying all the possible combination of two or more channels.

Feature combination The feature combination shows different behavior between kNNs and LDA-SVM to a two-feature analysis. This is not surprising, as LDA and SVM are close methods. Yet, the decrease of the DA is more unexpected. The choice of three channels relevant for a single feature analysis does not mean they are for a two features analysis. As shown on a further analysis of two-features classification applied on all the channels (see figure 3.19), the DA is actually increased when going from scratch. As did Rickert et al., we noticed that combination of a low frequency band with a high frequency band provides the best results.
Working with two features also adds complexity in an already noisy space, which might lead to more uncertain results. Indeed, Rickert et al. noticed that the combination of all the frequency bands did not further increase the DA because the relatively low amount of additional information added by the intermediate frequency band competes with the decrease in performance of the decoder as a result of the higher number of input signals. As a result, a trade-off has to be found between and increased number of features, an increased complexity of the feature space and the computation time (which was a major issue in our case).

EEG analysis Globally, high frequency ranges are extensively used. Yet, according to Waldert et al. 2005 and 2008 information about movement directions are present in the low (< 3 Hz), nearly absent in < 7 Hz, not present in high frequencies (62-87 Hz). As a result, our outcomes may have to be linked with our critics of the experimental protocol and the possible electromagnetic noise, which could lead to beta and high gamma artifacts.
However, we can see from figure 4.3 that frequency analysis for movements direction classification in EEG stays a weak method compared to time analysis.

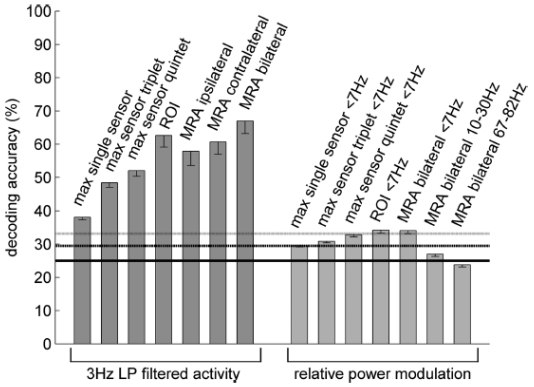

Figure 4.3: Topography of DA for single sensor-based decoding and different time windows. All DA values are averages across subjects. The sensor field is shown from above (in approximation to the head, nose pointing upward); all sensors (black dots) are visible. The top three panels show the DA for the three frequency bands, and the bottom shows the DA for the 3 Hz low-pass (LP) filtered MEG activity. Sensors showing significant DA are marked with an "x" [Waldert et al., 2008].

Classifier comparison At our knowlege, Lotte et al. is the only paper which attended to review classifiers in BCI research. Lotte et al. did not perform their own study but gather information from a corpus of published papers. The different articles we took into consideration to build our work are using different classifiers. It has to be said that an objective classifier comparison is extremely difficult due to all the parameters which can be modified in each classifier (mainly in Neural Network or SVM). The comparison performed by Lotte et al. has to be taken even more carefully because the used inputs provide from articles where the methods differ. In addition, the choice of a classifier is highly dependant of both the data set and the goal of the classification (e.g. offline vs. online).

For both iEEG and EEG data, our investigations show kNN methods globally lead to better results than LDA, SVM or NN. The impact of k is not obvious: it seems that an increased k decreases the DA on rest vs. movement or preparation while a $k > 1$ may lead to a better DA on directions classification. According to Lotte et al., kNN algorithms are not very popular in the BCI community, probably because they are known to be very sensitive to the curse-of-dimensionality, which made them fail in several BCI experiments. However, when used in BCI systems with low dimensional feature vectors, kNN may prove to be efficient. We talk about 'curse-of-dimensionality' when the number of training data is small compared to the size of the feature vectors, which is not the case in our experiment.

Despite Neural Network are universal approximators, these classifiers are very sensitive to overtraining, especially with such noisy and non-stationary data as EEG. Therefore, careful architecture selection and regularization is required [Lotte et al., 2007]. It could explain the bad results of the Neural Network in the direction classification, where the

features space is much more complex and noisy than for the movement vs. rest classification. Furthermore, due to time issues, we had to run the neural network on the best features found for LDA and kNN=3, which are not necessarily the most relevant with this method.
Finally, LDA is shown to provide slightly lower results than SVM, but is much more quick to run. We had the same impression. LDA can override SVM on some classifications though. A further optimization of the SVM methods (regularization parameter C and the RBF width if using kernel) could have increase the DA.
Ideally, classifiers should be tested within the same context, i.e., with the same users, using the same feature extraction method and the same protocol. It is what we did. But, the remaining problem would be to apply to each classifier the same level of optimization: layers and learning function for NN, k and distance measure for kNN, a-priori assumptions for LDA and parameters for SVM. For this reason some researchers have proposed general purpose BCI systems such as the BCI2000 toolkit [Schalk et al., 2004]. This toolkit is a modular framework which makes it possible to easily change the classification, preprocessing or feature extraction modules. With such a system it becomes possible to test several classifiers with the same features and preprocessing. The use of BCI2000 could help to choose the best a-priori classifier which has to be further optimized.

4.4 Prospectives

One future prospective would be to use both time and time frequency analysis in a BCI system. Indeed, the two methods might be complementary. Even if time frequency analysis performs equally or better than time analysis for the movement detection, it is a far less robust method. E.g. a mental calculation task lead to important changes in the time-frequency domain, and could thus be mistaken as a movement intention. On the contrary, MRCPs are specifically linked to motor tasks. This system could be useful for an online real-time and asynchronous analysis (e.g. prosthesis movement).
Another way of improving the system would be to use not only the early phase of the MRCP, but the whole MRCP, which could also enable a detection of the movement direction, rather than movement intention only. We could then use a "grading system" to determine the direction: each of the methods (time analysis, frequency analysis with LDA, kNN, k=3, and kNN, k=5) would lean for the classification of a direction, and the most represented direction would be taken as the direction of choice.
Modifying the experimental protocol might also lead to better and safer outcomes. For instance, a longer rest period and preparation period would bring benefit to the time-based movement detection. The visual cues could also be eliminated to avoid possible artifacts on the MRCPs in the brain signals. The subject would choose when to perform a movement (given certain specification). The mouse position could then be used in order to detect movement onset and course. Although more complex to analyse, such a recording is also closer to real-life BCI system.

In order to build a real life application, two other aspects could be further investigated. First, it would be interesting to test our algorithm robustness on an artificially noised dataset. Also, as a real time application would not let us know whether the subject is resting or not, it could be relevant to use a single baseline per subject (time frequency analysis) or a single noise per subject (time analysis) in the algorithm. Secondly, considering the heterogeneous results we have found among the different subjects for the EEG recordings (e.g. kNN methods provide best results for subjects 1 to 4 while LDA is better for subject 5), it seems difficult to design a system which could be efficient without fitting itself to the user (choice of a classifier, choice of the features, etc.). Given the above statements, two paths might be followed: trying to find patterns with cross comparison on large population of subjects, or trying to find a way to adapt the techniques of choice quickly and efficiently on a user. In this report, we followed the second path, enabling us to discover different techniques widely used in BCI, from the data preprocessing to the different analyses (time and frequency). Closed loop systems have shown to improve very quickly with short training periods. Leuthardt et al. reported 74-100 % final accuracy for a binary task performed across all subjects after short training periods (3-24 min) (see figure 4.4).

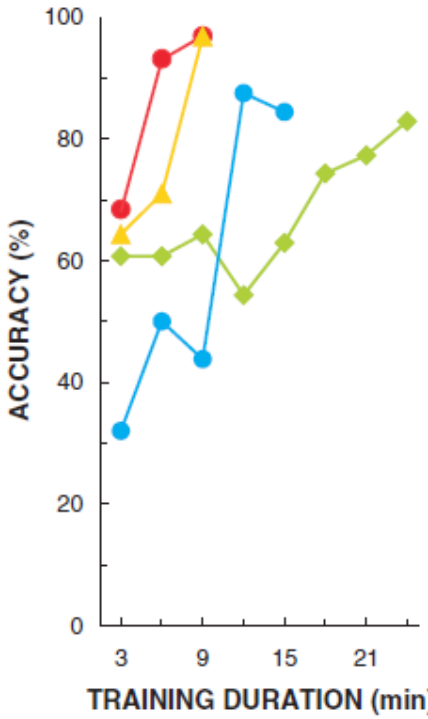

Figure 4.4: Learning curves for ECoG control of vertical cursor movement using motor imagery to move up and rest to move down). (Accuracy in the absence of control would be 50%) [Leuthardt et al., 2004]

A study conducted by Leuthardt et al. reported a substantial improvement from 71

% to 94 % of correct classification using closed loop system. In order to fit our classifier to a specific subject for a real time continue analysis, the use of a closed loop system seems very appealing, both in order to select the features of interest and to optimize the classifier. Furthermore, patterns may be discovered in the way the classification is optimized.

Chapter 5

Conclusion

The goal of this research project was to implement and apply multiple detection and decoding techniques to scalp and depth EEG recorded in subjects performing motor tasks in different directions. Two main techniques have been investigated: time analysis and time frequency analysis. The accuracy of the various decoding strategies has been compared at various levels:
(a) the type of EEG recordings: intracortical EEG (iEEG) and scalp EEG
(b) robustness to artifacts and noise with preprocessing, bipolarization methods and blinks discarding
(c) the different spatial filters (large Laplacian filter and Optimized Laplacian Filter) in the time analysis and the different classification methods with the time frequency analysis (LDA and kNN for scalp EEG data; LDA, SVM, kNN and NN for iEEG data).
(d) the features: different time windows, frequency ranges, number of features, channels combination and sort of normalization with the time frequency analysis.
Not surprisingly, iEEG recordings, which are less noisy and less affected by artifacts, led to better classification performances than scalp EEG signal. Movement detection has been performed with time analysis (up to 75% of correct movement preparation detection,) while movement detection and classification has been performed with time frequency analysis (up to 98 % of correct movement preparation detection, up to 78 % of correct two directions classification, up to 40 % of correct four directions classification).
We noticed that kNN classification methods with *subtraction then division* normalization globally performed better on our datasets (time frequency analysis) while the two spatial filters provide similar results (time analysis).
Finally, by using both time analysis and time frequency analysis we are able first to detect a motor task, and then identify the direction.
The reliable detection of human movement intention along with the knowledge about the direction of movement, has the potential implication in the control of external devices (such a prostheses or other robotic systems). Such BCI paradigm could be useful in a possible development of a patient-driven rehabilitation system which could induce plastic changes in the brain or even prosthetics control in amputees.

Bibliography

Allison, B., Graimann, B., and Gräser, A. (2007). Why use a bci if you are healthy. *proceedings of BRAINPLAY 2007, playing with your brain.*

Ball, T., Demandt, E., Mutschler, I., Neitzel, E., Mehring, C., Vogt, K., Aertsen, A., and Schulze-Bonhage, A. (2008). Movement related activity in the high gamma range of the human eeg. *Neuroimage*, 41(2):302–310.

Ball, T., Schulze-Bonhage, A., Aertsen, A., and Mehring, C. (2009). Differential representation of arm movement direction in relation to cortical anatomy and function. *Journal of neural engineering*, 6:016006.

Bashashati, A., Mason, S., Ward, R., and Birch, G. (2006). An improved asynchronous brain interface: making use of the temporal history of the lf-asd feature vectors. *Journal of neural engineering*, 3:87.

Besserve, M. (2007). Analyse de la dynamique neuronale pour les interfaces cerveau-machines: un retour aux sources. *PhD Thesis*, 18:43.

Birbaumer, N. (2006). Breaking the silence: brain–computer interfaces (bci) for communication and motor control. *Psychophysiology*, 43(6):517–532.

Boye, A., Kristiansen, U., Billinger, M., Nascimento, O., and Farina, D. (2008). Identification of movement-related cortical potentials with optimized spatial filtering and principal component analysis. *Biomedical Signal Processing and Control*, 3(4):300–304.

Bradshaw, L. and Wikswo, J. (2001). Spatial filter approach for evaluation of the surface laplacian of the electroencephalogram and magnetoencephalogram. *Annals of Biomedical Engineering*, 29(3):202–213.

Chaplais, F. (1998). A wavelet tutorial adapted for the web.

Dai, D. and Yuen, P. (2003). Regularized discriminant analysis and its application to face recognition. *Pattern Recognition*, 36(3):845–848.

Dalal, S., Vidal, J., Hamamé, C., Ossandón, T., Bertrand, O., Lachaux, J., and Jerbi, K. (2011). Spanning the rich spectrum of the human brain: slow waves to gamma and beyond. *Brain Structure and Function*, pages 1–8.

De Hoon, M., Van der Hagen, T., Schoonewelle, H., and Van Dam, H. (1996). Why yule-walker should not be used for autoregressive modelling. *Annals of Nuclear Energy*, 23(15):1219–1228.

Duda, R., Hart, P., and Stork, D. (2001). Pattern classification. *John Willey & Sons*.

Georgopoulos, A., Kalaska, J., Caminiti, R., and Massey, J. (1982). On the relations between the direction of two-dimensional arm movements and cell discharge in primate motor cortex. *The Journal of Neuroscience*, 2(11):1527–1537.

Graps, A. (1995). An introduction to wavelets. *Computational Science & Engineering, IEEE*, 2(2):50–61.

Hawkins, D. (2004). The problem of overfitting. *Journal of chemical information and computer sciences*, 44(1):1–12.

Hudson, D. and Cohen, M. (1999). *Neural networks and artificial intelligence for biomedical engineering*. Wiley-IEEE Press.

Jahanshahi, M. and Hallett, M. (2003). *The Bereitschaftspotential: movement-related cortical potentials*. Springer.

Jerbi, K., Ossandón, T., Hamamé, C., Senova, S., Dalal, S., Jung, J., Minotti, L., Bertrand, O., Berthoz, A., Kahane, P., et al. (2009). Task-related gamma-band dynamics from an intracerebral perspective: Review and implications for surface eeg and meg. *Human brain mapping*, 30(6):1758–1771.

Jerbi, K., Vidal, J., Mattout, J., Maby, E., Lecaignard, F., Ossandon, T., Hamamé, C., Dalal, S., Bouet, R., Lachaux, J., et al. (2011). Inferring hand movement kinematics from meg, eeg and intracranial eeg: From brain-machine interfaces to motor rehabilitation. *IRBM*.

Kandel, E., Schwartz, J., Jessell, T., et al. (2000). *Principles of neural science*, volume 4. McGraw-Hill New York.

Krepki, R., Blankertz, B., Curio, G., and Müller, K. (2003). The berlin brain-computer interface (bbci). *IEEE Transactions on Automatic Control*, 23(4):538–544.

Krepki, R., Blankertz, B., Curio, G., and Müller, K. (2007). The berlin brain-computer interface (bbci)–towards a new communication channel for online control in gaming applications. *Multimedia Tools and Applications*, 33(1):73–90.

Leeb, R., Friedman, D., Müller-Putz, G., Scherer, R., Slater, M., and Pfurtscheller, G. (2007). Self-paced (asynchronous) bci control of a wheelchair in virtual environments: a case study with a tetraplegic. *Computational intelligence and neuroscience*, 2007:7.

Leuthardt, E., Miller, K., Schalk, G., Rao, R., and Ojemann, J. (2006). Electrocorticography-based brain computer interface-the seattle experience. *Neural Systems and Rehabilitation Engineering, IEEE Transactions on*, 14(2):194–198.

Leuthardt, E., Schalk, G., Wolpaw, J., Ojemann, J., and Moran, D. (2004). A brain–computer interface using electrocorticographic signals in humans. *Journal of Neural Engineering*, 1:63.

Lotte, F., Congedo, M., Lécuyer, A., Lamarche, F., and Arnaldi, B. (2007). A review of classification algorithms for eeg-based brain–computer interfaces. *Journal of neural engineering*, 4:R1.

Martini, F. (2006). *Fundamentals of anatomy and physiology*. Prentice Hall.

Mehring, C., Nawrot, M., de Oliveira, S., Vaadia, E., Schulze-Bonhage, A., Aertsen, A., and Ball, T. (2004). Comparing information about arm movement direction in single channels of local and epicortical field potentials from monkey and human motor cortex. *Journal of Physiology-Paris*, 98(4-6):498–506.

Middendorf, M., McMillan, G., Calhoun, G., and Jones, K. (2000). Brain-computer interfaces based on the steady-state visual-evoked response. *Rehabilitation Engineering, IEEE Transactions on*, 8(2):211–214.

Millan, J., Rupp, R., Muller-Putz, G., Murray-Smith, R., Giugliemma, C., Tangermann, M., Vidaurre, C., Cincotti, F., Kubler, A., Leeb, R., et al. (2010). Combining brain-computer interfaces and assistive technologies: state-of-the-art and challenges. *Frontiers in neuroscience*, 4.

Mirkin, B. (2011). Data analysis, mathematical statistics, machine learning, data mining: Similarities and differences. In *Advanced Computer Science and Information System (ICACSIS), 2011 International Conference on*, pages 1–8. IEEE.

Niazi, I., Jiang, N., Tiberghien, O., Nielsen, J., Dremstrup, K., and Farina, D. (2011). Detection of movement intention from single-trial movement-related cortical potentials. *Journal of neural engineering*, 8:066009.

Noble, W. et al. (2004). Support vector machine applications in computational biology. *Kernel methods in computational biology*, pages 71–92.

Pfurtscheller, G., Muller-Putz, G., Scherer, R., and Neuper, C. (2008). Rehabilitation with brain-computer interface systems. *Computer*, 41(10):58–65.

Press, W., Teukolsky, S., Vetterling, W., and Flannery, B. (2007). *Numerical Recipes Source Code CD-ROM 3rd Edition: The Art of Scientific Computing*. Cambridge University Press.

Ramoser, H., Muller-Gerking, J., and Pfurtscheller, G. (2000). Optimal spatial filtering of single trial eeg during imagined hand movement. *Rehabilitation Engineering, IEEE Transactions on*, 8(4):441–446.

Rickert, J., de Oliveira, S., Vaadia, E., Aertsen, A., Rotter, S., and Mehring, C. (2005). Encoding of movement direction in different frequency ranges of motor cortical local field potentials. *The Journal of neuroscience*, 25(39):8815–8824.

Schalk, G., McFarland, D., Hinterberger, T., Birbaumer, N., and Wolpaw, J. (2004). Bci2000: a general-purpose brain-computer interface (bci) system. *Biomedical Engineering, IEEE Transactions on*, 51(6):1034–1043.

Shibasaki, H. and Hallett, M. (2006). What is the bereitschaftspotential? *Clinical Neurophysiology*, 117(11):2341–2356.

Soekadar, S., Birbaumer, N., and Cohen, L. (2011). Brain-computer interfaces in the rehabilitation of stroke and neurotrauma. *Systems Neuroscience and Rehabilitation*, pages 3–18.

Standring, S., Ellis, H., Healy, J., Johnson, D., Williams, A., Collins, P., and Wigley, C. (2005). Gray's anatomy: the anatomical basis of clinical practice. *American Journal of Neuroradiology*, 26(10):2703.

Waldert, S., Pistohl, T., Braun, C., Ball, T., Aertsen, A., and Mehring, C. (2009). A review on directional information in neural signals for brain-machine interfaces. *Journal of Physiology-Paris*, 103(3-5):244–254.

Waldert, S., Preissl, H., Demandt, E., Braun, C., Birbaumer, N., Aertsen, A., and Mehring, C. (2008). Hand movement direction decoded from meg and eeg. *The Journal of Neuroscience*, 28(4):1000–1008.

Yom-Tov, E. and Inbar, G. (2003). Detection of movement-related potentials from the electro-encephalogram for possible use in a brain-computer interface. *Medical and Biological Engineering and Computing*, 41(1):85–93.

Appendix A

The brain

A brief introduction to brain anatomy is described below. The following pages are based on [Martini, 2006] and [Standring et al., 2005].

The brain is one of the most complex parts of a human being. It accounts for up to 98% of the neural tissue within the entire body and has a weight of about 1.4 kg with large individual variance.

A.1 Protection and support

The brain tissue is tender and delicate and so it needs protection from potentially damage. Its protection is ensured by three layers: the cranial bones, the cranial meninges and the cerebrospinal fluid. The bones of the cranium supply a hard encapsulation of the brain. As show in figure A.1, the cranial meninges consist of multiple layers: dura mater, arachnoid mater and pia mater, in order of deepness. The dura mater has two fibrous layers, or lamellae, with tissue fluids and blood vessels in between. The arachnoid mater provides a smooth surface covering the entire brain, which does line the brain down into its sulci, as does the pia mater. Pia mater is a thin fibrous tissue, anchored to every fold of the brain, which encloses cerebrospinal fluid in order to protect the brain and allows blood vessels to pass through and feed the brain cells.
The cerebrospinal fluid has both a role in transport of nutrients, chemical messengers and other substances, and in protecting the brain from mechanical stress, partially preventing the brain from beating against the skull.

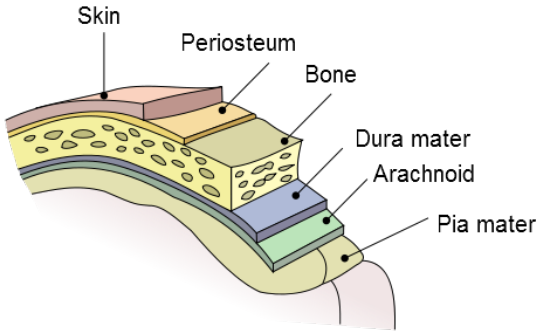

Figure A.1: Meninges surrounding the brain (adapted for own use from [Standring et al., 2005]).

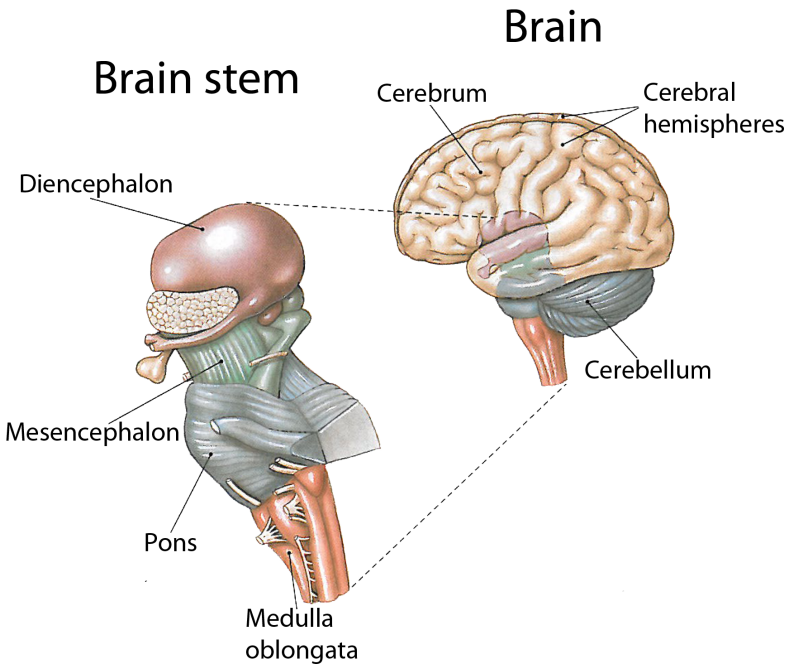

Figure A.2: Gross anatomy of the brain (adapted for own use from [Martini, 2006]).

A.2 Structure

The brain can be anatomically divided into four parts (see figure A.2): the brain stem, the diencephalon, the cerebellum and the cerebrum. The brain stem is located in the inferior part of the brain, connected and superior to the spinal cord.

A.2.1 The brain stem

The brain stem consists of several parts, which going superior from the spinal cord are: medulla oblongata, pons, mesencephalon. Sometimes the diencephalon is regarded as part of the brain stem.
The medulla oblongata transmits sensory information to the superior parts of the brain stem and regulates autonomic functions, such as heart rate and blood pressure. The pons connects the cerebellum to the brain stem and is involved in visceral and somatic motor control and transmits sensory information to superior parts of the brain stem and the cerebellum. The mesencephalon controls auditorily and visually triggered reflexes and helps maintaining consciousness.

A.2.2 The diencephalon

The diencephalon is a region composed by a left and right thalamus both relaying and processing sensory information. The inferior part is called hypothalamus and is involved in hormone production, emotions and autonomic functions.

A.2.3 The cerebellum

The second largest part of the brain is the cerebellum, located posterior at the level of the mesencephalon and covered by the cerebellar cortex. The main function of the cerebellum is to adjust the ongoing movements and to help to coordinate repeated advanced somatic motor patterns by receiving sensory information and comparing it to previously experienced movements, allowing to make smooth movements.

A.2.4 The cerebrum

The cerebrum consists of two highly folded cerebral hemispheres covered with neural cortex and, in general, each one controls the contralateral side of the body. Even if the hemispheres look similar, they do not have the same functionality neither the same size. The cerebrum plays a role in most higher mental functions, such as attention, awareness, thought, intellect, memory, highly complex movements, sensations and speech. The superficial layer of the cerebrum is the cerebral cortex, which together with the deeper basal nuclei, is part of the grey matter (formed from neurons and their unmyelinated fibers) and superficial to the white matter (formed predominantly by myelinated axons). The surface of the cerebral cortex is folded into the so called "sulci" and organized in different layers. The cerebral cortex can be topographically subdivided into four lobes: frontal, parietal, occipital and temporal lobe (see figure A.3), and is commonly

described as comprising three parts: sensory, motor, and association areas, depending on the functionality. Below, a short explanation of the main areas that compose the cortex.

Cortices

The primary motor cortex (M1) is located in the posterior part of the frontal lobe and is involved in performing voluntary movements, whereas the primary sensory cortex (S1), which is a part of the parietal lobe, il located posteriorly. It allows conscious sensation of vibration, touch, pressure, pain etc. The two cortices are named "primary" because they have a specifically defined topographic mapping of the body, so a specific area of the primary motor cortex is related to motion of a corresponding group of muscles or organ (for example a limb). The regions of the primary sensory and motor cortex are not of the same size: as the size increases, a finer control and sensitivity is allowed. The gustatory cortex, the visual cortex, the auditory and olfactory cortex are also worth to be mentioned.

Association centres

To each of the cortices mentioned above corresponds an association centre, which interprets signals and coordinates the motor response. The somatic motor association area stimulates the neurons of the primary motor cortex in order to achieve the planned movement, while the primary motor cortex initiates the actual movement. Moreover, the association area stores a pattern of stimulation, which matches the corresponding movement pattern.

Integrative centres

Integrative centres collect information from the association centres in order to perform highly complex motor or analytical tasks. The prefrontal cortex located in the frontal lobe, which integrates information from sensory association centres and Wernicke's area, which integrates sensory information while allowing coordinated access to visual and auditory memory, are two examples of integrative centres.

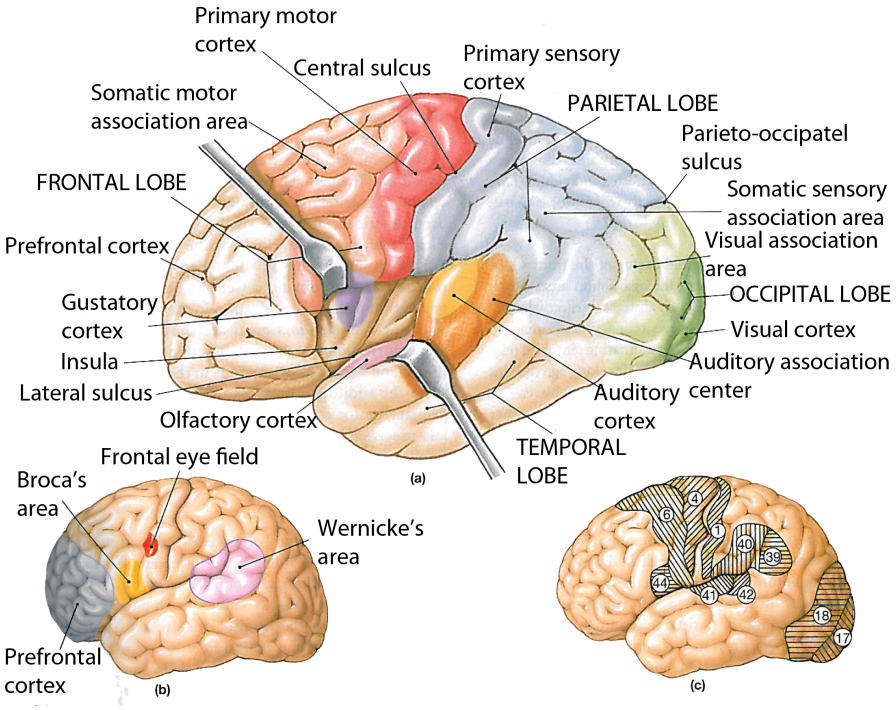

Figure A.3: The figure shows a) the major anatomical landmarks of the left cerebral hemisphere, b) the areas mainly involved in speech and c) histological distinct areas (adapted for own use from [Martini, 2006]).

Appendix B

Organization of movement

In this chapter a general overview about organization of movement and motor control is given. The following is mainly based on [Martini, 2006] and [Kandel et al., 2000] unless otherwise specified.

B.1 Motor cortices and motor planning

The cerebral cortex, the brain stem and the spinal cord are the most important parts of the nervous system involved in movement. Skeletal muscles can be controlled from many places in the central nervous system (CNS): the spinal cord, the pons, the basal ganglia, the cerebellum and the motor cortex, each part having its own role. The spinal cord can be described as the main path trough which signals from the brain are transmitted to the periphery of the body and the opposite. The structure is more complex than this, though: the spinal cord consists of several cord centres, which are commanded by the upper levels of the nervous system. These neuronal circuits in the cord are also responsible for walking movements or different reflexes. Pons, basal ganglia and cerebellum belong to the lower brain and control automatic, instantaneous muscle responses to sensory stimuli.
As it has already been said, the cerebral cortex is involved in processing and integrating sensory information and establishing motor commands. The motor cortex is, more specifically, in charge of complex movements that are controlled by thought processes and also functions as a storage of information for future control of motor activities. Each part of the body receiving somatosensory input corresponds to a specific area in the cortex; this is often represented with a somatosensory homonculus, as shown in figure B.1(a). In the same way, the primary motor cortex (M1) is organised in a topographical manner, containing a representation of each part of the body (see figure B.1(b)). Besides in M1 and S1, a complete map of the body is present in the premotor areas too. However, while stimulation in the M1 evokes simple movements of single joints, stimulation of the premotor cortex results in more complex movement involving multiple joints and resemble natural coordinated movements. The premotor areas consist of the premotor

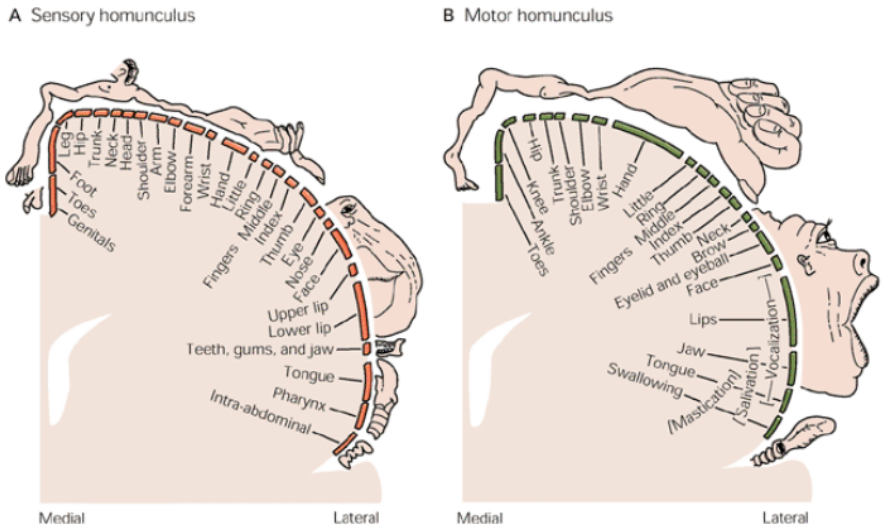

Figure B.1: The figure shows a) The somatotopic representation of the body in somatosensory cortex b) the topographic representation of the body in the motor cortex (adapted for own use from [Kandel et al., 2000]).

cortex and the supplementary motor area and are mainly involved in coordination and planning of movements.
All these areas in the brain are interconnected to each other in a complex network (see figure B.2).
I could explain in detail the connections but i think it's not necessary.

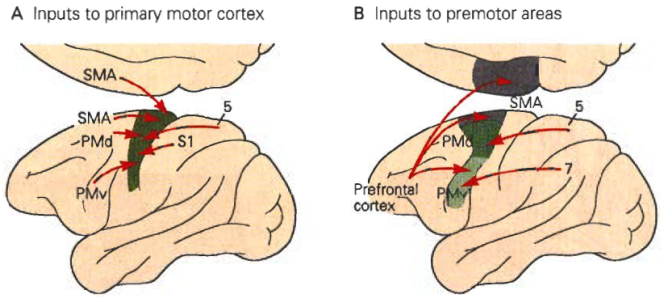

Figure B.2: The major inputs to the motor cortex in monkeys.
A. The major inputs to the primary motor cortex. (**PMd** = dorsal premotor area; **PMv** = ventral premotor area; **S1** = primary sensory cortex; **SMA** = supplementary motor area.)
B. The major inputs to the premotor areas. Dense interconnections between the premotor areas are not shown here. (adapted for own use from [Kandel et al., 2000]).

B.2 Types of movement

The corticospinal tract is considered as the direct pathway of voluntary movements. In the spinal cord, the projection neurons are connected either with interneurons or directly with motor neurons, which in their turn transmit the signals to skeletal muscles. Three types of movements may occur in respect of to ascending and descending signals via different pathways and at different levels: voluntary movement, reflexes and rhythmic movement.
Reflexes are performed subconsciously and can occur at an exclusively spinal level, though they may also be modulated by subcortical or cortical commands. A reflex is started by a sensory stimulus which then leads to excitations of motor neurons at a spinal level, resulting in a muscle contraction or relaxation, possibly even before sensation occurs. Distinct reflexes are initiated by different stimuli of the same sensory receptors or by stimuli of different receptors and can be modulated throughout excitation or depression of the level of the post-synaptic neuron excitability.
The latter, instead, are characterized by a stereotyped action involving repetitions of the same movements (e.g. walking, running, swimming, crawling, flying and allow control of movement at a 'low' (spinal) level without involvement of higher cortical control (conscious control). These can be triggered by peripheral stimuli that activate the underlying circuits or from higher cortical centres, which can also overrule them.
Here, though, we will focus on the voluntary movement planning, control and execution.

B.2.1 Voluntary movement

Voluntary movement is usually goal directed and therefore fully conscious. It arises in the motor cortex and is executed by the spinal cord. When a voluntary movement is started, neurons in the M1 send commands to upper and lower motor neurons. Neurons in the M1 are responsible for one specific somatic location respectively (see figure B.4); for example, the leg components are situated in the middle, the face components are

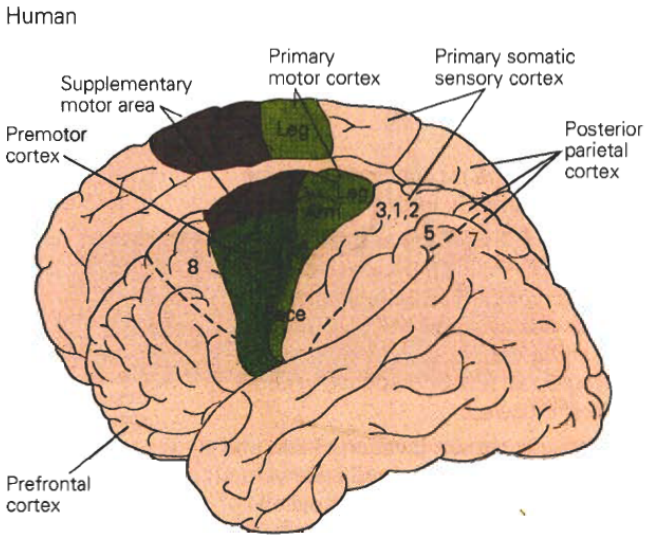

Figure B.3: The figure shows the motor cortices in humans. The sequence of representation of body parts is similar. The ankle control area is medial while the face, mouth, and mastication control areas are lateral. The face and fingers in the human motor cortex have much larger representations because of the greater degree of cortical control of these areas (adapted for own use from [Kandel et al., 2000]).

located laterally and so on. The largest representations belong to muscles which imply finest movement control (e.g. arms, legs and face, see figure B.3 and B.4).
Typically, every voluntary movement performance is based on movements the person has done several times before. In this case, the cortical motor area uses the pattern already memorised in deeper layers of brain stem, basal ganglia, cerebellum or spinal cord and combines

it with the information that comes from the S1. This constant feedback from the S1 enables a finer control and adjustment of the voluntary movement before and during the execution. The cerebellum, instead, plays an essential role as important control centre for unknown motor activities. When a new unknown movement is needed (*motor learning*), the cerebellum is not only in charge of the adaptation of the motor task to the new movement sequence, but it is also associated in planning, execution, controlling and refining of the movement execution.
The neuronal activity in the cortex and the subsequent effect in the muscles is specific. More precisely, it has been shown that the force of a movement is proportionally related to the firing rate of the associated cortical neurons: when the load opposing a movement increases, the firing rate of the active neurons increases too.

Direction of the movement

One of the first and most relevant studies on the direction of movement coding mechanism in the brain was achieved by Georgopoulos et al. preforming studies on primates'

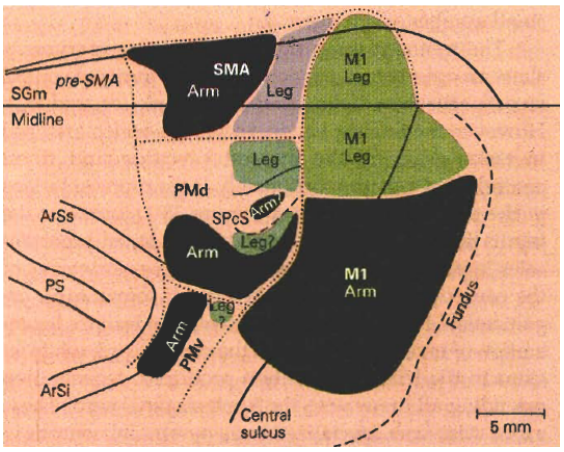

Figure B.4: Somatotopic oraganization of the medial and laterl motor cortex in the monkey, showing the arm and leg representations. (**ArSi**, arcuate sulcus, inferior limb; **ArSs** = arcuate sulcus, superior limb; **CS** = central sulcus; **M1** = primary motor cortex; **PMd** = dorsal premotor area; **PMv** = ventral premotor area; **PS** = precentral sulcus; **SGm** = superior frontal gyrus, medial wall; **SMA** = supplementary motor area; **pre-SMA** = presupplementary motor area; **SPcS** = superior precentral sulcus.) (adapted for own use from [Kandel et al., 2000]).

brain. Georgopoulos et al. trained monkeys to move a joystick toward visual targets located in different directions and recorded the associated changes in activity in the primary motor cortex. The experiment indicated that all neurons fired both before and during movement in a wide range of direction. It appears that motor cortical neurons are tuned to the direction of movement, but individual cells fire preferentially in connection with movement in certain directions. The raster plots in figure B.5 show the firing pattern of a single neuron during movement in eight direction show the cell firing at relatively higher rates during movements in the range from 90 degrees to 225 degrees, pointing out that different cells have different preferred movements directions. Cortical neurons with different preferred directions are all active during movement in a particular direction and the entirety of this activity results in a population vector that closely matches that of the direction of movement.

This means that movement in a particular direction is determined not by the actions of the single neurons, but by the net action of a large population of neurons, where the contribution of each neuron to movement in a particular direction can be represented by a vector whose length indicated the level of activity during movement in that direction and where the contributions of individual cells could then be added vectorially to produce a population vector.

Georgopoulos et al. also found a strong dependence between directionally tuned cell's firing rate and external load, suggesting that the activity of neurons in the primary motor cortex varies with the direction. This modulation depends on the amplitude of the force required to displace the limb; the neuron's firing rate increases if load opposes movement of the arm in the cell's preferred direction, while it decreases if the load pulls the arm in the cell's preferred direction.

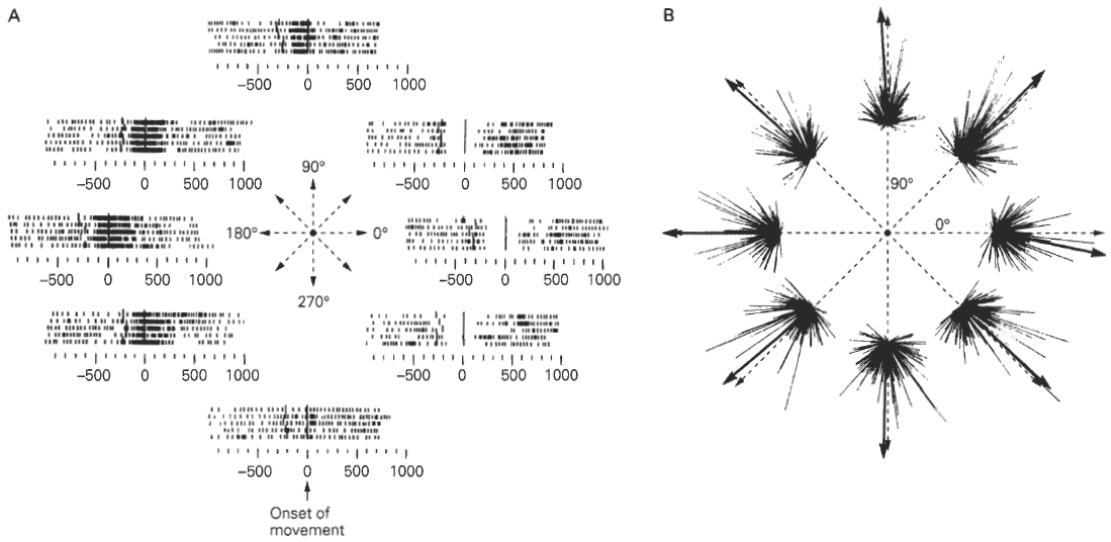

Figure B.5: The raster plots of the firing pattern of a single neuron during movement in eight direction. The cell fires at higher rates during movements in the range fro 90 degrees to 225 degrees. For these recordings a monkey was trained to move a handle to eight locations arranged radially in one plane around a central starting position. Each row of tics in each raster plot represents activity in a single trial. The rows are aligned at the onset of movement (zero time) (adapted for own use from [Georgopoulos et al., 1982]).

Movement planning

The M1 needs to be stimulated by neurons from the premotor cortex and the supplementary motor area (SMA), which support and coordinate the M1, in order to initiate a voluntary movement. The preparatory activity of a movement is performed in the premotor areas and the primary motor cortex. This planning results in a motor program (or *movement pattern*) describing extent, angle and velocity of movement of the joints involved. Thus the premotor cortex is in charge to provide sensory guidance of movement, while the SMA is responsible for planning and coordination of complex movements. The premotor cortex and the SMA are able to receive information from different decisional centres within the brain; these areas interpret the information and coordinate the execution commands and send it to the M1, which subsequently controls the actual signals sent to the muscles (effectors). A movement is the consequence of triggering of a pattern more that of the stimulation of each neuron separately, thus allowing to perform the movement more easily when it has been repeated.
The measure of activity in the motor cortex of the brain leading up to voluntary muscle movement is called Bereitschaftspotential or BP (from German, "readiness potential"), which is covered more extensively in chapter C.

Appendix C

The Bereitschaftpotential

The first report of electroencephalographic (EEG) activity preceding voluntary movement in humans was made by Kornhuber and Deecke in 1964, recording both the EEG and an electromyogram (EMG), with the aim of connecting in some respect the activity of the brain with the one of the muscles involved in the movement on a temporal scale. The experiment was conducted using an off-line averaging technique and led to the identification of two main components of the BP, one before and one after the EMG onset: the actual Bereitschaftspotential (BP), also known as readiness potential (RP), and the reafferente potential. Later they found two more components which appear before the movement onset: the pre-motion positivity (PMP) and the motor potential (MP). Although a relatively high number of studies have been conducted on the movement-related cortical potentials (MRCPs), the actual physiological significance of each component, among others that of BP, has not been fully clarified yet [Shibasaki and Hallett, 2006].
In its original formulation by Kornhuber and Deecke, the BP was seen as 'readiness potential', so as an index of motor preparation. Further experiments have shown new and wider interpretations of the BP, such as anticipation and expectancy, attention, preparatory activity, intention to act, resource mobilization, effort, timing of movements and degree of effort associated with movement. Jahanshahi and Hallett proposed that it is possible to differentiate the contributions to BP associated with cognitive, motivational and motor processes among the different areas of the motor cortex, rising the hypothesis that while prefrontal areas may be involved in the decision-making process necessary for response selection timing and initiation of the motor action, the pre-SMA motor areas and lateral premotor cortex may take care of preparatory precesses [Jahanshahi and Hallett, 2003].
The BP has become a common tool in motor physiology laboratory in the past years, not only to investigate movement parameters such as force, rate, movement complexity and mode of movement, but its latency and/or shape have been reported to change in case of neurological disorders. Various methods are used to record BPs, e.g. scalp electroencephalography (EEG), magnetoencephalography (MEG), intracranial EEG recordings, combined EEG and positron emission tomography (PET), combined EEG and MEG,

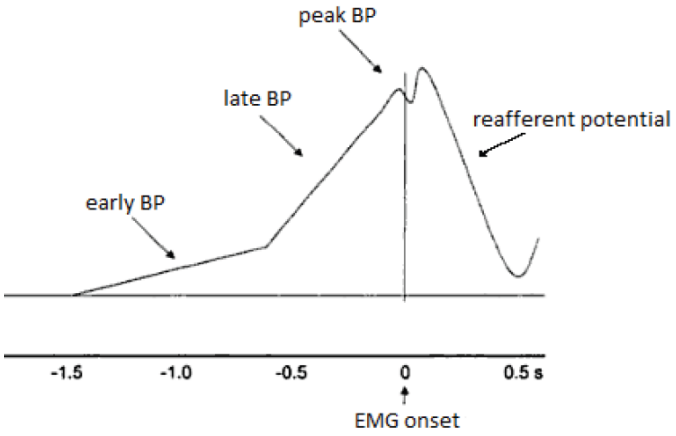

Figure C.1: A schematic representation of the time course and the Bereitschaftpotential (BP) prior to movement (adapted for own use from [Jahanshahi and Hallett, 2003])

combined EEG and functional magnetic resonance imaging (fMRI).
A comprehensive book which describes in detail the Bereitschaftspotential was published in 2003 ([Jahanshahi and Hallett, 2003]), used hereby as main reference and integrated with more recent findings, trying, when possible, to focus on hand movements in electroencephalographic recordings

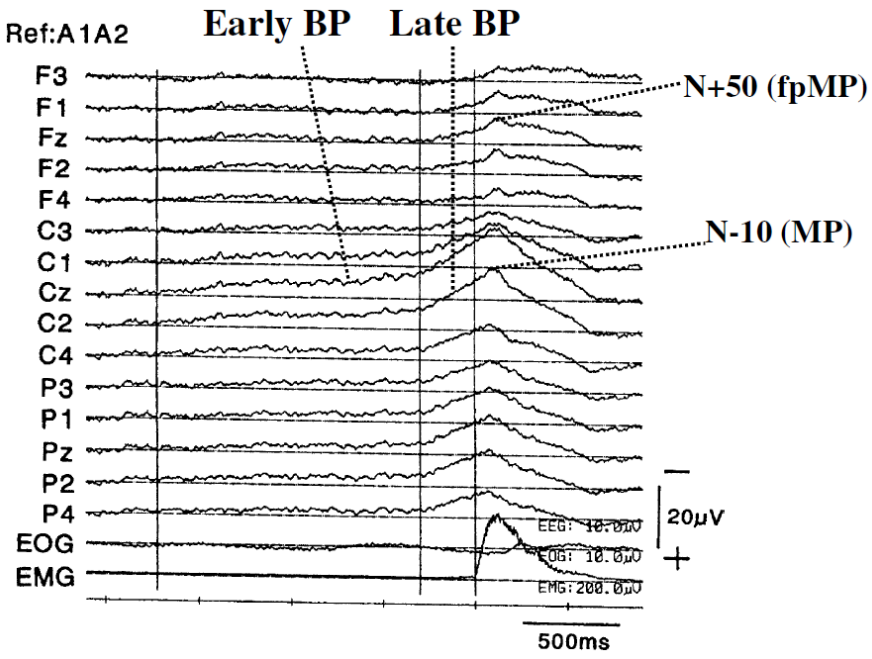

Figure C.2: Waveforms and terminology of MRCPs from a single normal subject in self-iniated left wrist extention. Avarage of 98 trials.
Reference (Ref): linked ear electrodes (A1A2). Early pre-movement negativity (early BP) starts 1.7 s before the onset of the averaged, rectified EMG of the left wrist extensor muscle, and is maximal at the midline central electrode (Cz) and widely and symmetrically distributed on both hemispheres. Later negative slope (late BP) starts 300 ms before the EMG onset and is much larger over the right central region (contralateral to the movement). A negative peak localized at the contralateral central area (C2) is N-10 or motor potential (MP). Another negative peak occurring shortly after N-10 is localized over the midline frontal region and corresponds to N+50 or the frontal peak of motor potential (fpMP).
(adapted for own use from [Shibasaki and Hallett, 2006])

C.1 Morphology of BPs

BPs are considered to represent neuronal activation, which is the outcome of an increase of extracellular K^+ concentration and decrease of Ca^{++} concentration. This activation of brain regions result in negative slow potentials, such as the BP. More specifically, the BP is a negative cortical potential which develops beginning about 1.5 to 1 s prior the onset af a self-placed movement (see figure C.1 and C.2), although the onset of BP with respect to the movement onset significantly differs among diverse conditions of movement and among subjects. For example, when the subject is requested to repeat the same movement, the BP starts much earlier as compared to the same movement executed in natural conditions, because in such experimental conditions the subject has a longer time to prepare for the movement. It is important to stress that its onset is related to an actual, intended or imaginary voluntary movement. Thus the BP can be defined as a movement-related cortical potential (MRCP).
Initially a distinction between the slowly rising phase of BP waveform and change in the steepness of the slope, which suddenly occurs around 400 to 500 ms prior to movement onset, was made (see figure C.1). The early and late BP differ in term of distribution over the scalp: the early BP is bilaterally symmetrical, but the late and peak BP are asymmetrically distributed and maximal over the contralateral precentral areas [Jahanshahi and Hallett, 2003]. The early slow, rising negativity has been usually referred as early BP, BP1, and NS1 (negative slope 1), whereas BP2, NS' and NS2 stand for the second phase of negativity [Jahanshahi and Hallett, 2003]. The late BP was thought to be more specific for the site of movement while the early BP was thought to represent the more general preparation for the forthcoming movement because of its diffuse distribution, but neither the physiology nor the functional significance of change of steepness is currently completely known (see section C.2). Later, a third negative component was distinguished, occurring 50 to 60 ms prior to movement onset, the 'motor potential' (MP, peak BP or peak NS'), which is the point of maximum negativity over the hand area contralateral to the moving hand. BP midline maximal, symmetric distribution is likely due to the summation of electrical fields generated from homologous areas of both hemispheres [Shibasaki and Hallett, 2006].
Different groups have proposed wide range of different terminologies, according to their findings and different opinions about origin, location and physiological meaning of BP components (see table C.3 for details), however, in this report, in order to avoid confusion about the use of the term BP, we call the early segment 'early BP' and the late, steeper segment 'late BP', and just BP for the early BP and the late BP inclusive (see figure C.2).

	Pre-movement components				Post-movement components			
Kornhuber and Deecke (1965)	BP		PMP	MP				RAP
Vaughan et al. (1968)	N1		P1	N2 (?)	N2 (?)			P2
Shibasaki et al. (1980a)[a]	BP	NS′	P−50	N−10	N+50	P+90	N+160	P+300
Dick et al. (1989)	NS1	NS2						
Lang et al. (1991)	BP1	BP2						
Tarkka and Hallett (1991)	BP	NS′	PMP	isMP ppMP	fpMP			
Kristeva et al. (1991)[b]	RF			MF	MEFI	MEFII	MEFIII	PMF
Cui and Deecke (1999)	BP1	BP2		MP		PMPP	MEPI	MEPII

[a] Peak of each component, except for BP and NS′, was measured from the peak of averaged, rectified EMG.
[b] Based on movement-related magnetic fields.

Figure C.3: Terminology of movement-related cortical potentials (adapted for own use from [Shibasaki and Hallett, 2006])

C.2 Generator sources of MRCPs

The generator sources of MRCPs have to be fully understood yet. In order to achieve this challenge, various dipole source localization techniques have been applied to estimate the generator sources of MRCPs, as already mentioned above. The identification of generators of single MRCP components is a controversial topic in the existing literature. The complexity of the problem occurs due to several different factors, such as the specific localization technique which was used, the type of movement under investigation, the movement performance or the investigated time frame. However, it is a common opinion among the literature that the BP is mainly generated by sources located in the supplementary motor area (SMA) (both the proper SMA as well as the cingulate motor area (CMA) should be considered in this context) and in the M1 (particularly in the contralateral motor cortex) to a lesser or greater extent. [Shibasaki and Hallett, 2006]. Moreover, also regarding the time course of activation of the SMA and M1 there are still doubts. Some suggest that the BP reflect serial activation of the SMA preceding M1, others propose that SMA and M1 are activated in parallel [Jahanshahi and Hallett, 2003]. The current consensus on the generator source of each MRCP component is summarized in table C.4. At least regarding self-paced repetition of simple movements at slow rate, the early BP begins about 2 s before the movement onset in the pre-SMA with no site-specificity and is bilaterally generated from the localized area of the SMA according to the somatotopic organization and shortly thereafter in the lateral premotor cortex bilaterally, again with relatively clear somatotopy. About 400 ms before the movement onset, suddenly the steepness of the waveform changes and the late BP occurs in the contralateral M1 and lateral premotor cortex with precise correspondence to a somatotopic organization. The generator sources of post-movement components have not been clearly identified yet [Shibasaki and Hallett, 2006].

Shibasaki and Hallett, in his review, has reported some experiments concerning the case of hand movements. SMA and lateral precentral gyrus were shown to be the main generator sources for early BP. It has been proposed that there are three dipole sources of the early BP, one in the SMA and two others in bilateral M1, and that only the source recorded in the SMA was influenced by the mode of movement selection in such a way that it was larger before freely selected movements than fixed ones. Based on

Component	Generator sources
Early BP	
Earliest	Pre-SMA (bilateral)
	SMA proper (bilateral)[a]
Next earliest	Area 6 (bilateral)[a]
Late BP (NS′)	Area 6 (mainly contralateral)[b]
	Area 4 (mainly contralateral)[b]
MP (N−10)	Area 4 (contralateral)[b]
fpMP (N+50)	Area 3 (contralateral)[b]

[a] Somatotopically organized to some degree.
[b] Somatotopically organized precisely.

Figure C.4: Generator sources of each component of movement-related cortical potentials (MRCP) (adapted for own use from [Shibasaki and Hallett, 2006])

the high-resolution DC-EEG analysis, it has been estimated that BP occurs earlier in the SMA and cingulate motor areas, after in the contralateral M1, and finally in the ipsilateral M1. Principal component analysis and fMRI-constrained EEG dipole source analysis were used, determining that the main source of early BP was the crown of the precentral gyrus bilaterally (specifically hand area of area 6), the source of late BP in both area 4 and area 6, and MP in area 3. Most studies have localized the source of MP or N-10 in the M1 hand area.
For this report, it is important to record EEG from multiple electrodes, including C1 and C2, because the late BP is maximal over the contralateral central area (approximately C1 or C2 of the International 10-20 System) for the hand movement.

C.3 Factors influencing BP

Lang W. (as reported by [Shibasaki and Hallett, 2006]) reviewed extensively the factors that contribute to magnitude and time course of BP recorded in a self-paced condition. Taken together the amplitude and the time course of the MRCP is affected by various factors, such as: level of intention; speed, precision, mode (free versus fixed), pace og repetition, discreteness, complexity of the movement; preparatory state; learning and skill acquisition; perceived effort; force exerted and pathological lesions of brain structures.
Below are listed some studies supporting the information given by table C.5, which summarizes the findings about this issue so far [Shibasaki and Hallett, 2006].

The effect of the complexity of a movement on BP was investigated in several studies, mostly involving comparison of single, simultaneous and sequential movements. Below are reported (cited by Shibasaki and Hallett; Jahanshahi and Hallett) a number of experiments which confirms that more complex movements translate in a larger late BP.
Comparison of isolated single finger extension with simultaneous finger extension of

Factors	Early BP	Late BP
Level of intention	Larger[a]	
Preparatory state	Earlier onset[a]	
Movement selection	Larger	No effect
Learning	Larger during learning[a]	
Praxis movement	Start parietally[a]	
Force	Larger[a]	
Speed	Later onset[a]	
Precision	No effect	Larger
Discreteness	No effect	Larger
Complexity	No effect	Larger
Parkinsonism	Small	No change
Cerebellar lesion	Small	Small
Dystonia	No change	Small
Hemiparesis recovery	No change	Involved
Mirror movement	No change	Involved

Figure C.5: Differential influence of various factors on early and late BP in normal and pathological conditions. As for the factors in normal conditions. (adapted for own use from [Shibasaki and Hallett, 2006])

two fingers revealed significantly larger BP at the pre-central area contralateral to the movement, in the case of single finger activation; although only half of the muscles are activated. This phenomena can be explained by the fact that single finger movements are finer and more discrete, therefore requiring a more 'precise' motor program and M1 activation (Kitamura et al., 1993). Another study was comparing single isotonic elbow flexion and single isometric finger flexion with sequential and simultaneous activation of these two movements, finding a larger BP for the sequential and simultaneous movements compared to single flexion (Benecke et al., 1985). Kitamura found that, when middle and index finger were moved consecutively, the negative slope started earlier, but no amplitude changes of the BP were observed, compared to simultaneously activation of the fingers. Thus it was hypothesised that the execution of unilateral sequential movement requires a greater and earlier activation of the SMA and the primary hand sensorimotor areas(Kitamura et al.). Earlier onset and larger amplitude of BP in the sequential movement than in the simple movement was also reported by Simonetta et al.(1991), in a study involving comparison of a simple movement with a more complex motor sequence (starting with the simple movement).
The exerced force is another factor that was shown to increase the BP (Slobounov et al., 2004; Masaki et al., 1998). In a study conducted by Masaki et al. (1998), when subjects were asked to produce a specific force, a larger negative slope was observed compared to movements performed in a non-purposive manner although the same amount of force was produced. This leads to think about the involvement of a planning process which is required to produce a particular force and subsequently leads to a larger BP amplitude. Again, a possible explanation is that the preparation process in order to develop larger forces requires a higher level of activity of the involved brain areas.
As for the mode of movement, investigation showed that freely selected movements led to higher amplitude of BP as opposed to pre-determined repetitive movements. This influence does not seem to involve all the areas of the brain, though. By using a spatio-

temporal decomposition, three dipole sources of the BP were estimated: one located in the SMA and two in the M1 in each hemisphere, finding that only the source in the SMA was influenced by the mode of the movement (Praamstra et al.,1995). In contrast Dirnberger et al. (1998) observed a larger lateralized readiness potential for freely selected movements compared to fixed repetitive movements, considering this by a result of a greater involvement of M1 activity in the selected movement mode.
Furthermore, the BP onset is affected by the speed with which the movement is conducted. The BP starts later if the movement is performed with a higher speed (Shibasaki and Hallett, 2006). The time course of the early BP is also influenced by the level of experience of the movement under study. Libet et al.(1983), for example, observed a 1 s earlier onset when the movement is associated with a preplanning or preparation time to act shortly compared to movements which are associated with a more specific or endogenous intention to act (about 500 ms prior onset).